KU LEUVEN

ARENBERG DOCTORAL SCHOOL
Faculty of Science

Characterization and optimization of a versatile laser and electron-impact ion source for radioactive ion beam production at ISOLDE and MEDICIS

Yisel Martinez Palenzuela

Dissertation presented in partial fulfillment of the requirements for the degree of Doctor of Science (PhD): Physics

Supervisor:
Prof. dr. T. E. Cocolios
Prof. dr. P. Van Duppen, co-supervisor

April 2019

Characterization and optimization of a versatile laser and electron-impact ion source for radioactive ion beam production at ISOLDE and MEDICIS

Yisel MARTINEZ PALENZUELA

Examination committee:
Prof. dr. R. Raabe, chair
Prof. dr. T. E. Cocolios, supervisor
Prof. dr. P. Van Duppen, co-supervisor
Prof. dr. G. Neyens
Prof. dr. M. Huyse
Prof. dr. N. Severijns

Dr. T. Stora
(CERN, Geneva, Switzerland)
Dr. P. Delahaye
(GANIL, Caen, France)

Dissertation presented in partial fulfillment of the requirements for the degree of Doctor of Science (PhD): Physics

April 2019

Uitgegeven in eigen beheer, Yisel Martinez Palenzuela, Celestijnenlaan 200D - box 2418, B-3001 Leuven (Belgium)

Acknowledgements

A huge thank you to Piet and Mark who were my supervisors at the start of this PhD. You made me feel very welcome at IKS from the first day. Special thanks to Thomas who became my main supervisor in my second year. Thank you for your constant guidance and motivation which helped enormously to see this thesis to completion. I am also very thankful to my jury members Pierre, Gerda, Nathal, Riccardo and Thierry, I really enjoyed the interesting discussions during my defence.

I remember wishing as a summer student that I could one day work at ISOLDE, and luckily enough I joined in 2015. A long list of people made my time there really enjoyable. Many thanks to the ISOLDE operators, the RILIS team, my colleagues at the TISD group, the workshop, the MEDICIS collaboration, the magnets section and the Interdisciplinary Research Group led by Thomas.

Lots of people gave their time and hard work to help me with various aspects of this thesis: Stef, Bernard, Mike, Ermanno, Andres, Joao, Jochen, Sebastian, Vincent. Thanks Kati for being a good friend and colleague over the last years. Also thanks to Tom and Alex for hosting me in TRIUMF.

In probably the loudest office in any CERN corridor, I couldn't have had better officemates. Annie, Nhat-Tan, Carlos, Stu and Bea to mention a few. I really enjoyed the constant silliness and fun times. Also my friends and colleagues during my time at IKS: Simon, Sasha, Rafael, Ruben, Wouter, Liam, Paul, Dani, Ana, Hilde, Philippe, Camilo, Isabelle, Danielle, Fabienne and many others. And thank you Yero for looking after me in Leuven!

I would like to thank two people in particular: Jonny and Bruce. I worked with Jonny on VSim simulations for uncountable hours. I loved the periods in Manchester, running simulations at late hours in various pubs. I am also forever in debt to Bruce, who helped me in many aspects of my thesis, from the many hours in the lab to the thesis writing/proof-reading. Despite the hard work, we always managed to fit in a decent number of coffee breaks and climbing sessions.

My non-ISOLDE friends, the Geneva crew. I am so lucky I got to meet you all. Theo, John, Matevz, Jess, Urska, Debs, Tobi, Steve, Bea, Slawosz, Marta, Laura, Vale, Lena, Matteo, Christian, Hana, Tom, Kira, Johannes, Claire, Marko, Laure, Mati, Silvia, Samir, Dan, my French parents Brigitte and Eric and so many others that made these last years in Geneva unforgettable.

Jean-Pierre, my first supervisor at CERN and good friend. Hope there will be many more table tennis matches to come.

I am so lucky to have such a wonderful family. Big thanks to Cian for preparing the best midnight gin-and-tonics that certainly helped me get through the writing period. The unconditional love and support you have given me these years, despite the emotional roller-coaster really meant a lot to me. Thanks to my brother for being always there for me. You are, most of the time, the best brother I could have wished for. And thanks to Ella for always being so kind to me. To my mum and my dad: I know you have enjoyed and suffered with me every second of this journey. I can't wait to be back home celebrating this chapter of my life with you.

Preface

The work reported in this thesis concerns the new CERN-MEDICIS (MEDical Isotopes Collected from ISOLDE) facility. It presents details of the first stable and radioactive beams, and developments to optimize its operation. Chapter 1 lays out the motivation behind this work. In Chapter 2, details on the infrastructure and operation of the MEDICIS facility are given. It includes calculations of ion optics for the design and characterization of the MEDICIS beamline. The results obtained during the commissioning phase, where both stable and radioactive beams have been produced, demonstrate the readiness of the facility to enter full production mode.

Chapter 3 gives a review of the ion sources employed at ISOLDE, summarizing the latest developments and ongoing work. In Chapters 4 and 5, which together with Chapter 2 constitute the bulk of this thesis, computational and experimental studies performed to characterize, optimize, and improve the performance of the VADIS and VADLIS ion sources are discussed. Part of the research on the VADLIS has been published in a peer-reviewed scientific journal and is included in Chapter 5:

- Y. Martinez Palenzuela *et al* "Enhancing the extraction of laser-ionized beams from an arc discharge ion source volume", NIMB, vol. 431, pp. 59–66, 2018. https://doi.org/10.1016/j.nimb.2018.06.006

The final chapter (Chapter 6) gives an overview of the main findings from the simulations and experimental work, with suggestions for further studies.

Abstract

This work describes the operating regime of the newly commissioned CERN-MEDICIS facility and reports on the first extracted ion beams. To achieve this milestone and to ensure that the facility is capable of meeting the performance requirements, simulation software is used to optimize the ion beam extraction, mass separation and transport. The MEDICIS mass separator, recovered from the LISOL facility [1], has been characterized and optimized for this application: laser-window installation, electromagnetic field mapping and assessment of mass resolving power amongst others.

In the quest of improving the performance of the ISOLDE FEBIAD (VADIS) ion source, a study of the dependence of the ionization efficiency on the operational parameters has been performed. The role of the cathode temperature, anode voltage, ion source magnetic field and gas load have been investigated, leading to recommendations for the optimal operation of the ion source. The ionization efficiencies for magnesium, manganese, gallium, tin and mercury were measured, with values ranging from 1-21 % recorded.

Particle-in-cell software was used to visualize the electrostatic field distribution within the VADIS and VADLIS and to perform ion tracking. By doing so, the VADLIS, which has been recently developed at ISOLDE for the application of element-selective laser ionization in the FEBIAD cavity, was modified for enhanced extraction of laser-ions. This modification allows for the recovery of the extraction capabilities of the VADLIS when operated in the so-called RILIS mode.

The modified VADLIS prototype, presented here, was used for the production of laser-ionized ^{24}Mg, ^{71}Ga, ^{98}Mo and ^{196}Hg beams, both off-line and on-line. An efficiency improvement greater than a factor of two was achieved in all cases, although, for species exclusively laser-ionized inside the FEBIAD anode, a seven-fold increase in efficiency was measured.

Beknopte samenvatting

Dit werk beschrijft de operationele werking van de in gebruik genomen CERN-MEDICIS faciliteit en de eerste geproduceerde ionenbundels. Simulatie software is gebruikt voor de optimalisatie van de extrahering van de ionenbundel, de massa separatie en het transport om zowel deze mijlpaal te behalen als de vereiste performantie van de faciliteit te garanderen. De massa separator van MEDICIS, afkomstig van de LISOL [1] faciliteit, is gekarakteriseerd en geoptimaliseerd voor deze toepassing. Dit betreft het installeren van het venster voor de laser, opmeten van het magnetische veld, bepalen van het resolverende vermogen van de magneet, etc.

In het kader van de verbetering van de ISOLDE FEBIAD (VADIS) ionenbron is de rol van de operationele parameters op de ionizatie efficientë bestudeerd. De temperatuur van de cathode, het voltage van de anode, het magnetisch veld van de ionenbron en de gasdruk zijn in rekening gebracht, wat geleid heeft tot een voorstel voor een optimale werking van de ionenbron. De ionizatie efficiëntiës van Mg, Mn, Ga, Sn en Hg zijn opgemeten, welke allemaal tussen 1-21% vallen.

Particle-in-cell software is gebruikt voor de visualisatie van de distributie van het elektrostatisch veld in VADIS en VADLIS, en ook voor het bepalen van de baan van de ionen. Hierbij is de VADLIS, recent ontwikkeld in ISOLDE voor element-selectieve laser ionizatie in de FEBIAD, aangepast voor verhoogde extrahering van laser geïoniseerde deeltjes. Deze aanpassing laat het herstellen van de extraherende mogelijkheden van de VADLIS toe wanneer deze wordt gebruikt in de zogenaamde RILIS-modus.

Het aangepaste prototype van VADLIS, wat hier besproken wordt, is gebruikt geweest voor de productie van laser geïoniseerd ^{24}Mg, ^{71}Ga, ^{98}Mo and ^{196}Hg, zowel on-line als off-line. Een verbetering van de efficiëntië met meer dan een factor twee is behaald voor alle gevallen, hoewel exclusief voor laser geïoniseerde deeltjes in de FEBIAD anode een verhoging van de efficiëntië van een factor zeven opgemeten is.

List of Abbreviations

ISOL - Isotope Separator On-Line
ISOLDE - Isotope Separator On-Line DEvice
FEBIAD - Forced Electron Beam-Induced Arc Discharge
GPS - General Purpose Separator
HRS - High Resolution Separator
LISOL - Leuven Isotope Separator On-Line
MEDICIS - MEDical Isotopes Collected from ISOLDE
MRP - Mass Resolving Power
RCS - Rail Conveyor System
RILIS - Resonance Ionization Laser Ion Source
SIS - Surface Ion Source
VADIS - Versatile Arc Discharge Ion Source
VADLIS - Versatile Arc Discharge and Laser Ion Source

Contents

Acknowledgements i

Abstract v

Beknopte samenvatting vii

List of Abbreviations ix

Contents xi

List of Figures xv

List of Tables xxiii

1 Introduction 1

1.1 Motivation and relevance 1

1.2 The ISOL technique 3

1.3 Computational tools for optimizing the ISOL process 4

1.3.1 SIMION: A simulation tool for ion tracking 4

1.3.2 VSim: A simulation tool for ion source optimization and characterization 4

1.3.3 OPERA-3d/TOSCA: A simulation tool for magnetic field characterization 5

1.4 The ISOLDE facility 5
1.4.1 The ISOLDE off-line separator 6

2 CERN-MEDICIS: A new facility for the production of medical radioisotopes 7

2.1 The CERN-MEDICIS facility in the context of ISOLDE 8
2.2 MEDICIS operating cycle 9
2.3 Infrastructure 12
2.3.1 Irradiation point 12
2.3.2 Ventilation system 12
2.3.3 Vacuum system 13
2.3.4 Target storage 13
2.4 Beamline elements and ion beam optics simulations 14
2.4.1 Target unit and materials 14
2.4.2 The ion source 15
2.4.3 Front-end 16
2.4.4 Mass separator 17
2.4.4.1 Focal plane distance and orientation 19
2.4.4.2 Characterization of the magnetic field with the OPERA software 21
2.4.4.3 Mass resolving power 23
2.4.5 Beam emittance 25
2.4.6 Collection box 26
2.5 First stable beams produced at MEDICIS 28
2.6 First radioactive beams produced at MEDICIS 31

3 Ion sources for the production of radioactive beams at ISOL facilities 33

3.1 Ion sources used at ISOLDE: principle of operation 34

3.1.1 Surface ion source 34
3.1.2 Hot-cavity RILIS (Resonance Ionization Laser Ion Source) 37
3.1.3 Forced-Electron Beam Induced Arc-Discharge Ion Source (FEBIAD) and the VADIS series 39
3.1.4 Negative ion source 43
3.1.5 Versatile Arc Discharge and Laser Ion Source (VADLIS) 45
3.2 Other ion source technologies in use or under development at ISOLDE 47

4 Insights into the Versatile Arc Discharge Ion Source (VADIS) 49

4.1 Experimental studies 50
4.1.1 Dependence on the cathode temperature 53
4.1.2 Dependence on the anode voltage 55
4.1.3 Dependence on the ion source magnet 58
4.1.4 Dependence on the ion load capacity 59
4.1.5 Ionization efficiency measurements 64
4.2 VSim: A Particle-in-Cell software for the study of the VADIS ion source 66
4.2.1 Influence of the magnetic field on the charge density distribution 67
4.2.2 Influence of the ion population on the electrostatic field distribution 70

5 The Versatile Arc Discharge and Laser Ion Source (VADLIS) 75

5.1 **Paper:** Enhancing the extraction of laser-ionized beams from an arc discharge ion source volume 76
5.2 Performance of the modified VADLIS on-line at ISOLDE . . . 85
5.2.1 Magnesium 86
5.2.2 Molybdenum 87
5.2.3 Mercury 88

5.3 Electrostatic field distribution in the VADLIS: other considerations 90
5.4 Influence of the extraction voltage on the mass resolving power 92
5.5 Effect of neutral atom density and ion load 93

6 Conclusions **100**

6.1 Contribution of this work 100
6.2 Future directions 102

Bibliography **105**

List of Figures

2.1 CERN accelerator complex. 8

2.2 CERN-MEDICIS laboratory next to the ISOLDE facility and target area. 9

2.3 a) Storage room for new and used ISOLDE/MEDICIS targets. The targets are handled by a KUKA® robotic arm, also used at ISOLDE. b) KUKA robotic arm placing/retrieving a target from the rail conveyor system (RCS) or MONTRAC®. 11

2.4 The MEDICIS target is positioned behind the ISOLDE target for irradiation in the ISOLDE target area. 12

2.5 a) MEDICIS target with thermal shielding made out of Sigratherm replacing the standard 5 layers of metal shields used for ISOLDE targets. b) ANSYS simulations to visualize heat homogeneity and distribution when applying 900 A to the container electrodes in the new MEDICIS target design. (Images courtesy of J.P. Ramos, M. Ballan and S. Marzari). 14

2.6 Proton fluence (p/cm^2) in the ISOLDE-MEDICIS target region [6] simulated using the FLUKA software. (Image courtesy of R.S. Augusto). 15

2.7 MEDICIS front-end after modifications to reduce the pumping volume in the target sector and fulfil requirements concerning the available space in the MEDICIS bunker. 17

2.8 Geometry of the MEDICIS beamline simulated with SIMION. Figure a) shows the geometry and electromagnetic elements included in the simulations. Figure b) shows the potential energy surface, the vertical axis representing the electrostatic potential. 18

2.9 Mass separator donated by KU LEUVEN to the MEDICIS experiment. a) Exit of the dipole magnet at the LISOL bunker. b) Dipole magnet installed at the MEDICIS bunker. A window was installed to allow lasers to be sent towards the ion source for resonance ionization. 18

2.10 SIMION simulations to determine the focal distance and angle of the focal plane. 21

2.11 Magnetic field homogeneity of the magnet using the OPERA software for I=70.3 A. 22

2.12 Comparison between OPERA models without (model #1) and with (model #2) the window for the lasers 22

2.13 Relative integrated field error [10^{-4}] for I=70.3 which corresponds to A=300 amu at 30 keV. Left-model #1 (no hole), right-model #2 (hole) 23

2.14 MRP as a function of einzel lens voltage. a) Geometry 1. b) Geometry 2. 24

2.15 Emittance at magnet entrance. The quoted emittance values correspond to the area of the ellipse containing 95 % of the simulated events. a) Emittance geometry 1. b) Emittance geometry 2. 25

2.16 Horizontal beam profile for masses 99, 100 and 101 at the focal plane. 26

2.17 Simulation of the beam spot size at the focal plane for masses 99, 100, 101. a) Simulated with SIMION. b) Simulated with OPERA. 27

2.18 Sample holder positioning. Three different sample positions are shown (blue, green and yellow). A vacuum valve separates the sample container from the collection box. Once the container is attached to the collection box, the valve is opened, the samples moved into the collection box and the vacuum valve is closed. a) Fresh samples to be placed at irradiation position. b) Samples are in position to be irradiated. 27

2.19 Option for the MEDICIS switchyard system to be installed for a future upgrade of the facility. This system is inspired from the one used at the LISOL experiment in Louvain-la-Neuve, allowing the collection of 3 different masses simultaneously. 28

2.20 Calibration curve of the MEDICIS dipole magnet. The quadratic expression shown in the figure was fitted through the data points (red curve). 29

2.21 First mass separated beams at the CERN-MEDICIS facility. The horizontal axis shows the acquisition time while varying the magnetic field strength (by varying the current in the magnet coils) and the vertical axis the amplitude. The blue curve represents the acquisition at each given time while the red curve averages the last 5 data points taken. 30

2.22 Xe beam profile. The heatmap shown in the left panel (data represented by colours, with red and blue being the maximum and minimum values of the beam intensity respectively) shows the relative intensities for A=129 to A=132. Figures in the right side show the scanner images for the horizontal axis (top panel) and vertical axis (lower panel) 30

2.23 Gamma spectrum of the second radioactive sample collected at MEDICIS. The collection time was 30 minutes. The target (tantalum rolls) and ion source (tungsten surface ionizer) temperature were 1950 and 2150 °C respectively. 32

3.1 The ISOLDE hot cavity surface ion source (SIS). The products of the nuclear reactions from the primary proton beam with the target material reach the surface ionizer via a transfer line. . . 35

3.2 Elements for which the hot-cavity SIS has been applied for ion beam production at ISOLDE [40]. The different color shades are associated to the ionization potential of the element. 36

3.3 Principle of resonance photo-ionization. 37

3.4 The hot-cavity surface ion source used as laser-atom interaction region for RILIS applications. 38

3.5 Elements for which RILIS has been applied at ISOLDE according to [41]. The ionization schemes are accessible through an online resource known as 'The RILIS Elements Database' [42]. 38

3.6 Geometry of the ISOLDE FEBIAD ion source (VADIS). The electrons released by the hot cathode are accelerated towards the anode volume where the atoms (which reach the anode through the hollow cathode, connected to the target using a transfer line) are ionized mainly by electron impact ionization. The structure shown on top going through the cathode support, serves to connect the anode to its power supply. 40

3.7 Elements produced at ISOLDE using the FEBIAD or VADIS ion source indistinctly from the ion source subtype [40]. 42

3.8 Negative ion source used at ISOLDE. A magnet and an electron catcher ensure the emitted electrons are not accelerated downstream of the ion source. A low ϕ pellet is placed near the exit to enhance the interaction probability with an atom. . . . 43

3.9 Elements for which the negative ion source as been applied at ISOLDE for the production of negative ion beams [40]. 44

3.10 (a) RILIS lasers directed onto the anode volume. Boron nitride insulators are used to independently bias the voltage of the extraction plates for improved laser-ion extraction. (b) Anode voltage scan to identify the different modes of operation of the VADLIS. For more details see Section 5.1. 46

4.1 Sketch of the ISOLDE off-line laboratory. 51

4.2 Efficiency of the noble gases as a function of the cathode temperature. The anode voltage was kept at 125 V. The red curves (values on the right-hand side axis of the figure) correspond to the drain current, both experimental and theoretical (the latter calculated according to the Richardson-Dushman equation for thermionic emission) and total ion current. 54

4.3 f-factor calculated using equation 3.5, for the efficiencies shown in Fig. 4.2. 55

4.4 Mass separated ion current as a function of the anode voltage (ion source magnet ON). (a) For gallium. Two curves were taken: first with voltage increasing from 0 to 200 V; second one with voltage decreasing from 200 to 0 V. (b) For krypton. 56

4.5 Experimental measurement of the cathode current as a function of the anode voltage for different cathode temperatures. 57

4.6 Scan of the anode voltage with ion source magnet ON and OFF at 2000 °C. Both curves were taken under identical experimental conditions. 59

4.7 Normalized extracted ion current for the noble gases as a function of the extracted CO^+ ion beam. 61

4.8 Extracted CO^+ ion beam and total current as a function of the CO gas load in the VADIS. The anode voltage is set to 100 V. The set point labelled on the x-axis indicate the position of the leak valve, where 1 is 'closed' and 1000 means 'fully open' . . . 62

4.9 Extracted ion beam for different elements at the start of the measurement (blue bars-Mn oven cold) and at maximum Mn ion extraction (orange bar-oven hot). A decrease in efficiency for the main elements contributing to the total beam is observed under the presence of high Mn beam current. A manganese beam of about 160 nA is present at the beginning of the measurement (oven cold) due to indirect heating. 63

4.10 Determination of the efficiency of mercury off-line. The extracted current is shown as a function of the necessary time it took to evaporate the sample (x-axis). The 'oscillations' observed correspond to the heating of the mass marker to promote the release of Hg atoms. The measured current is integrated to determine the ion source efficiency. 64

4.11 Experimentally measured efficiency of metals at the ISOLDE off-line laboratory as a function of the cathode temperature. The efficiency for the noble gases at 2125 °C are also shown, taken from 4.2. 66

4.12 Field map, electron and ion density distributions with (left-hand side) and without (right-hand side) the presence of the ion source magnetic field. The results are also shown for two different electron currents: 40 mA (panel **a**, **b**, **c**) and 100 mA (panel **d**, **e**, **f**). 69

4.13 Number of electrons and ions in the ion source volume. The ion number is 'boosted' during the iterative process to gain an insight on how the electron number and electrostatic field distribution evolve. 72

4.14 Evolution of the electrostatic field, electron and ion distribution as the ratio of ions and electrons in the ion source varies (see stages shown in Fig. 4.13). The first column shows the potential along the axis of ion source. 73

5.1 Building of the modified VADLIS with extraction plates for first off-line tests. a) Anode body mounted on BN insulator with thread. b) Connections to anode body and extraction plates. . 85

5.2 Ionization schemes used for the study of laser-ionized beams of magnesium [42], molybdenum [78] and mercury [42]. 86

5.3 ^{24}Mg ion current as a function of the voltage applied to the extraction plates for 1, 5 and 250 V anode settings. 87

5.4 ^{24}Mg ion current before and after blocking the Blaze laser to observe heating effect. 88

5.5 Scan of the voltages V_a and V_e to optimize the extraction of ^{98}Mo. 89

5.6 Simulated number of electrons as a function of time in the anode cavity (top panel) and electron current (drain current) emitted by the cathode as a function of time (lower panel). 91

5.7 Temporal evolution of the location of the ions in a 100 μs window (time between two laser pulses at 10 kHz repetition rate, 5 to 30 ns laser pulse duration). The particles are color-tagged according to their initial position from left (blue) to right (red), as shown in the top-left figure (0 μs). See text for a description of the four stages depicted in the figure. 92

5.8 Beam profile measured at the scanner position (focal plane downstream of the dipole magnet) when the extraction plates are set to 0 and -200 V. 93

5.9 $^{71}Ga^{+}$ signal enhancement as CO_2 is injected into the source in RILIS-mode (again, we measure the CO content in the RGA). The 'dips' going to zero correspond to the insertion of the Faraday cup in the way of the beam for total current measurements. The large 'dips' correspond to periods where the laser beams were blocked or the wavelength was being readjusted. 95

5.10 Amount of CO in the ion source as a function of time measured by the residual gas analyzer, placed at the exit of the ion source. (The y-axis shows relative values since a calibration of the RGA is not available.) 96

5.11 Anode voltage scan for different pressures of CO within the anode volume. 98

5.12 ^{71}Ga ion current in RILIS-mode dependence on the ion load capacity. The cathode temperature is 2035 °C. 99

List of Tables

4.1 Experimental efficiencies measured at the ISOLDE off-line laboratory. Unit # refers to the target/ion source assembly used. T is the cathode temperature, A the mass of the element, W_i the ionization potential, V_a the anode voltage, I_a the electron (drain) current, ϵ the ion source efficiency and f the f-factor as defined in equation 3.5. The transmission through the mass separator was 76 %. 65

5.1 ^{196}Hg ion current enhancement when V_e is optimized for maximum ion extraction in the RILIS region. (This dataset is different from the one used to get the results shown in Table 2, Section 5.1). 90

Chapter 1

Introduction

This introductory chapter states the motivations for this research work, and places it in the context of radioactive beam production for fundamental research and for applications in medicine. The isotope separator on-line technique (ISOL) is described, which is used worldwide for the production of a wide range of radioactive beams. The main computational tools used to optimize the ISOL process are introduced, as are the instrumentation and experimental facilities relevant to this work.

1.1 Motivation and relevance

Before the advent of nuclear reactors (<1942), our access to the isotopes of the chart of nuclides was limited to those naturally occurring on earth (stable, and long lived species) ∼500 isotopes. Nuclear fission reactors expanded our range of isotopes to those which could be extracted from the reactor material and processed (treated/purified chemically after extraction) to ∼800 isotopes, with half-lives down to several hours/days. The purpose of the Isotope Separator On-Line (ISOL) approach is to overcome this radioisotope lifetime limit by coupling the production, extraction, purification and transport of the desired radioisotope in a single machine. This was first achieved at the Niels-Bohr Institute in 1951. Thanks to facilities such as ISOLDE (Isotope Separator On Line DEvice) [2] at CERN in Geneva, Switzerland, the number of discovered isotopes has grown considerably (∼3000), with half-lives as short as several milliseconds, and can be often provided to experimentalists in the form of pure, high quality ion beams.

While such facilities were developed primarily for fundamental research projects in nuclear astrophysics, nuclear structure and reaction physics, their use has been expanded to many other fields of applied science such as solid state, biophysics, life sciences, material physics, etc.

This thesis places particular emphasis on the application of ISOL technology for the production of novel radioisotopes for medical applications. According to the World Health Organization, cancer is the second largest cause of death globally. The disease was responsible in 2018 for an estimated 9.6 million deaths. The field of nuclear medicine offers many opportunities to study and refine our understanding of cancer biology. Radiopharmaceuticals, drugs that can be used either for the diagnosis or treatment of cancer, are composed of radioisotopes that bind to organic molecules. The radioisotope is chosen for its therapeutic or imaging capabilities while the molecule conveys it to specific cells, tissues or organs. For example, the $^{223}RaCl_2$ (Xofigo®) is used as a pain relief and treatment drug in advanced bone cancer. ^{18}F-FDG, a radioactive sugar equivalent, is by far the most widely used diagnostic tracer for Positron Emission Tomography (PET) imaging.

Radioisotopes that are currently commercially available for nuclear medicine are not always optimal in terms of their effectiveness in the treatment or diagnostics of cancer. Innovative isotopes with better nuclear-decay properties for use in medicine have emerged, and efforts to scale up their production are ongoing.

The ISOLDE facility provides a large catalogue of radioisotopes for a variety of physics experiments. The production of radionuclides for medical applications is dictated by the facility's scientific programme, heavily dominated by fundamental research in nuclear physics. This leaves only about one quarter of the total beamtime to be split between atomic and solid-state physics, biology, beam development and the production of medical isotopes, which translates to approximately two weeks of collections for medical research per year. In spite of this, the diversity and high quality of the mass-separated (therefore high specific activity radiopharmaceuticals) beams at ISOLDE provide novel and interesting isotopes for the nuclear-medicine community.

For example, ^{149}Tb (collected from ISOLDE) emits both α and β particles. This property of the radioisotope enables targeted therapeutic use and PET imaging to be combined [3]. ^{152}Tb and ^{155}Tb (also produced at ISOLDE) have proven to be suitable candidates for PET and SPECT imaging [4, 5].

In order to help to overcome the production shortage of medical isotopes for research, a new facility named MEDICIS (MEDical Isotopes Collected from ISOLDE) [6] has been built next to the ISOLDE laboratory. It broke ground in September 2013 and extracted its first radioactive beams in 2017. MEDICIS

constitutes a dedicated facility for the production of novel, medically interesting and relevant radionuclides throughout the year, with minimum interference with ISOLDE operations. Beyond MEDICIS, a network has been established with European partners called MEDICIS-PROMED, with the aim of bridging different disciplines across hospitals, private companies and research institutes.

The ISOLDE and MEDICIS facilities are complex experiments with many parts that have to work in synchrony to produce the radioisotopes of interest. In this thesis, we dedicate a chapter to the MEDICIS facility, providing details on its infrastructure and operation. An overview chapter describing the principle of operation of the ion sources most commonly used at ISOL facilities is included, before dedicating two chapters to the research performed here for a better understanding and further optimization of these devices for use at ISOLDE and MEDICIS. The radioactive quantities produced should be large enough to allow research in small animals and pilot studies in human patients. To this end, it is important to optimize the different stages of the production process for radioisotopes: choosing the right target material, optimizing the extraction and transport efficiency to the collection point, and matching the expected beam purity while striving for high production yields.

1.2 The ISOL technique

The isotope separator on-line (ISOL) method aims for the production of radioactive beams with good ion optical quality, purity, wide energy range and abundance. The radioisotope production process must then be selective, fast (in case one wants to produce beams from short-lived isotopes), efficient and have a high production rate.

The ISOL technique is described in detail in [7]. To produce a radioactive ion beam, a primary beam impinges on a target material, where a nuclear reaction takes place. The products of the nuclear reaction recoil and/or diffuse out of the target material and effuse towards the ion source via a transfer line or through a gas medium. The transfer line is in general kept at high temperature to avoid condensation of the elements on its surface, but may also be actively cooled to selectively favour gaseous species. Once in the ion source, the atoms are ionized via different ionization mechanisms. The type of ion source is chosen depending on the required beam characteristics (e.g. purity, yield, ion charge). The ions are extracted and accelerated towards an analyzing magnet, which separates the ions according to their mass-to-charge ratio. Given that most beams consist of singly-charged ions, those devices are often referred to as mass separators. The

formed beam is transported using optical elements to the different experimental setups, where the detection/collection systems are located.

Other elements can be placed in the beamline in order to change or modify the characteristics of the ion beam. Radio frequency coolers and Penning traps can be used to reduce the axial and radial energy spread of the ion beam and bunch them if necessary [8, 9, 10]. Charge-state breeders can be used to produce multiple-charge state ion beams. This can be achieved by using an Electron Beam Ion Source (EBIS) or the Electron Cyclotron Resonance (ECR) ion source [11]. The multiple-charge or single-charge ion beam is then injected into the accelerator; a process known as post-acceleration.

1.3 Computational tools for optimizing the ISOL process

1.3.1 SIMION: A simulation tool for ion tracking

The SIMION software package [12] is used in the present work to perform simulations of ion beam optics for the MEDICIS front-end and beamline. SIMION uses finite difference methods to solve the Laplace equation. It calculates the electromagnetic fields and particle trajectories under such fields given the initial conditions are provided by the user.

SIMION has been used to determine the optimal configuration of electromagnetic elements in the beamline, given space constraints within the MEDICIS laboratory, while keeping the desired beam characteristics. The beam profiles, emittance and settings for the optical elements calculated with SIMION were validated with experimental results.

1.3.2 VSim: A simulation tool for ion source optimization and characterization

This thesis presents experimental and theoretical studies to better understand and optimize the VADIS (Versatile Arc Discharge Ion Source) and VADLIS (Versatile Arc Discharge and Laser Ion Source). The VSim software package [13, 14] from Tech-X Corporation [15] allows the modelling of electron and ion distributions, as well as the electric and magnetic field distribution within the ion source volume. VSim is also used to visualize the trajectories of the

laser-ionized gallium ions from their creation point within the source to their extraction.

The particle-in-cell approach VSim follows is favoured over fluid-based models due to its ability to model non-local-thermal-equilibrium distributions for electrons and ions, such as they are generated in the plasma volume. In this approach, fields are initialized taking into account magnetic fields, the potentials on the electrodes and the charge density in order to solve Poisson's equation, using a high performance scalable linear solver. New fields are computed, and electric and magnetic fields are interpolated to the location of so-called macroparticles (a macroparticle represents a large group of physical particles). The Boris algorithm [16] is used to make the particles move under these fields, and a new charge density distribution, and therefore new fields, are found to be used at the next time-step. Care has been taken to resolve the Courant condition and Debye heating in the plasma simulations.

1.3.3 OPERA-3d/TOSCA: A simulation tool for magnetic field characterization

OPERA-3d/TOSCA [17] - a software suite for electromagnetic, thermal and structural simulations - was used to obtain electromagnetic field maps of the CERN-MEDICIS dipole magnet. It uses a static module to compute magnetostatic and electrostatic fields or DC current flow in three dimensions. It solves Maxwell's equations using the Finite Element method. Within the static module, the properties of magnetic material can be specified and coils/solenoids can be simulated with the Biot-Savart integral to calculate magnetic fields from coils. The program calculates the potential at each node of the mesh with a sophisticated, iterative-solution technique, offering high computer speed and great memory efficiency.

Particle tracking was performed using OPERA, and the results compared to those from SIMION. The magnet was modified in order to install a window for the lasers. OPERA was used to assess the field homogeneity of the modified magnet and determine the homogeneous field region.

1.4 The ISOLDE facility

At CERN, proton beams are delivered to any of the two ISOLDE target stations with an energy of 1.4 GeV and with an average proton current intensity up to 2 μA. Reaction processes such as spallation, fragmentation and fission take

place within the target material and the products ionized using, for example, the hot cavity, laser or plasma ion sources (see Chapter 3 for an overview of the ion sources used at ISOLDE). The target/ion source assembly can be coupled to two different mass separators: the high resolution separator (HRS) or the general purpose separator (GPS). The ions are then extracted and accelerated towards different experimental setups located within the ISOLDE experimental hall. For the on-line measurements performed at ISOLDE and discussed in Chapter 5, the ISOLDE tape station [18] was used for the detection of the radioactive isotopes extracted from the ion source/target assembly.

A detailed description of the ISOLDE facility and latest achievements can be found in [2].

1.4.1 The ISOLDE off-line separator

The experimental work for this thesis was mostly carried out at the ISOLDE off-line laboratory. This laboratory is also used for the preparation and characterization of the ISOLDE targets before they are taken to ISOLDE for on-line experiments. New prototypes are characterized in this experimental facility, such as the modified VADLIS ion source described in Chapter 5.

The off-line separator consists of a target/ion source unit, an extraction electrode, electrostatic deflectors for both axis, an einzel lens and Faraday cups for the measurement of the total and mass separated beam currents. The mass separator consists of a 60° bending dipole magnet. At the end of the beamline a diagnostics box is located, containing a horizontal wire scanner, horizontal slits and a Faraday cup. The extracted beams are accelerated towards the dipole magnet at typically 30 keV and sent to the collection box. More details on the off-line laboratory are given in [19] and in Section 4.1.

Chapter 2

CERN-MEDICIS: A new facility for the production of medical radioisotopes

The CERN-MEDICIS (MEDical Isotopes Collected from ISOLDE) facility aims to produce innovative radioisotopes for applications in the field of nuclear medicine [6]. It had its ground-breaking ceremony in September 2013 and collected the first radioactive isotope batch in December 2017. MEDICIS operates hand-in-hand with the ISOLDE facility and makes use of the knowledge and expertise gained at ISOLDE during more than 50 years of operation. The ISOLDE facility underwent a major upgrade during the CERN Long Shutdown 1 (LS1) period (February 2013-July 2014), offering a time window to add/upgrade HIE-ISOLDE [20] infrastructure and build an extension of building 179, which hosts the CERN-MEDICIS class A laboratory for the production of medical radioisotopes. The new building also hosts a new area for target storage, for both MEDICIS and ISOLDE.

This chapter gives an overview of the MEDICIS laboratory infrastructure that allowed integration to the ISOLDE facility. The results of the simulations using software like SIMION and OPERA are discussed, which were essential for the design of the MEDICIS beamline. First results on the production of stable and radioactive beams are reported at the end of the chapter.

2.1 The CERN-MEDICIS facility in the context of ISOLDE

The MEDICIS laboratory is located in the Meyrin site of CERN, next to the ISOLDE facility. It has a dedicated irradiation target station located between the ISOLDE HRS target and its beam dump. ISOLDE and MEDICIS receive protons on their targets from the PS Booster which forms part of the CERN accelerator network as shown in Fig. 2.1.

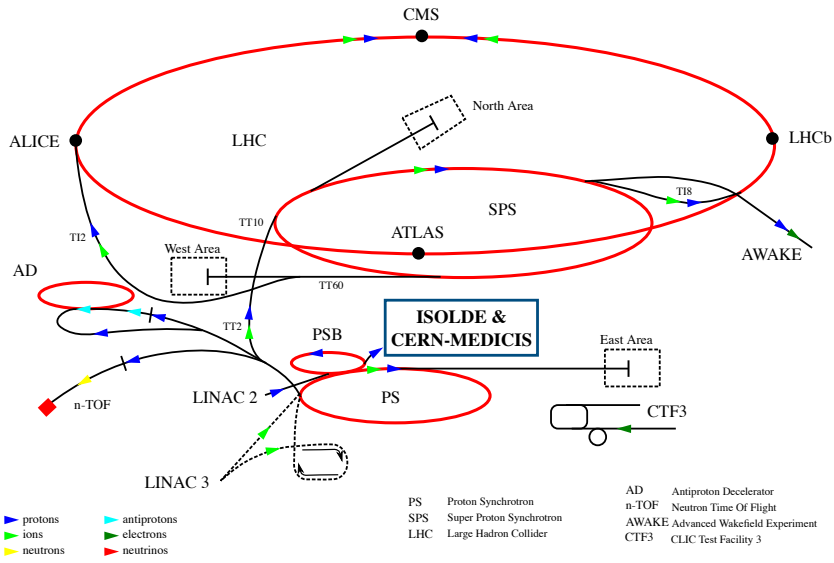

Figure 2.1: CERN accelerator complex.

Although the current energy specifications of ISOLDE are a 1.4 GeV proton beam impinging on the HRS target, the MEDICIS facility has been conceived considering an energy increase to 2 GeV primary beam energy, where up to $6{\cdot}10^{20}$ protons per year are expected. Both laboratories are connected through a corridor as shown in Fig. 2.2.

MEDICIS and ISOLDE's operation schedules may seem strongly linked at first sight, but the specificities allow for decoupled operation. Even when ISOLDE stops operations (physics with the GPS front end, Year End Shut-Down or Long Shut-Down), MEDICIS can continue its normal activities provided the availability of CERN's infrastructure resources like water, electricity, etc. This is because besides operating with freshly irradiated targets, MEDICIS can

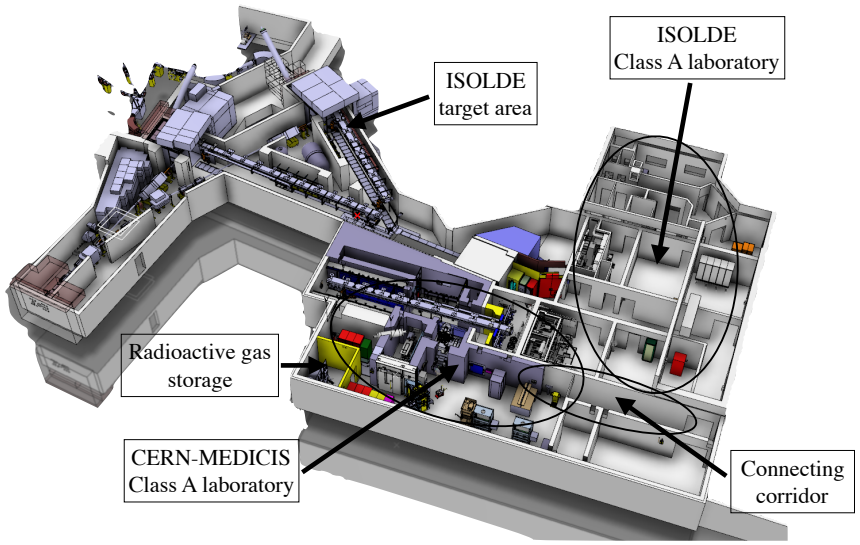

Figure 2.2: CERN-MEDICIS laboratory next to the ISOLDE facility and target area.

re-use previously irradiated ones from ISOLDE. ISOLDE operates around 30 targets per year and once the physics programme is finished, they can be used for the extraction of medical isotopes at MEDICIS if desired. MEDICIS can also operate with imported target ion source systems, in which external, activated material is inserted inside a standard target unit for isotope separation.

During the time the MEDICIS targets are being manipulated by the target handling robots, protons are prevented from irradiating the HRS and GPS targets. Details on the MEDICIS guidelines for target irradiation and operations are given in [21, 22].

2.2 MEDICIS operating cycle

When the proton beam impinges the HRS target, more than 85 % of the beam traverses it without interacting and may reach the MEDICIS target located 400 mm further downstream. Radioactive isotopes are produced this way, benefiting from the otherwise lost proton beam.

After irradiation, the MEDICIS target is brought back to the MEDICIS building by a rail conveyor system (RCS). The target is then retrieved by a

robotic arm which couples the target to the MEDICIS off-line front-end. The target container is heated to promote diffusion of the nuclear recoils out of the target material and enhance the diffusion towards the ion source, through a hot transfer line, that can be also cooled to condense non-volatile elements and extract gaseous species. The elements reaching the ion source are then ionized, as discussed later in Section 2.4.2.

An accelerating voltage of 30-60 kV is applied and the extracted ion beams are accelerated towards a dipole magnet for mass-over-charge separation. Isotopes are collected after separation onto different possible substrates (e.g. metallic foils, salt samples) at the end of the beam line. The collected samples are finally retrieved from the collection box and transferred to a fume hood or glovebox using a trolley, where they can be processed in preparation for shipping to partner institutions specializing in radiochemistry, radiolabelling, and nuclear medicine research.

The following list describes (though not in an exhaustive way) the main aspects of the MEDICIS operation cycle from target irradiation to isotope extraction.

1. Target delivery: The operation starts with the delivery of a fresh target to the MEDICIS radioactive area through the supply point. It is handled by the KUKA® robotic arm (Fig. 2.3), which places the target in the Rail Conveyor System (RCS), also known as MONTRAC®. This supply point can also be used to deliver targets for operation at the GPS and HRS front-ends of ISOLDE.

2. Transport to target area: The target is transported in ∼12 minutes to the ISOLDE target area and placed between the HRS target and its beam dump by the RCS where the irradiation starts. Inspections of the ISOLDE target area can be done using a RCS module equipped with a camera, as well as monitoring radiation levels with portable radiation detectors. A rescue shuttle, also equipped with a camera can be used to retrieve the RCS shuttle in case of failure.

3. Irradiation: The incoming 1.4 GeV proton beam traverses the ISOLDE HRS target. About 85 % of the beam continues without interaction towards the MEDICIS target and the irradiation process begins. The irradiation time lasts until saturation for the isotope of interest is reached (depending on half-life and operation schedule).

4. Transport to the MEDICIS laboratory and decay point after irradiation: The irradiated target is transferred back to the MEDICIS laboratory by the RCS and placed in the decay point. Radiation monitors keep track of

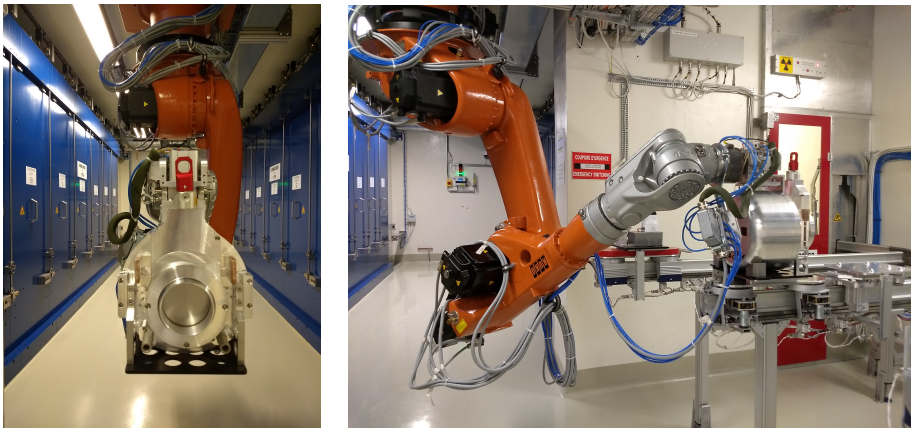

(a) (b)

Figure 2.3: a) Storage room for new and used ISOLDE/MEDICIS targets. The targets are handled by a KUKA® robotic arm, also used at ISOLDE. b) KUKA robotic arm placing/retrieving a target from the rail conveyor system (RCS) or MONTRAC®.

the radiation levels. The time the target spends at the decay point varies depending on irradiation time, target material used, primary proton beam intensity and isotope to be extracted amongst others. The target can safely be removed from the decay point once the dose rate falls below 1 Sv/h (measured at 26 cm distance)

5. Mass separation: The target is placed by the KUKA® robotic arm in the MEDICIS front-end (located in the MEDICIS bunker) where mass separation takes place. The products of the nuclear reaction diffuse out of the target material after the target has been heated and effuse to the ion source where ionization takes place. The beam is accelerated at 30-60 keV towards the mass separator, consisting of a 55° bending angle dipole magnet. The beams are deflected according to their A/Q ratio (where Q is the charge state) and the beam of interest is implanted in a metallic foil in the collection box.

6. Chemical separation: The MEDICIS chemical laboratory (still under preparation as of February 2019) will receive in its fume hoods the collected samples for further chemical purification when deemed necessary. The fume hoods are shielded spaces made out of corrosion-resistant material to operate strong acids. For higher activities, glove boxes or hot cells will be used. They will be installed at a later stage of the commissioning

phase of the chemical laboratory, once experience with lower activities has been gained.

7. Delivery of samples: The final product is delivered to partners of the CERN-MEDICIS collaboration in sealed transport containers.

2.3 Infrastructure

2.3.1 Irradiation point

To make this irradiation process possible, the new MEDICIS target had to be accommodated in the HRS Faraday cage. The HRS target is kept at high-voltage (on-line extraction of isotopes after proton impact) while the MEDICIS one is grounded (isotopes are extracted off-line at a further stage in the MEDICIS laboratory). The MEDICIS target is surrounded by a shielding box which creates a sub-environment within the Faraday cage. The positioning of the MEDICIS target behind the ISOLDE one is shown in Fig. 2.4.

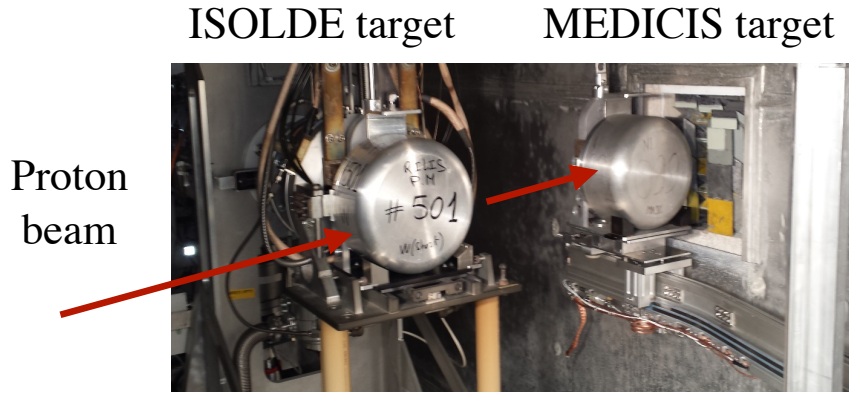

Figure 2.4: The MEDICIS target is positioned behind the ISOLDE target for irradiation in the ISOLDE target area.

2.3.2 Ventilation system

The ventilation system of ISOLDE's laboratories was upgraded to fulfil the requirements of the MEDICIS facility and ensure that the ISOLDE facility

complies with the latest Swiss regulation for Class-A laboratories. The ventilation system of ISOLDE's target area stays however independent from the rest. It follows the principle of pressure differentials to ensure the air flows from areas with lower to higher risk of radiation contamination. The hot-cell and glove boxes will have independent extraction systems. To ensure the activated air by the proton beam from the target area does not reach the MEDICIS laboratory, two Special Airlock Systems (SAS) were installed between the Class A laboratory and the target area. More details can be found in [23].

2.3.3 Vacuum system

The MEDICIS beamline is held under vacuum during isotope collection. Three vacuum sectors exists: one for the front-end, one for the separator and one for the collection chamber. The estimated volume of each sector is 11, 375 and 15 litres (each collection chamber) approximately. During operation, the pressure along the beamline must not exceed 10^{-6} mbar, except for the target where it must not be higher than 10^{-5} mbar.

As the pumped volume contains radioactive isotopes, the contaminated gas is stored in tanks located behind the MEDICIS bunker (see Fig. 2.2). The gas is held there so that the radioisotopes may decay and once the radioactivity level has reached a sufficient low level, the accumulated air may be released into the atmosphere. For more details on the MEDICIS vacuum system see [24].

2.3.4 Target storage

The MEDICIS building has a new storage area for targets for both MEDICIS and ISOLDE. It has an area of 50 m^2 and can host 104 targets. It consists of two shielded shelf assemblies on each side of the target handling KUKA robot corridor with 4 levels each (see Fig.2.3). More details on the target handling devices, transport and storage area can be found in [23].

2.4 Beamline elements and ion beam optics simulations

2.4.1 Target unit and materials

During the commissioning phase of the MEDICIS facility, standard ISOLDE targets were used, consisting on a tantalum tubular oven of 2 cm diameter and 20 cm length. In a future stage of the facility, a larger target container will be used to match the ISOLDE yields, accounting for beam losses after the the proton beam traverses the ISOLDE target. In this design, the resulting volume equals ∼200 cm^3 (compared to ∼60 cm^3 for the ISOLDE one). The 5 cm diameter is chosen so that most of the scattered proton beam is caught in the target volume. The novel material Sigratherm is proposed to replace the standard 5 layers of metal thermal shields (see Fig. 2.5a with shielded target).

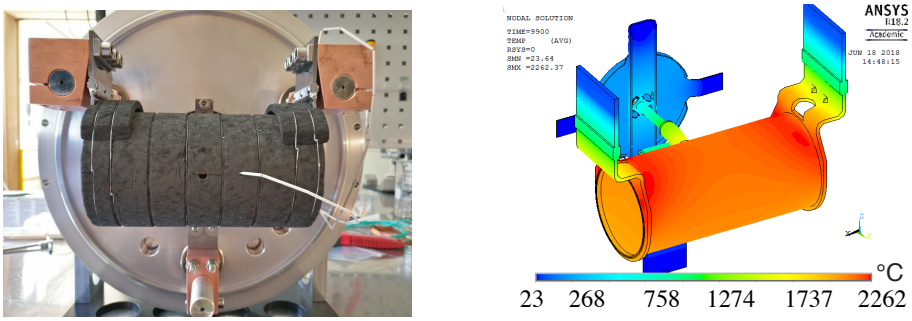

(a) (b)

Figure 2.5: a) MEDICIS target with thermal shielding made out of Sigratherm replacing the standard 5 layers of metal shields used for ISOLDE targets. b) ANSYS simulations to visualize heat homogeneity and distribution when applying 900 A to the container electrodes in the new MEDICIS target design. (Images courtesy of J.P. Ramos, M. Ballan and S. Marzari).

The thickness of the target container will be reduced from 0.5 mm to 0.3 mm so that the resistance increases, in order to obtain the standard target temperature of ∼2000 °C for the available current (max. 1200 A) delivered by the power supplies.

A temperature of ∼2140 °C has been reached inside the target container during the tests of the prototype by applying a current of 900 A to the container electrodes, dissipating 2.9 kW. These values were in agreement with simulations

performed using the ANSYS software [25] (see Fig. 2.5b). More details on the MEDICIS target design can be found in [26, 27].

The FLUKA software [28] was used to calculate the proton fluence on the ISOLDE-MEDICIS target region as shown in Fig. 2.6 [6, 29]. In this specific example, a target material consisting of four tantalum cylinders (2.5 cm length, 2.5 cm radius each) were considered. The optimal distance between the ISOLDE and MEDICIS targets was found to be 400 cm. In these conditions, ∼90 % of the initial proton beam intensity hitting the HRS target unit irradiated the MEDICIS target. The material of the HRS target considered was UCx with a density of ∼2.35 g/cm^3.

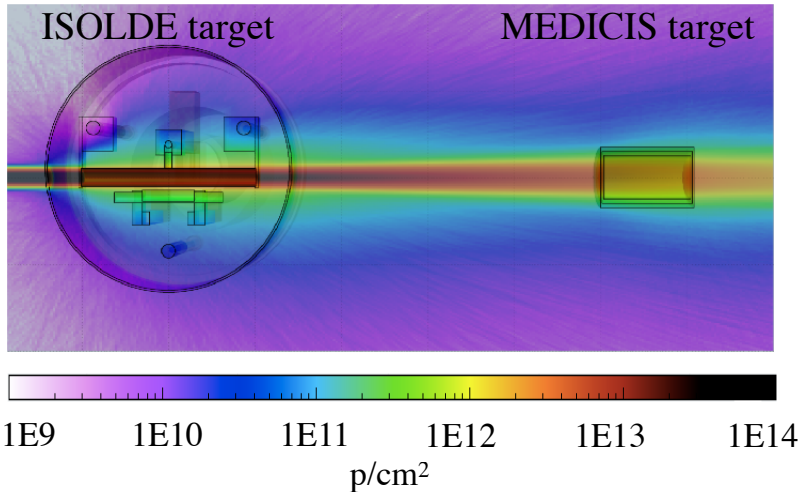

Figure 2.6: Proton fluence (p/cm^2) in the ISOLDE-MEDICIS target region [6] simulated using the FLUKA software. (Image courtesy of R.S. Augusto).

2.4.2 The ion source

The first beams, both stable and radioactive, were produced at the CERN-MEDICIS facility using a standard ISOLDE surface ionizer. It consists of a tubular cavity of 3 mm inner diameter and 34 mm length typically made of tantalum or tungsten. More details on the working principle of the hot cavity can be found in Section 3.1.1. This geometry served as an input for particle tracking, emittance and mass resolving power calculations using the SIMION software [12].

To simulate the ion beam extraction and transport, ions were distributed homogeneously inside the ion source following a Gaussian energy distribution with a mean energy of 0.25 eV (∼3000 K) and a 10 % energy spread. Ions drift towards the exit of the hot cavity due to a longitudinal voltage drop of ∼2 V (this voltage gradient was also taken into account for the simulations) and are extracted due to the field penetration created by the extraction electrode. The ions are then accelerated towards the dipole magnet where they will be separated according to their mass-over-charge ratio.

FEBIAD-type (VADIS) ion sources have been already operated at MEDICIS, following those used at ISOLDE. In the future, the MEDICIS facility will diversify its ion sources. A laser ion source, MELISSA (MEDICIS Laser Ion Source Setup), is currently under development [30]. Altogether, MEDICIS is seeking an ideal ion source that would allow for a versatile operation between surface, laser, and plasma ionization. This concept will be discussed later in chapters 4 and 5.

2.4.3 Front-end

The ISOLDE front-end 5 (FE5) was adapted for use at MEDICIS. The main components are the target coupling flange and a movable extraction electrode, usually operated at 30 kV, placed after an acceleration gap of 50-100 mm from the ion source exit. Due to the limited available space at the MEDICIS bunker, an einzel lens was used instead of an electrostatic quadrupole triplet like the ones used at ISOLDE to shape the ion beam downstream of the extraction electrode. The einzel lens makes it possible to have a parallel beam at the entrance of the mass separator (more details in Section 2.4.4.1). Between the extraction electrode and the einzel lenses, an X-Y electrostatic deflector is used to adjust for misalignments that may cause the transport of the beam with a wrong angle. This can be achieved by applying a voltage of up to ± 5 kV to the deflectors.

The initial position of the vacuum valve in the separator sector was changed to reduce the pumping volume and minimize the radioactive gas load going into the gas storage. Simulations using the SIMION software were done to ensure that such modifications would not be detrimental to the mass resolving power. Figure 2.7 shows a technical drawing of the MEDICIS front-end and mass separator after modifications.

Einzel lenses consisting of three separated cylindrical electrodes are used to guide the ions during flight. The central lens is kept at high (variable) potential to create the lens effect while the outer ones are kept at ground potential. The einzel lenses in this set-up are used to ensure a parallel beam at the entrance of

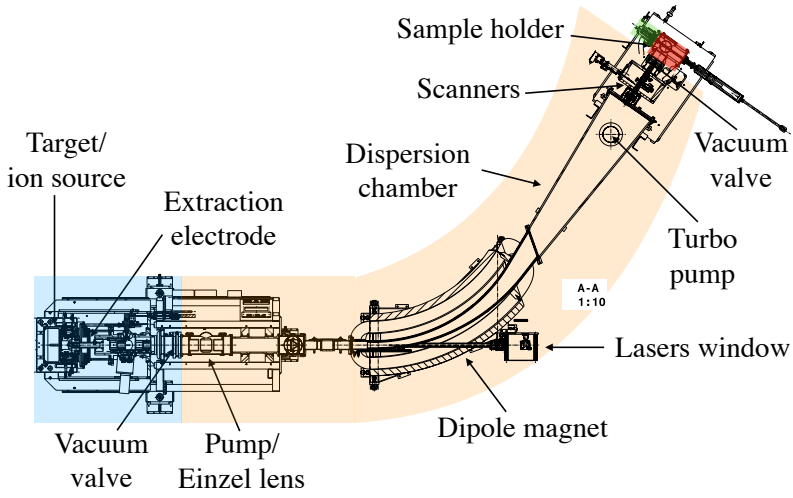

Figure 2.7: MEDICIS front-end after modifications to reduce the pumping volume in the target sector and fulfil requirements concerning the available space in the MEDICIS bunker.

the mass separator. This is a requirement for horizontal and vertical focusing at the focal plane for the kind of magnet employed (see Section 2.4.4.1 and Ref. [1]). The radius of the electrodes of the einzel lens are 45 mm and their length 77, 90 and 77 mm respectively. The gap between them is 20 mm. Those parameters were used as input for the geometry in the SIMION simulations (Fig. 2.8a). More details can be found in [31].

2.4.4 Mass separator

The mass separator dipole magnet used at CERN-MEDICIS was provided by the University of Leuven (KU Leuven) in Belgium. This magnet was used for 40 years at the LISOL experiment [1] in Louvain-la-Neuve at the Centre de Recherche du Cyclotron. Figure 2.9 shows the magnet before decommissioning at LISOL and the magnet once it was installed at the MEDICIS bunker during the commissioning phase of the facility.

The mass separator is a 55° double focusing magnet with a bending radius of

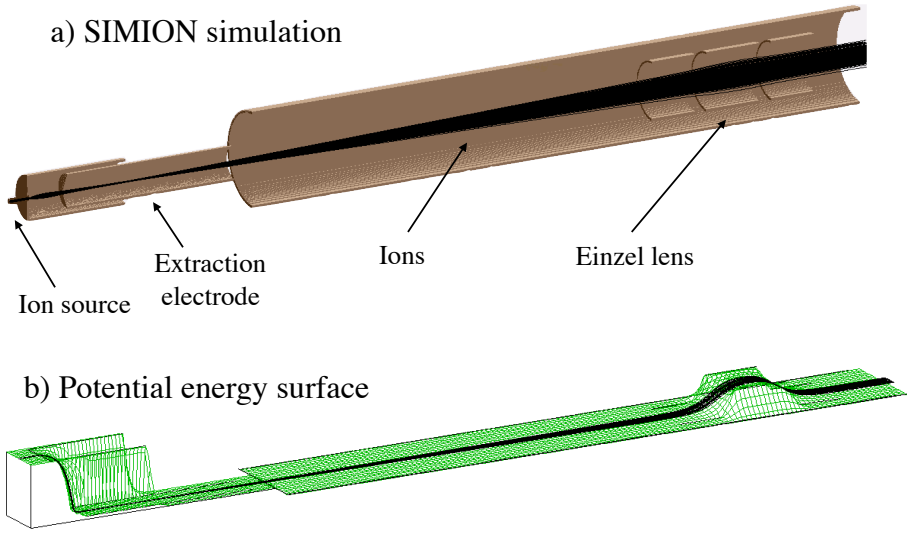

Figure 2.8: Geometry of the MEDICIS beamline simulated with SIMION. Figure a) shows the geometry and electromagnetic elements included in the simulations. Figure b) shows the potential energy surface, the vertical axis representing the electrostatic potential.

(a) (b)

Figure 2.9: Mass separator donated by KU LEUVEN to the MEDICIS experiment. a) Exit of the dipole magnet at the LISOL bunker. b) Dipole magnet installed at the MEDICIS bunker. A window was installed to allow lasers to be sent towards the ion source for resonance ionization.

1.5 m. The entrance angle of the magnet is 90° and 35.5° at exit. The magnet has a curved, H-type yoke made of solid iron, with an aperture of 200 mm wide and 55 mm height (full mechanical aperture). It has an indirect water cooled, bedstead coil electrically connected in series. The required maximum integrated field strength in T · m is provided by 90 turns per coil with a current of 120 A.

Ions are bent in the horizontal plane following a 55° curvature radius. The integrated field homogeneity $\Delta \mathrm{B}_y \mathrm{d}_z / \mathrm{B}_y(0,0,\mathrm{z})\mathrm{d}_z$ must be better than $2{\cdot}10^{-4}$ inside the rectangular homogeneous field region, where Z is the distance along the central trajectory. The requirements on the integrated field homogeneity have to be respected at all operational field levels.

The mass separator was modified to enable use with a resonance ionization laser ion source (MELISSA). MELISSA will become available in a next phase of upgrades of the facility, however it was essential to perform this modification from the early stage of the laboratory, before any risk of contamination in the magnet. With this purpose in mind, a window for the lasers with a 33 mm diameter was incorporated to the vacuum chamber to allow a clear line-of sight to the ion source (see Fig. 2.9b). A shutter was installed in front of the window to prevent contaminating it when e.g. the dipole magnet is off but the high voltage is on.

2.4.4.1 Focal plane distance and orientation

In here we determine the position of the focal plane and its orientation using the SIMION software [12]. The geometry of the magnet used as an input for the simulations was kept as close as possible to the geometry described in the technical specifications of the mass separator. It determines most of the optics of the entire beamline. The 90° angle at the entrance and 35.5° at the exit with respect to the central beam trajectory ensures double focusing given an incoming parallel beam.

When the ions enter in the magnet they are bent by the magnetic field according to their A/Q ratio. For ions flying along the central trajectory, the corresponding magnetic field can be calculated using the Lorentz law:

$$eQ\vec{v} \times \vec{B} = m_n A \frac{\vec{v}^2}{R} \tag{2.1}$$

where e is the electron charge, Q is the ion charge state, $\vec{B}$ the magnetic field, m_n the mass of a nucleon, A the ion mass number, $\vec{v}$ its velocity and R the curvature of its trajectory under the magnetic field. By substituting:

$$v = \sqrt{\frac{2eQV}{m_n A}} \tag{2.2}$$

in equation 2.1 for an acceleration voltage of 30 kV, $R = 1500$ mm and $A = 100$ amu we obtain B=0.166 T.

The distance to the focal plane can be calculated using the matrix formulation for the focusing of charged particles. The transfer matrix H in the horizontal plane can be found in [32] to be:

$$\begin{pmatrix} 1 & \frac{f}{R} & 0 \\ 0 & 1 & 0 \\ 0 & 0 & 1 \end{pmatrix} \times \begin{pmatrix} cos\phi & sin\phi & 1 - cos\phi \\ \frac{-sin(\phi-\beta)}{cos\beta} & \frac{cos(\phi-\beta)}{cos\beta} & sin\phi + (1 - cos\phi)tg\beta \\ 0 & 0 & 1 \end{pmatrix} = \begin{pmatrix} H \end{pmatrix}$$

where f is the focal distance, $\phi = 55°$, $\beta = 35.5°$ and R=1500 mm. The focusing condition from a parallel beam to a focal point is $H_{11} = 0$ [32] we find:

$$f = R\frac{cos\phi \times cos\beta}{sin(\phi - \beta)} \tag{2.3}$$

Finally we obtain $f = 2098.3$ mm.

Different masses will have their focus at different locations from the magnet exit. The focal plane is therefore not normal to the central trajectory but has an inclination as shown in Fig. 2.10. The focal plane distance and inclination with respect to the central beam were found using SIMION. Particles with $A = 99$, 100 and 101 were launched from either side of the central trajectory, upstream of the dipole magnet at 30 keV.

Good agreement between the theoretically calculated focal distance as given by equation 2.3 and the SIMION simulations is observed as shown in Fig. 2.10. The angle of the focal plane with respect to the central trajectory is $\sim 24°$. These results were used to determine beam instrumentation specifications. The scanner moves along the focal plane with the calculated inclination angle. The collection point is then placed as close as possible to the focal point for the beam on the central trajectory.

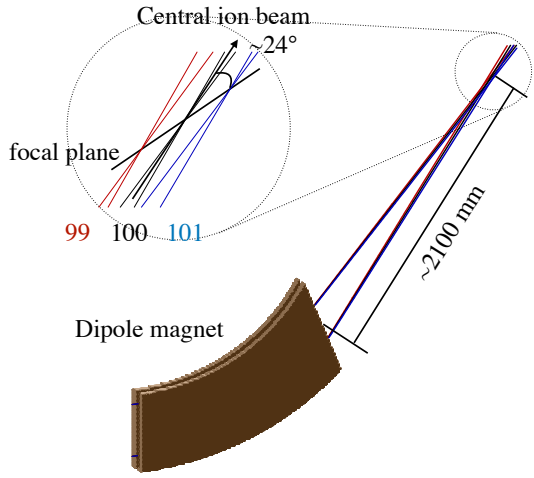

Figure 2.10: SIMION simulations to determine the focal distance and angle of the focal plane.

2.4.4.2 Characterization of the magnetic field with the OPERA software

Magnetic field calculations of the dipole magnet were performed using the Opera-3D/TOSCA program [17]. Fig. 2.11 shows the field distribution on the surface of the magnet when applying a current of 70.3 A, which would be the current necessary to keep ions of mass 300 on the central trajectory.

The magnetic field distribution along the central trajectory for 3 different values of current was also determined. In Figure 2.12, model #1 refers to the original structure of the magnet (no hole for laser window) and model #2 takes into account the yoke with the hole of 40 mm diameter (outer diameter) for the laser window.

The homogeneity of the magnetic field was calculated to determine the homogeneous field region of the magnetic field. The field was calculated at different heights (Y-direction, different colours in Fig. 2.13). The X-axis represents the shift from the central trajectory.

The integrated field errors were calculated according to the expression:

$$\epsilon = \frac{\int B dz - \int B_0 dz}{\int B_0 dz} \tag{2.4}$$

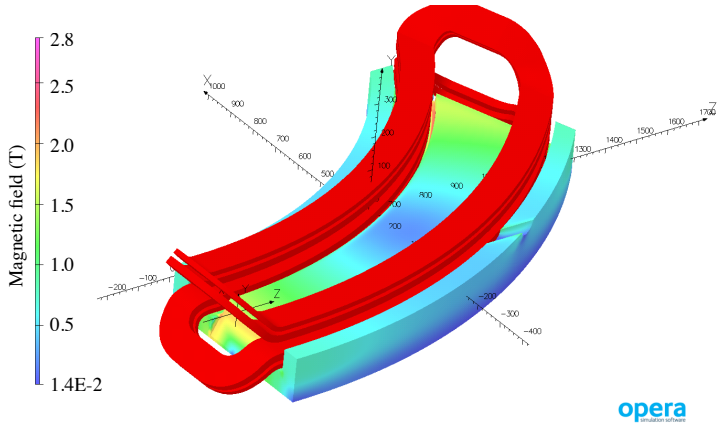

Figure 2.11: Magnetic field homogeneity of the magnet using the OPERA software for I=70.3 A.

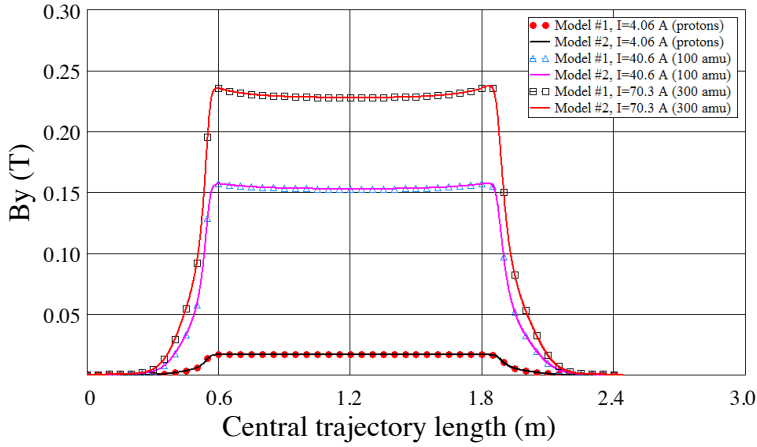

Figure 2.12: Comparison between OPERA models without (model #1) and with (model #2) the window for the lasers

where B_0 is the magnetic field along the central trajectory at Y=0.

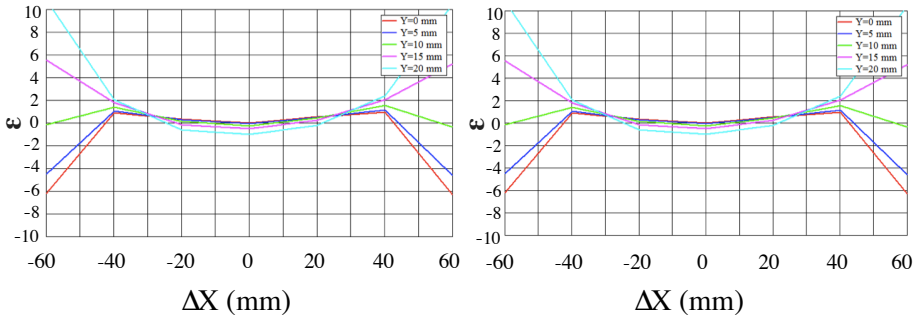

Figure 2.13: Relative integrated field error [10^{-4}] for I=70.3 which corresponds to A=300 amu at 30 keV. Left-model #1 (no hole), right-model #2 (hole)

It is seen then that the impact of the hole in the return yoke (laser window, model #2) on the field strength is negligible compared to model #1. In order to keep an integrated field homogeneity better than $\pm 2 \cdot 10^{-4}$, the beam should stay within a rectangle of 40 mm in the X-direction (horizontal) and 20 mm in the Y-direction (vertical).

2.4.4.3 Mass resolving power

An important property that expresses the quality of the system is the mass resolving power (MRP). The resolving power depends on the properties of the magnet and of the ion optical properties of the ion beam. In here we will use the MRP definition given in [1], which defines it as:

$$MRP = d \cdot \frac{M}{FWHM} \tag{2.5}$$

where d is the distance between two adjacent peaks with masses M and $M+1$ and FWHM is the full width at half maximum of a beam of ions with mass M in the focal plane of the separator. This value must be maximized to decrease the cross-contamination from neighbouring masses. Typical values for ISOL systems vary from a few hundred to a few thousand. Under normal off-line working conditions, the MRP has been measured to be larger than 1500 for the LISOL magnet (refurbished for use at MEDICIS) when operational at the LISOL facility [1].

As mentioned in Section 2.4.3, the ISOLDE FE5 front-end had to be adapted to be compatible for use at MEDICIS. The modifications, as a consequence, influences the mass resolving power. SIMION calculations were performed to demonstrate the feasibility of modifying the geometry without strongly affecting the MRP.

The MRP was calculated for the original configuration (geometry 1), in which the vacuum valve for vacuum sector 1 (target sector) is placed behind the einzel lenses. The results are compared with a new geometry (geometry 2), in which the vacuum valve is placed before the einzel lenses to reduce the pumping volume of the target sector. The einzel lenses were moved 80 mm away from the ion source as a result. Other elements of the beamline were also discarded/replaced during the modifications. More details can be found in [31].

In the simulations, the voltage of the einzel lens was scanned for both geometries as shown in Fig. 2.14. Ions with mass A=100 were launched with the parameters described in 2.4.2 and accelerated towards the mass separator under a 30 kV acceleration voltage.

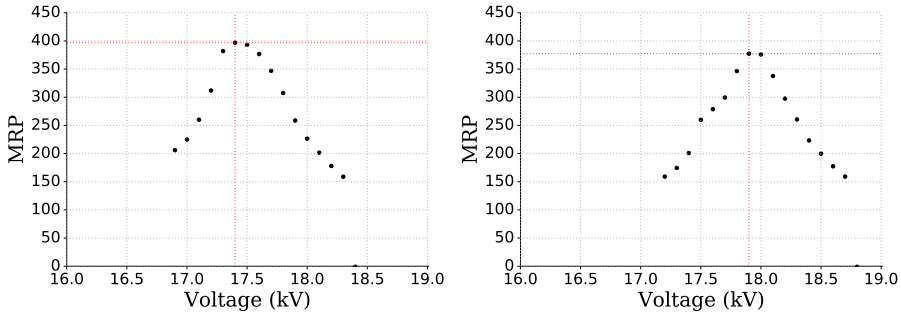

(a) (b)

Figure 2.14: MRP as a function of einzel lens voltage. a) Geometry 1. b) Geometry 2.

The MRP were 400 and 380 respectively, which shows that the MRP is not strongly affected by an 80 mm displacement of the einzel lens. From the simulations it can be observed that a change in 500 V applied to the einzel lenses can affect the MRP significantly. This sensitivity of the MRP on the applied voltage to the einzel lens has also been observed at the MEDICIS facility while tuning the beamline for isotope extraction and collection.

2.4.5 Beam emittance

The emittance of the beam gives a measure of its quality. It is related to the volume occupied by the particle beam in the phase space determined by the position and momentum of the particles in the beam. Often, only the two directions transversal to the beam direction are of interest (in here, y and z are considered the transverse directions). When calculating the emittance, the momentum p_y can be replaced with y'=$(d_y/d_x) = (d_y/d_t)/(d_x/d_t) = v_y/v_x$, often referred as trace space. In the paraxial approximation this slope y' can be represented as an angle θ with units of radians.

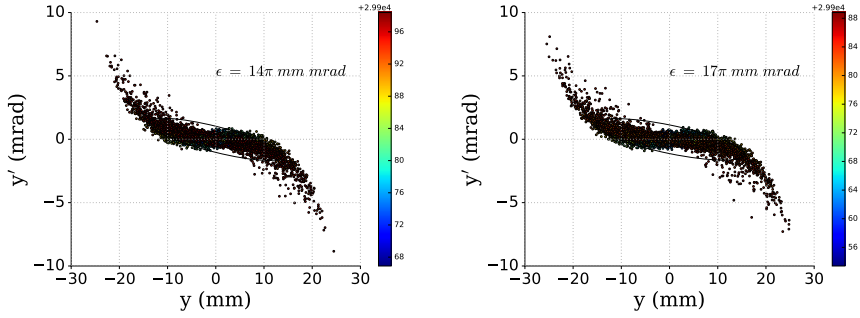

(a) (b)

Figure 2.15: Emittance at magnet entrance. The quoted emittance values correspond to the area of the ellipse containing 95 % of the simulated events. a) Emittance geometry 1. b) Emittance geometry 2.

The simulated beam emittance was computed at the entrance of the magnet for geometries 1 and 2 as defined in subsection 2.4.4.3. The emittance plots are displayed in Fig. 2.15. The ellipse that has been drawn and the values computed encompass 95 % of the simulated events. By comparing the emittance for geometries 1 and 2 we can see that the beam quality stays similar for both geometries. Therefore, to fulfil the requirements of operation of the MEDICIS facility, geometry 2 was chosen.

The beam profile at the focal plane seen in Fig. 2.16 shows that at mass A=100, a cross-contamination at the level of 1-2 % exists (assuming a Gaussian distribution). Two adjacent masses are separated by ∼14 mm.

The beam spotsize is shown in Fig. 2.17a as calculated using SIMION, which takes into account an initial energy spread and angular distribution of the ions leaving the ion source (details in subsection 2.4.2). The positions of the mass

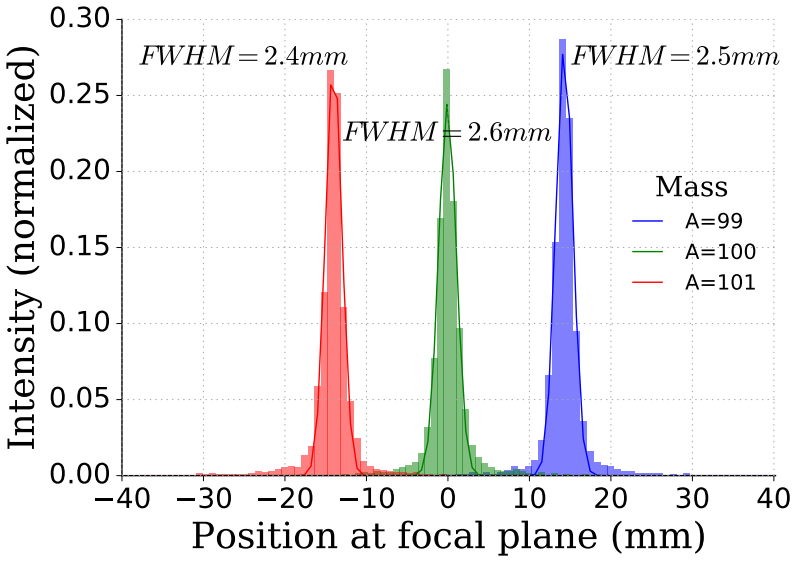

Figure 2.16: Horizontal beam profile for masses 99, 100 and 101 at the focal plane.

centroids correspond to those predicted by the OPERA simulation (Fig. 2.17b). OPERA considers only a mono-energetic, parallel beam, perpendicular to the magnet entrance plane with a radius of 15 mm. On the other hand, OPERA takes into account an accurate magnetic field distribution (as seen in 2.4.4.2) while for the SIMION simulation, an homogeneus magnetic field between the poles is considered.

2.4.6 Collection box

The main components of the collection box are the beam diagnostics instrumentation, the beam switchyard and the sample collection system. Up to three samples can be placed in the sample holder separated by 15 mm with a size of 10 by 10 mm. Before the holder for the sample plates a collimator and electron deflector are placed. The current in the sample should be maximized while it should be minimized in the collimator.

The position of the sample is controlled by a moveable arm that can move perpendicular to the beam direction. Figure 2.18 shows two different positions.

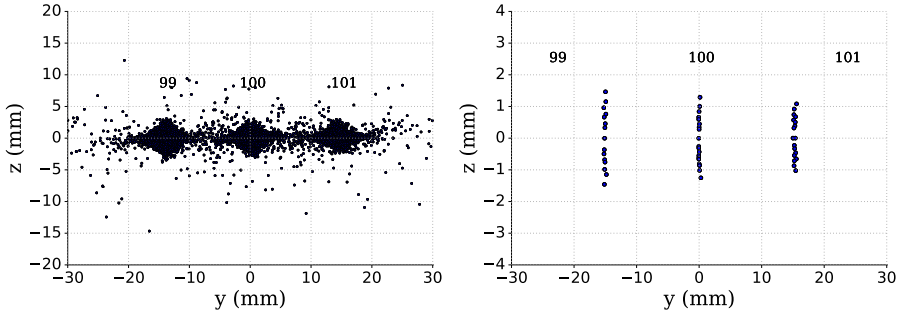

(a) (b)

Figure 2.17: Simulation of the beam spot size at the focal plane for masses 99, 100, 101. a) Simulated with SIMION. b) Simulated with OPERA.

In Fig. 2.18a the samples are still outside the collection box and in Fig. 2.18b the sample intercepts the beam in the central trajectory.

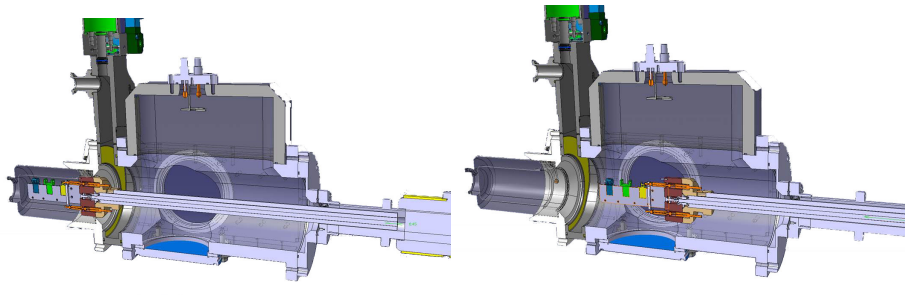

(a) (b)

Figure 2.18: Sample holder positioning. Three different sample positions are shown (blue, green and yellow). A vacuum valve separates the sample container from the collection box. Once the container is attached to the collection box, the valve is opened, the samples moved into the collection box and the vacuum valve is closed. a) Fresh samples to be placed at irradiation position. b) Samples are in position to be irradiated.

As for the beam instrumentation, Faraday cups are used, one for total beam current measurements (before the mass separator) and one to measure the separated beam (in the collection box). Wire scanners are used for beam profile and quality assessment in the YZ plane.

A beam switchyard was not used at the start-up of the facility. Instead, samples were collected at the collection point, in the central beam trajectory. For the upgrade of the facility, a beam switchyard is foreseen to enable collections of different masses at the same time. The purpose of the switchyard, which is made of electrostatic slits, is to divert the beams towards the collection chambers. The required electric field applied to the slits will depend on the energy and mass of the selected beam. The slits will be mounted on rails and moved by stepmotors along the focal plane. The MEDICIS switchyard model is shown in figure 2.19.

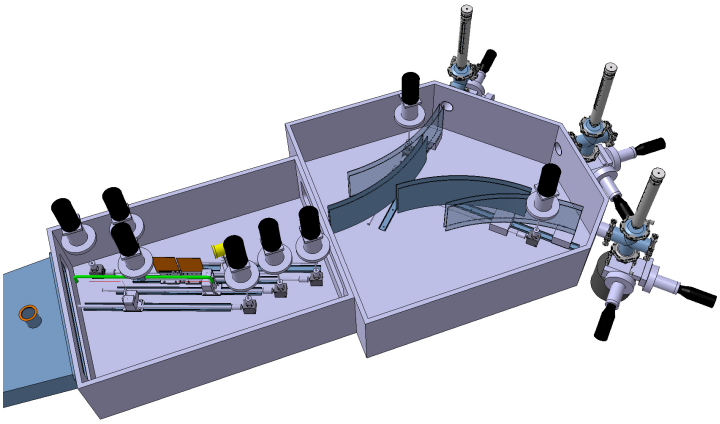

Figure 2.19: Option for the MEDICIS switchyard system to be installed for a future upgrade of the facility. This system is inspired from the one used at the LISOL experiment in Louvain-la-Neuve, allowing the collection of 3 different masses simultaneously.

2.5 First stable beams produced at MEDICIS

The first stable mass-separated beams at CERN-MEDICIS were produced on November 15th, 2017. Tantalum rolls of 25 μm thickness were used as target material with a standard ISOLDE hot cavity ion source (target unit #Ta621M). Mass markers of europium (A=151, 153) and erbium (A=162, 164, 166-168, 170) were connected for calibration of the magnet in the region of interest - the terbium isotopes (A=149, 152, 155).

The target was kept at $\sim$1220 °C while the ion source was heated to $\sim$1850 °C. The target/ion source assembly was kept at 30 kV during the

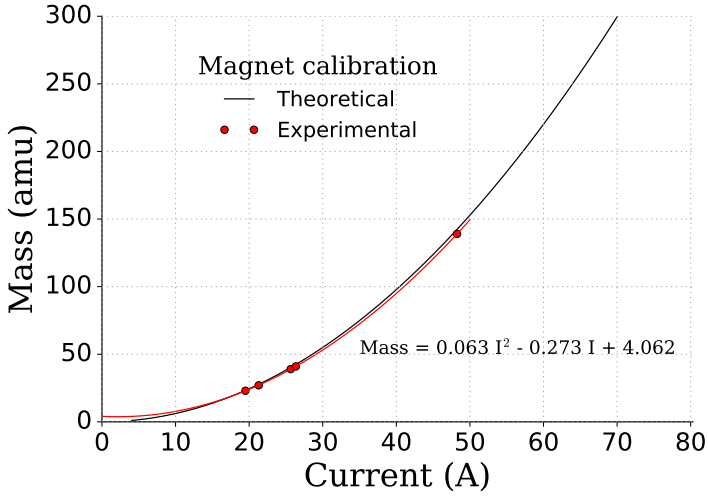

Figure 2.20: Calibration curve of the MEDICIS dipole magnet. The quadratic expression shown in the figure was fitted through the data points (red curve).

commissioning phase. The relation between current and mass was found using the calibration shown in Fig. 2.20. Figure 2.21 shows a scan done on the first day of commissioning of the stable beams. The scan was done by slowly increasing the magnet current manually. The X-axis shows time and Y-axis amplitude.

A VADIS (Versatile Arc Discharge Ion Source) was coupled to the MEDICIS front-end on March 2018 to further characterize the mass separator and continue with the beam commissioning phase, producing this way the first noble gas beams. A gas mixture of helium, neon, argon, krypton and xenon (20 % each) was connected to the target unit (#Ta649M) through a calibrated leak. The beam profile in the xenon region can be seen in Fig. 2.22, in which masses 129, 130, 131 and 132 are visible and with intensity at each mass reproducing the expected natural abundances. The extraction electrode was 40 mm away from the exit of the ion source. The measured total beam was 1.33 μA while the separated beam for ^{132}Xe was 135 nA. The cathode temperature was kept at 1950 °C.

The information provided by the beam profile taken with the scanners give information on the mass resolving power (MRP). Considering the FWHM for A=131 is 3 mm and the distance between the peaks is ∼11 mm, we get an approximate value for the MRP of 480. For LISOL, a MRP of 1500 was measured. A reason for this drop in the measured MRP could lie in the fact that at MEDICIS, the scanners are not located at the focal plane, resulting

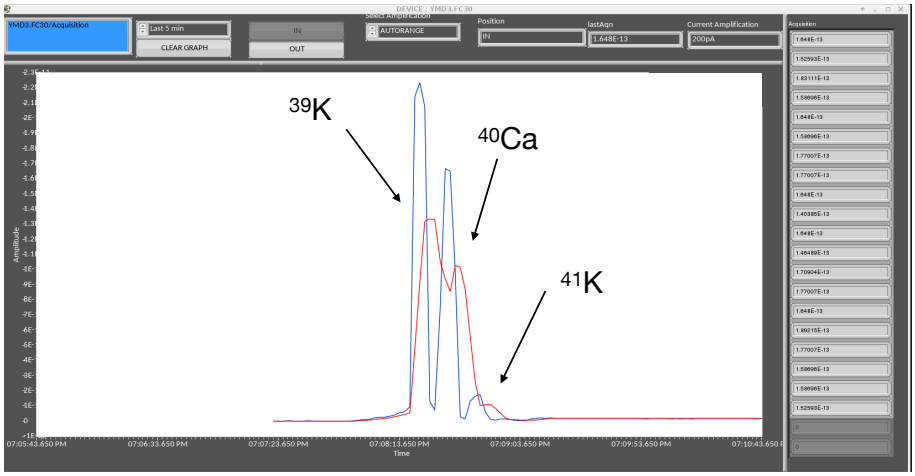

Figure 2.21: First mass separated beams at the CERN-MEDICIS facility. The horizontal axis shows the acquisition time while varying the magnetic field strength (by varying the current in the magnet coils) and the vertical axis the amplitude. The blue curve represents the acquisition at each given time while the red curve averages the last 5 data points taken.

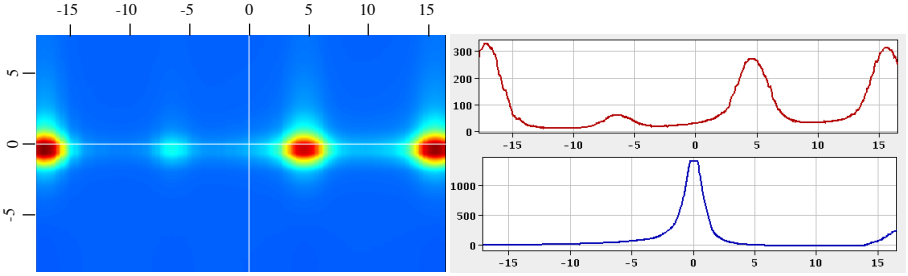

Figure 2.22: Xe beam profile. The heatmap shown in the left panel (data represented by colours, with red and blue being the maximum and minimum values of the beam intensity respectively) shows the relative intensities for A=129 to A=132. Figures in the right side show the scanner images for the horizontal axis (top panel) and vertical axis (lower panel)

in a larger measured FWHM. Also, different ion sources were used, and as a consequence the extracted beams have different energy spread, influencing the measured MRP.

Even though the beam profiles shown in Fig. 2.21 and Fig. 2.22 are not fully Gaussian and tails at low masses can be observed, the ability of the experimental setup to separate the beams of interest was demonstrated. The first stable beams produced during the commissioning phase showed that the facility was ready to start collection and delivery of the first radioactive isotope batches. The agreement between simulations and experiment demonstrate its usefulness to continue the studies for the future upgrade phases of the laboratory.

2.6 First radioactive beams produced at MEDICIS

The target #621M was installed at the irradiation point at the ISOLDE target area on December 5th 2017. The target/ion source assembly consisted of a standard ISOLDE target container filled with tantalum rolls (25 μm thickness) and a tungsten surface ionizer.

An overnight irradiation took place with a low intensity beam from the PS Booster. The target received a total $\sim 1.65 \cdot 10^{17}$ protons in 24 hours. One full day after the end of the irradiation, the target unit was installed at the MEDICIS front-end. The mass separator was tuned using the calibration curve shown in Fig. 2.20 for A=155. The target was slowly heated to 1950 °C (once the separator was properly tuned and ready to start the extraction) and the ion source to 2150 °C. The extraction was done at 30 keV. The first radioactive beam collections took place on the 11th and 12th of December 2017.

The collected samples were sent to IRA [33] in Lausanne, Switzerland and to IST-C2TN [34] in Portugal. For the latter, the collection time was 30 minutes. Fig. 2.23 shows the gamma spectrum highlighting some of the isotopes identified. A summary report by the CERN radioprotection group identified 218 Bq ± 9% of ^{155}Tb ($T_{1/2}$=5.3 days) and 64.8 Bq ± 15% of ^{139}Ce ($T_{1/2}$=137.6 days) which can appear at mass A=155 as an oxide.

The commissioning period of the facility, both with stable and radioactive beams offered the opportunity to gain operational experience and identify potential issues. The separator magnet was calibrated as well as the sample holder position which was, initially, done manually. The transmission was assessed ($\sim$90%) and software were debugged.

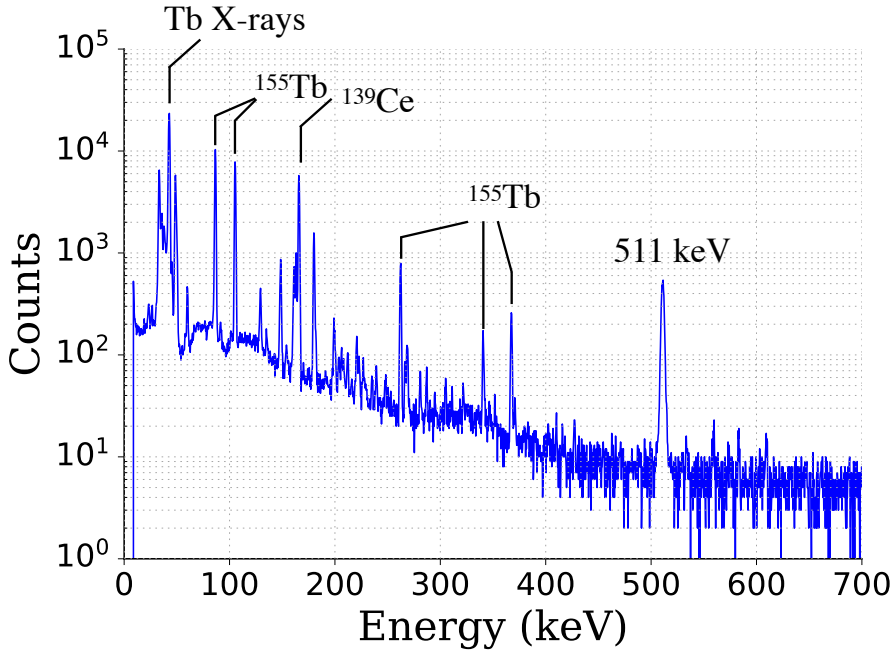

Figure 2.23: Gamma spectrum of the second radioactive sample collected at MEDICIS. The collection time was 30 minutes. The target (tantalum rolls) and ion source (tungsten surface ionizer) temperature were 1950 and 2150 °C respectively.

The first collections done during this commissioning phase demonstrated the readiness of the facility, which then allowed to enter in full production mode for the 2018 campaign at CERN.

Chapter 3

Ion sources for the production of radioactive beams at ISOL facilities

The ion source is the starting point for all particle accelerators. A wide spectrum of ion sources have been developed to serve the many thousands of particle accelerators that are operated worldwide. Ion sources can be compared and characterized based on the following performance criteria: intensity, efficiency, selectivity, versatility, universality, stability, reliability. To complicate the picture, for a given ion source, these parameters will vary according to the required ion species, energy spread, emittance, charge state and purity.

A universal ion source does not exist, instead the correct ion source type and mode of operation must be selected depending on the relative importance of each of the parameters discussed here:

Intensity: The intensity is defined as the extractable ion current from the ion source. For example, in the case of negative hydrogen sources for fusion reactors, the injected atom flow comes from an unlimited supply (e.g. hydrogen bottle), compromising in efficiency and other parameters for beam intensity. For radioactive beam facilities, sample injection comes from radiogenic in-target production. These radioisotopes are a valuable commodity to be preserved, and do not generally pose an intensity limit on the ion source. For radioactive beam production (RIBs), the efficiency becomes the most important parameter.

Efficiency: The ionization efficiency ϵ is defined as $\epsilon = \mathrm{N}_{ions}/\mathrm{N}_{atoms}$ where

N_{ions} is the number of ions extracted from the source and N_{atoms} the number of atoms in the sample.

Selectivity: The selectivity of the ion source refers to its capability to ionize just the desired element. It could be defined as the ionization efficiency of the element of interest divided by the mean ionization efficiency of all other elements. In combination with mass separation, which typically relies on a dipole magnet separator to select isotopes with mass $A = N + Z$, an element-selective ion source, providing Z-selectivity, ensures unambiguous isotope selection.

Versatility: This is a measure of the scope for a particular ion source to be optimized as required for a variety of different applications. It should not be confused with **Universality**, which is purely a measure of the range of species that can be ionized with the source.

Stability: This refers to the ability of the ion source to sustain its performance without fluctuations during the course of an experiment (e.g. maintain its efficiency/intensity/beam quality properties in time).

Reliability: The reliability is a combined measure of the mean time between failure, reproducibility in performance between one unit and the next, and the long-term survivability of the ion source under typical operating conditions.

This chapter will describe the principles of operation of the ion sources used at ISOLDE that are relevant for the discussions that follow in Chapters 4 and 5.

3.1 Ion sources used at ISOLDE: principle of operation

3.1.1 Surface ion source

The process of surface ionization was well described by Saha and Langmuir [35] in the first half of the 20^{th} century, during the early days of radioactive beam production using the ISOL technique. Positively charged ions can be produced when an atom with a low ionization potential W_i, hits a heated surface with a higher work function ϕ, losing a valence electron in the process.

The ionization probability will depend strongly on the temperature of the surface and the difference between the work function of the material and the ionization potential of the atom. It will be given by:

$$\alpha = \frac{N_{ions}}{N_n} = \frac{g_+}{g_0} exp\left(\frac{\phi - W_i}{kT}\right) \tag{3.1}$$

Equation 3.1 is called the Langmuir equation. Here N_n is the number of neutrals, T is the temperature of the hot surface and g_+ and g_0 are the statistical weights of the ionic and atomic ground state respectively.

The hot cavity surface ion source (SIS) used at ISOLDE is a hollow cavity 34 mm long, with a 3 mm internal diameter and walls 0.5 mm thick. It is connected via a transfer line to the target container. A transversal view of its design is shown in Fig. 3.1.

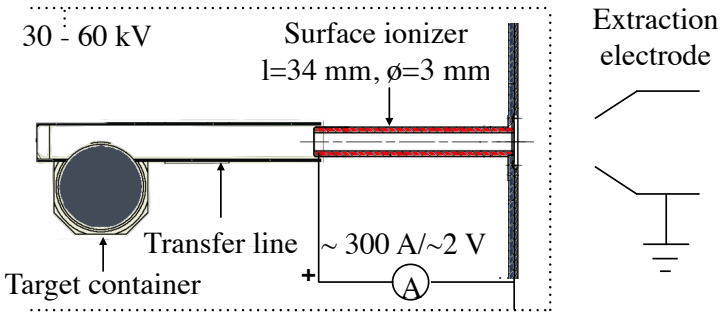

Figure 3.1: The ISOLDE hot cavity surface ion source (SIS). The products of the nuclear reactions from the primary proton beam with the target material reach the surface ionizer via a transfer line.

In this geometry, it has been observed that the ionization efficiency of the SIS greatly exceeds the ionization probability predicted by equation 3.1 for a single atom/wall collision. This is because of the well documented and much discussed 'hot-cavity effect', which stems from the transverse plasma potential generated by the thermionic emission of electrons from the cavity walls [36, 37]. As a result, when under the influence of this effect (with sufficient electron emission), each ion leaving the cavity walls is confined in the transverse plane, thus avoiding further wall interactions. They are guided towards the extraction region by the longitudinal electrical potential of the resistively heated cavity. Thus, the ion survival may approach 100 %. The overall efficiency of the ionization process in the hot cavity is therefore enhanced and will be given by:

$$\beta = \frac{\omega k \alpha}{1 + \omega k \alpha} \tag{3.2}$$

where k accounts for the number of collisions with the hot surface the ion suffers before being extracted and ω is the trapping efficiency of the created ion in the potential well of the low density plasma created inside the cavity.

The ideal SIS material will have a combination of high melting point, mechanical stability and reliability under heating and cooling cycles, high work function and low thermal expansion coefficient. The most commonly used materials are tungsten (ϕ=4.53 eV), tantalum (ϕ=4.19 eV) and rhenium (ϕ=5.1 eV). At the IRIS facility (PNPI, Gatchina), a high temperature, and therefore high efficiency SIS has been developed from a single tantalum crystal tube [38, 39].

Figure 3.2 shows the elements produced at ISOLDE using the SIS, and a summary of the advantages and disadvantages of this ion source is given below.

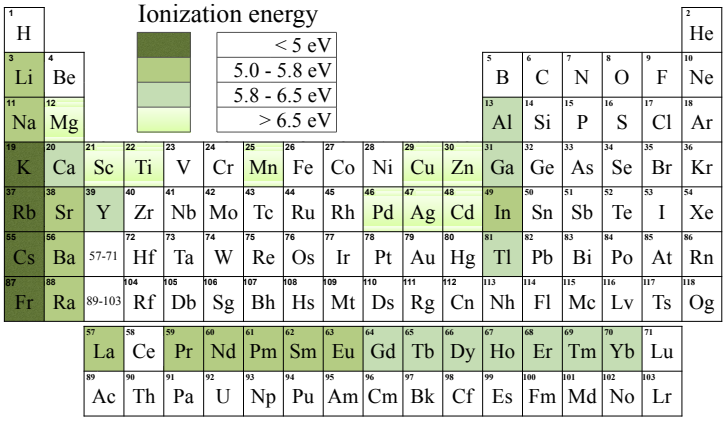

Figure 3.2: Elements for which the hot-cavity SIS has been applied for ion beam production at ISOLDE [40]. The different color shades are associated to the ionization potential of the element.

Advantages	Disadvantages
• simple • robust and reliable • high efficiency for low W_i elements (< 6 eV)	• low efficiency for high W_i elements (> 6 eV) • limited element selectivity

3.1.2 Hot-cavity RILIS (Resonance Ionization Laser Ion Source)

The Resonance Ionization Laser Ion Source (RILIS) is the most commonly used ion source at ISOLDE, providing 60 % of all the beams delivered in 2017 and 2018 and more than 85 % in 2016.

Figure 3.3 shows the principle of resonance laser ionization.

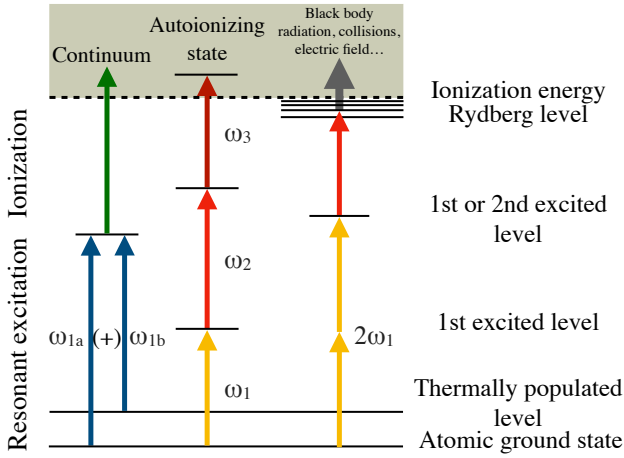

Figure 3.3: Principle of resonance photo-ionization.

The atoms are stepwise excited by precisely tuned laser light, so that the energy of the photon matches successive transitions of the electrons to excited states. One or two resonant excitations are used to bring the electron to the continuum through the absorption of a further photon, in a non-resonant ionization step or a transition to an auto-ionizing state (AIS).

The standard way of applying laser ionization at ISOLDE is to make use of the fact that the hot cavity, described in 3.1.1, offers a simple and robust laser-atom interaction region as shown in Fig. 3.4.

The hot-cavity offers the following favourable characteristics for RILIS applications:

- Atom confinement within the laser beam path for the duration of time between laser pulses (100 μs)
- Cavity plasma potential (as discussed in 3.1.1) for survival and efficient extraction of laser-ions
- Simplicity and reliability

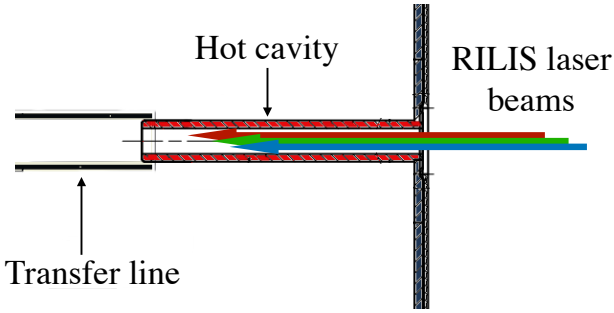

Figure 3.4: The hot-cavity surface ion source used as laser-atom interaction region for RILIS applications.

Full details of the RILIS system and the applications can be found in [41]. Figure 3.5 shows the currently available list of RILIS ionized elements at ISOLDE.

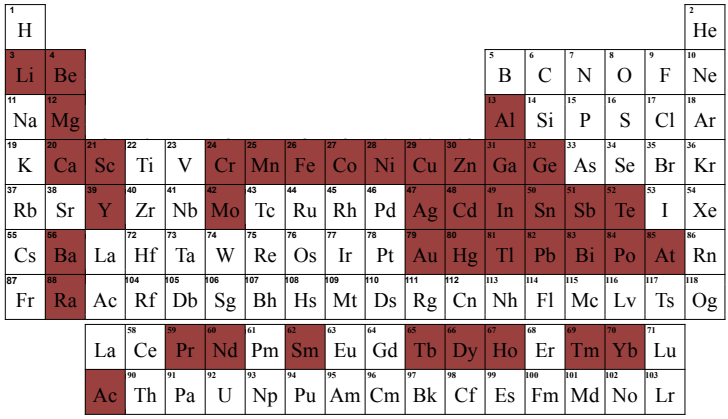

Figure 3.5: Elements for which RILIS has been applied at ISOLDE according to [41]. The ionization schemes are accessible through an online resource known as 'The RILIS Elements Database' [42].

Advantages	Disadvantages
• simple • robust and reliable • high efficiency can be achieved (typically exceeding 10 %) • over 40 elements so far available at ISOLDE • element selective ionization mechanism • beam diagnostics benefit with laser ON/OFF procedure • isomer selectivity in some cases [43]	• surface ionized isobars may limit the achievable selectivity • efficiency decreases with high ion rates of the order of 100 nA (laser plus surface ions)

3.1.3 Forced-Electron Beam Induced Arc-Discharge Ion Source (FEBIAD) and the VADIS series

FEBIAD ion sources [44] rely on electron impact ionization. The ISOLDE FEBIAD is shown in Fig. 3.6. The products of the nuclear reaction taking place in the target (the target material is placed in a cylindrical container) reach the anode volume of the ion source via a transfer line. Electrons are extracted from a heated cathode in a shape of a flat disc and accelerated towards an anode where ionization takes place. To reach the anode, the electrons traverse a grid with a transparency of 50 to 75 %. The energy of the electrons is typically in the range of 100-200 eV.

The electron current emitted by the cathode is described by the Child-Langmuir equation when the space-charge limit has been reached:

$$j_e[mAmm^{-2}] = \frac{4}{9}\epsilon_0 \left(\frac{2e}{m_e}\right)^{1/2} \frac{V^{3/2}}{d^2} \tag{3.3}$$

where j_e is the electron current density emitted from the cathode, e and m_e the charge and mass of the electron respectively, V[V] is the voltage applied

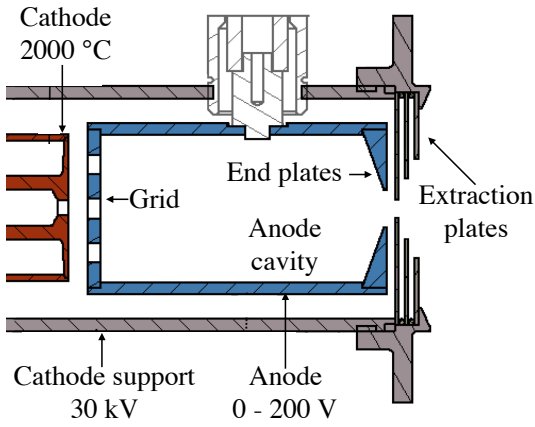

Figure 3.6: Geometry of the ISOLDE FEBIAD ion source (VADIS). The electrons released by the hot cathode are accelerated towards the anode volume where the atoms (which reach the anode through the hollow cathode, connected to the target using a transfer line) are ionized mainly by electron impact ionization. The structure shown on top going through the cathode support, serves to connect the anode to its power supply.

to the anode and d[mm] the distance between the cathode and the anode grid. At low temperatures, the electron emission from a hot cathode is limited and follows the Richardson-Dushman equation:

$$j_e[mAmm^{-2}] = AT^2 exp(-\phi/kT) \tag{3.4}$$

where A is the material-dependent Richardson's constant.

Several factors can influence the ionization efficiency for a given species:

- Residence time in the anode (lighter elements typically spend less time in the anode volume)
- Cross section for ionization (influenced by atomic radius and electron impact ionization energy)
- Volatility of the element of interest (also applies to the SIS and RILIS)
- Chemical compatibility with ion source parts and insulators
- Collisions with atoms and ions in the ion source
- Total gas/ion load

The parameters that can be controlled are:

- Cathode temperature, which influences electron emission rate and anode temperature
- Anode voltage, which determines the electron energy
- Magnetic field strength (this source is embedded in a weak axial magnetic field), which influences the electron trajectory

At ISOLDE, several subtypes of the FEBIAD ion sources were used [45] until 2009 when they were replaced by the VADIS (VD) series [46]. A wide experimental investigation of the main mechanisms influencing the ionization efficiency of the ISOLDE FEBIAD, was carried out by L. Penescu during his PhD work [19]. It was based on the work of R. Kirchner, inventor of the FEBIAD [47]. Penescu identified that the MK7 geometry was inferior to that of the MK5 [45] in terms of ion extraction efficiency. Furthermore, to mitigate any efficiency loss due to ion load limits caused by CO^+ ion creation, it was proposed that the carbon anode body should instead be made of molybdenum. These two changes constitute the so-called VADIS series of FEBIAD ion sources now used as standard at ISOLDE.

In reference [19], progress is reported towards the development of a model for the ion source operation based on experimental investigation and computer modelling (using the software CPO [48]) of many parameters. From this model, an expression was obtained for the efficiency ϵ:

$$\epsilon = 2.33 \cdot 10^4 \cdot f \cdot V_{source} \cdot A \cdot exp\left(\frac{-W}{kT}\right) \cdot l \cdot \frac{ln\left(\frac{U}{V_{ioniz}}\right)}{U \cdot V_{ioniz}} \cdot \frac{\sqrt{M}\sqrt{T}}{S_{out}} \qquad (3.5)$$

where V_{source} is the ion source volume, A the Richardson's constant, W the work function of the cathode material, T the cathode temperature, l the number of electrons in the valence shell, U the anode voltage, V_{ioniz} and M the ionization potential and mass of the element under study respectively and S_{out} the area of the outlet hole.

Nevertheless, the model still requires the inclusion of an adjustment factor, f, referring to the ion survival and extraction efficiency. Since this factor incorporates the interplay between many phenomena occurring within the ion source (plasma potential, ion confinement, trapping, collisions, chemistry, recombination, and so on), the scope for further understanding of the FEBIAD operation is evident.

Details on recent developments at ISOLDE of the FEBIAD for improved efficiency, selectivity and robustness will be given in Chapters 4 and 5. Figure 3.7 highlights the elements for which the FEBIAD has been used at ISOLDE. The term 'Cold plasma' is used when the transfer line is kept at room temperature and 'Hot plasma' when the transfer line is kept at 1900 °C or higher.

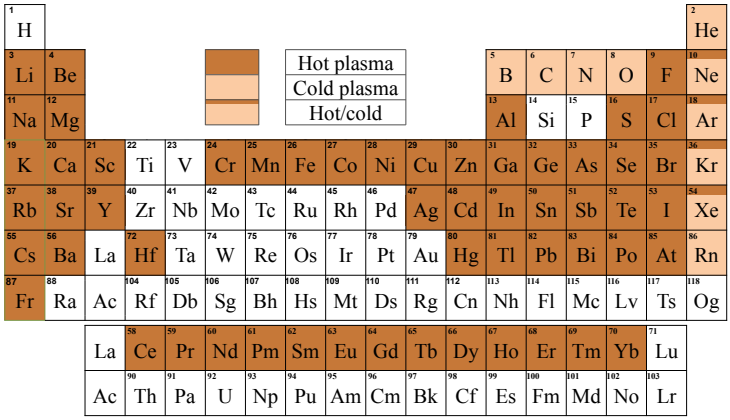

Figure 3.7: Elements produced at ISOLDE using the FEBIAD or VADIS ion source indistinctly from the ion source subtype [40].

Advantages	Disadvantages
• high efficiencies are achievable, independent of ionization energy (universal) • molecular species can be ionized • total ion output can be higher than that of the hot-cavity surface ion source (typically 10 times more) • gas injection and mass markers can be used for beam tuning, optimization and efficiency checks • compatibility with liquid targets at ISOLDE	• increased complexity with respect to SIS • ion source dynamics are not fully understood • reliability concerns when operating at maximum efficiency (insulator breakdown and cathode failure) • little to no element selectivity • low operating temperature with respect to maximum target temperature (and lower temperatures compared to the hot cavity): not suitable for the most refractory elements produced at ISOLDE

3.1.4 Negative ion source

A negative beam can be extracted from a surface ion source following similar processes as the ones described for its positive counterpart, described in 3.1.1. In this case, the material with which the atoms interact should have a low work function ϕ so that the expression:

$$\alpha = \frac{X^-}{X^0} = \frac{g_-}{g_0} exp\left(\frac{E_A - \phi}{kT}\right) \tag{3.6}$$

is maximum, where E_A is the electron affinity. The ionization efficiency is given by equation 3.2. But in this case the multiplication factor is a simple geometrical factor corresponding to the probability of an atom coming into contact with the ionizing surface.

Figure 3.8 shows the ISOLDE negative ion source (MK4) with the main components highlighted. A magnet that creates a perpendicular magnetic field (∼0.08 T) is placed closed to the exit of the ion source to deflect the emitted electrons. The electrons are collected at a polarized electrostatic deflector, typically biased to 1 kV.

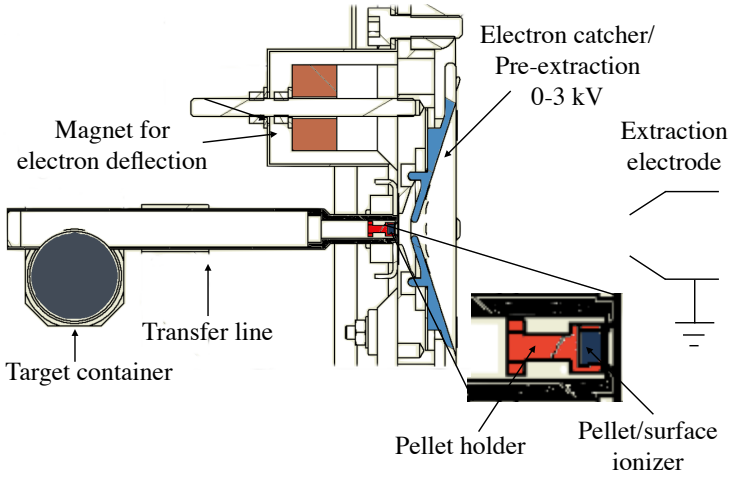

Figure 3.8: Negative ion source used at ISOLDE. A magnet and an electron catcher ensure the emitted electrons are not accelerated downstream of the ion source. A low ϕ pellet is placed near the exit to enhance the interaction probability with an atom.

A LaB_6 pellet (⌀=2 mm, thickness=1.5 mm) is placed at the cavity exit (as shown in Fig. 3.8). In this geometry, each atom has a roughly 50 % probability of coming into contact with the material. The well defined point of origin of the ions and the penetration of the extraction field from the electron deflector ensures efficient (∼100 %) extraction of the negative ions as a monoenergetic beam.

Even though this is the geometry traditionally used at ISOLDE for the production of negative beams, hollow-tube ionizers have also been used, for example for the production of Br^- and I^-, with an efficiency of 10 % [49]. While this improves the probability of atom contact with the ionizing surface, the hot-cavity plasma potential which is beneficial for the positive SIS, is actually detrimental for negative ion extraction. To mitigate this, attempts have been made to enhance ion extraction by injecting a flow of Cs^+ ions from the cavity exit. This adds extra complexity and the efficacy of this process has not proven reliable.

The negative ion beams produced at ISOLDE using the MK4 and tubular geometries are highlighted in Fig. 3.9. Halogens are practically the only isotopes that can be negatively ionized, therefore negative beams are very pure.

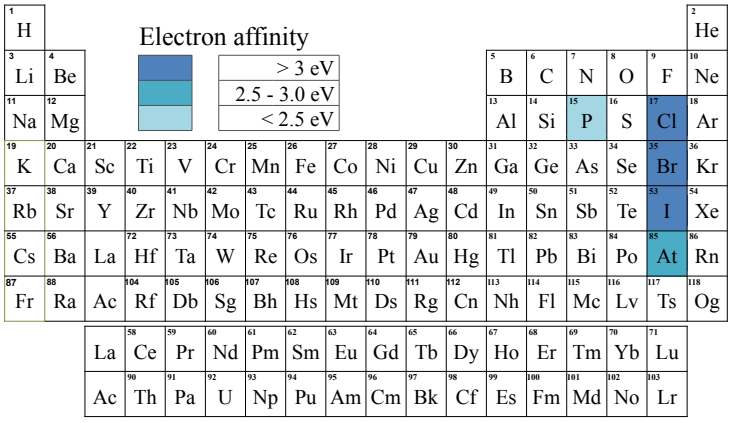

Figure 3.9: Elements for which the negative ion source as been applied at ISOLDE for the production of negative ion beams [40].

Advantages	Disadvantages
• only option for producing beams of negative ions • high purity negative ion beams • high efficiency for halogens (several %)	• low operation temperatures (below 1600 °C) • only suitable for elements with high electron affinity (halogens) • ionizing materials prone to poisoning by target outgassing

3.1.5 Versatile Arc Discharge and Laser Ion Source (VADLIS)

As the name suggests, here the ISOLDE FEBIAD (VADIS) volume is used as a laser-atom interaction region. The anode voltage can be tuned to allow for only resonance ionization (RILIS-mode) or electron-impact ionization (VADIS-mode) depending on the element of interest or the required beam purity [50].

The VADLIS with grounded extraction plates has been used at ISOLDE on several occasions since 2015. Figure 3.10a shows the RILIS lasers being directed into a modified FEBIAD anode volume [51]. By inserting a boron nitride insulator as depicted in Fig. 3.10a, the extraction plates can be independently tuned, modifying the electrostatic field inside the cavity, allowing for better laser ion extraction. Figure 3.10b shows the modes of operation (RILIS-mode, VADIS-mode) depending on the anode voltage. Further details are given in a dedicated chapter (Chapter 5).

So far, the VADLIS has been used for the production of Ga and Ba beams off-line while Hg [52], Mg, Cd and Mo have been produced during on-line operations at ISOLDE [50, 51]. The first on-line physics application of the VADLIS was for the laser spectroscopy of the mercury isotope chain produced in a liquid-lead target (the first application of RILIS with a liquid target [52]).

In Chapter 5, we report on the characterization of the VADLIS operation as well as simulations conducted to better understand the ion dynamics and extraction process. The motivation and performance benefits of the modifications implemented in this thesis work (addition of an adjustable extractor voltage) are presented.

The following is a list of the known advantages and disadvantages of the VADLIS. A comprehensive list will require a more complete understanding of the characteristics and performance of the ion source. For example, the ion capacity in RILIS-mode has not yet been evaluated.

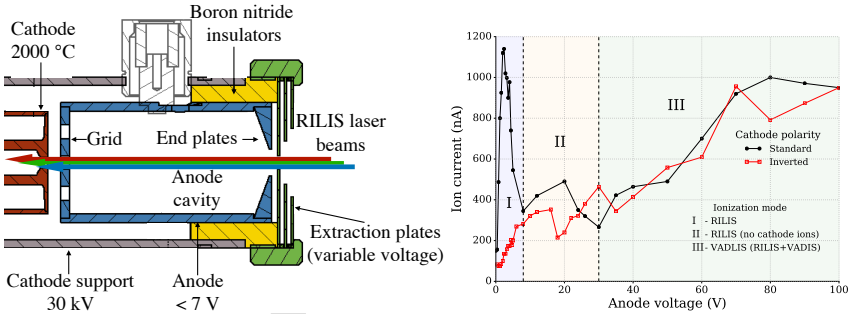

Figure 3.10: (a) RILIS lasers directed onto the anode volume. Boron nitride insulators are used to independently bias the voltage of the extraction plates for improved laser-ion extraction. (b) Anode voltage scan to identify the different modes of operation of the VADLIS. For more details see Section 5.1.

Advantages	Disadvantages
• versatility (only ion source that can ionize all elements produced at ISOLDE e.g. noble gases in VADIS-mode and selective ionization of metallic elements in RILIS-mode) • provides RILIS compatibility with liquid targets • enhanced RILIS selectivity compared to the hot-cavity in certain cases when the anode grid repels surface ions coming from the cathode tube • ability to switch to electron impact ionization to evaluate the presence of the desired RILIS ionized element prior to laser optimization	• increased complexity compared to hot-cavity RILIS • lower operation temperature than the hot-cavity RILIS • same reliability concerns as for the VADIS

3.2 Other ion source technologies in use or under development at ISOLDE

The **Laser Ion Source and Trap (LIST)**, first proposed in 2003 [53], has been implemented in a simplified form at ISOLDE as the most effective means of applying resonance ionization with active suppression of surface ions from the hot-cavity. This is achieved by surrounding the region immediately downstream of the hot-cavity exit by an RFQ structure and separating this region from the hot-cavity with an electrostatic ion repeller. In LIST-mode, the ion repeller is positively charged and suppresses ions from the hot-cavity (suppression factor $>10^5$) and laser ionization takes place inside the RFQ (RILIS efficiency loss factor 20-50). The LIST can operate in ion guide mode (negative repeller voltage), in which case the performance is comparable to that of hot-cavity RILIS [54, 55].

The **Time-of-Flight Laser Ion Source (ToF-LIS)** proposed by V. Mishin [56] is an alternative approach to RILIS surface ion suppression based on the exploitation of the time structure of the laser ionization process. The ToF-LIS combines a hot-cavity with an increased field gradient, and a shortened LIST RFQ ion guide structure (length equal to the hot-cavity dimensions). The laser ions created inside the hot-cavity drift through the RFQ structure and reach a narrow time focus (few μs) at the end of the RFQ and are extracted by the penetrating field of an extraction electrode. By fast beam gating of the ion beam, synchronized with the time focused laser ion bunch, a selectivity enhancement equal to the laser duty cycle (100 μs), divided by the beam gate width is achieved. This has yet to be implemented at ISOLDE but it is believed to be a promising means of enhancing RILIS selectivity without the efficiency loss associated with the LIST [57].

The application of RILIS using **Doppler-free two-photon excitation** is under investigation for the following reasons: enabling In-Source Resonance Ionization Spectroscopy studies without the resolution limitation or Doppler broadening in the high temperature cavity; isomer selective ionization of elements with a hyperfine structure of less than a few GHz; laser ionization of elements with high-lying first excited states (non metals such as carbon). This method was tested at ISOLDE in 2018, with promising results to demonstrate that the Doppler broadening limitation is indeed overcome by using two counter-propagating laser beams, provided that a narrow linewidth laser is used (Fourier limited linewidth). The relatively low excitation cross-section for the 2-photon transition is somewhat compensated for by the increased spectral brightness of the narrow linewidth laser. The hot cavity (with a mirror placed in the transfer line), the VADLIS (with a mirror surface at the centre of the anode grid) or the

LIST (using a newly developed perpendicular illumination geometry [58]) are all under further investigation as possible solutions to the requirement of reflecting the incident laser back upon itself, within the laser/atom interaction volume. The initial feasibility study of this technique is reported by K. Chrysalidis [59] and the development of the method is the subject of her PhD thesis.

The **Helicon** and **COMIC** ion sources are both low temperature plasma ion sources that rely on RF, rather than electrostatic voltage induced plasma generation. As such they are designed for the ionization of volatile species such as noble gases. Their low operating temperature make them potential candidates for the production of ion beams of heat-sensitive volatile molecules of refractory metals (such as the carbonyls). These ion sources are therefore being tested at ISOLDE in attempts to produce refractory metal beams. Results of ongoing developments will be given in the PhD thesis work of J. Ballof. More information about the Helicon and COMIC ion sources can be found in [60] and [61].

Chapter 4

Insights into the Versatile Arc Discharge Ion Source (VADIS)

The FEBIAD (Forced Electron Beam Induced Arc Discharge) is one of the most widely used ion sources for the production of radioactive beams at ISOL facilities around the world. It was first introduced by Kirchner in 1976, aiming for high ionization efficiencies at low current densities [44]. A different cathode design was adopted at ISOLDE, making the ion source more robust and reliable, leading to longer lifetimes. A series of FEBIAD subtypes, namely MK3, MK5, MK6 and MK7 were born [45, 46]. The subtype choice depended on the ion beam to be produced. In 2009, the VADIS (Versatile Arc Discharge Ion Source) series were introduced and a model for the ionization efficiency proposed [46]. More details are given in subsection 3.1.3.

In the present work, several studies were performed to gain better understanding on how different operational parameters affect the extraction efficiency of the VADIS. With this goal, both experimental and theoretical studies based on simulations using the VSim software were carried out.

Section 4.1 discusses the dependence of the extracted ion beam current and/or efficiency on operational parameters like cathode temperature, anode voltage, ion source magnetic field and ion load within the anode volume. It also reports on the efficiencies measured for a series of metals. Section 4.2 discusses

simulations using the VSim software package to characterize the influence of the ion source magnetic field and charge density on the electrostatic field distribution.

4.1 Experimental studies

The list below specifies the parameters that can be controlled experimentally, the specific operating conditions that change as a result, and the performance criteria affected by these changes. For an optimal operation of an ion source, an understanding of how the different operational parameters affect the performance is essential. The relation between them is complex and difficult to disentangle. For example, for space-charge limited electron emission from the cathode, increasing the anode voltage results in an increased electron density in the source. Furthermore, the change in electron energy has an influence on the probability of electron impact ionization. Together, these change the ion density in the source. Secondary to this, increased electron bombardment of the anode, results in a temperature change of the ion source. Finally, the ion extraction potential and electrostatic potential profile rely on the potential difference between the anode and the grounded extraction plates. Therefore the ion extraction probability is also influenced by the anode voltage. Together, these changes in operating conditions can influence all of the measurable performance criteria of the ion source.

Variable parameters	**Operating conditions**	**Performance**
Anode voltage	Ion density	Ionization efficiency
Magnetic field strength	Temperature	Selectivity
Cathode heating current	Electron energy	Emittance
Buffer gas type	Electron density	Reliability
Buffer gas pressure	Neutral pressure	
Extraction voltage	Electrostatic potential	
Cathode material		
Anode material		
Anode geometry		

In the assessment of the ion source performance, in response to changes of operating conditions when adjusting the variable parameters, an important (and the simplest) performance criteria measure is the efficiency. This can

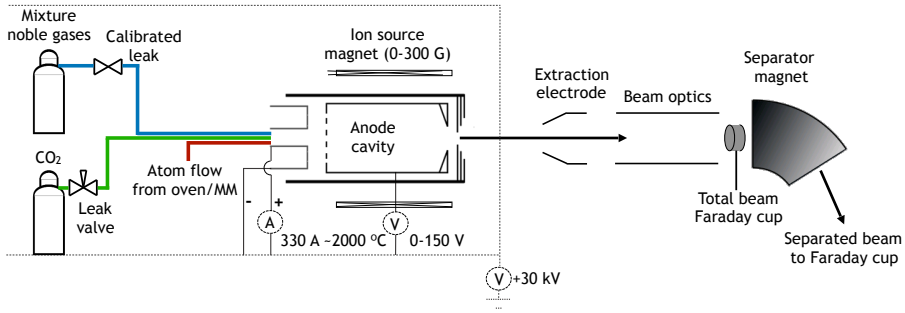

Figure 4.1: Sketch of the ISOLDE off-line laboratory.

be evaluated by an absolute efficiency measurement where the atom sample size that is injected into the ion source is known, or relative measurements based on changes in instantaneous ion rate. The ion rate is measured using a secondary-electron suppressed Faraday cup (FC), with an approximately linear response in the hundreds of fA to mA range. One FC is positioned before the separator magnet to measure the total beam current and another one after the magnet, measuring the separated ion beam current. A layout of the experimental set-up is shown in Fig. 4.1 and the various means of determining efficiency are described below:

Absolute efficiency measurements

- Gas injection with calibrated leak: The ionization efficiency of the noble gases can be measured by injecting into the source a support gas of which the composition is well known. The leak used is 2.6×10^{-6} $mbar\ l/s$. The support gas is a mixture of 40 % helium and 20 % neon, krypton and xenon each (unless otherwise specified)
- Sample evaporation from calibrated mass marker (MM): the ionization efficiency for condensable elements can be measured by attaching a capillary to the rear of the transfer line, containing a well known amount of the element of interest. The sample is evaporated into the ion source and the current of the mass-separated beam I_s is integrated using a Faraday cup. The efficiency can be found as:

$$\epsilon = \frac{\int I_s dt}{e \times N_A \times n_s \times t_{FC}} \tag{4.1}$$

with $e \times N_A$=96485 C/mol^{-1} being the Faraday constant, n_s the molar quantity of the atom inserted and t_{FC} the beam transmission to the Faraday cup.

Relative efficiency measurements

- Evaporation of atoms from an oven or excess mass marker (or atoms evaporating from the materials of the target/ion source assembly): measuring the ion rate enables assessment of relative improvements in the operation of the ion source. The sample size deposited in the oven is not known, but should be large enough to provide a continuous flow of atoms throughout the experiment.
- Gas injection with an adjustable leak valve (uncalibrated): a leak valve can be used to inject slowly and in a controlled manner gas into the ion source. It covers a range of 1000 steps, where 1 is closed and 1000 means the valve is fully open (a Nenion leakvalve F3 was used in these studies).

The determination of the efficiency of the ion source is subject to two main sources of uncertainties. One is the measurement error and the other the uncontrollable variation in experimental conditions between measurements. The former is relatively easy to estimate but the latter is harder to assess and typically results in a scattering of values between measurements.

Amongst the measurement errors we find:

- Beam transmission: From the ion source to the Faraday cup is calculated as the ratio of the sum of the contribution of the separated beams and the total current. These values depend on the background pressure which might be changing during the measurement, or drift of ion source characteristics. A value for the transmission was estimated by averaging values obtained from 5 different mass scans, leading to 76±15% transmission.
- Mass marker preparation: An instrumental error of 1-2 % is introduced when depositing the precipitate in the foil before being evaporated in the oven.
- Calibrated leak: uncertainty in the leak rate when using calibrated leaks for the injection of support gas.

Difficult to control experimental conditions:

- Electron emission: Cooling and heating of the cathode may change the properties of the cathode surface, shape and degradation of the thermal shielding and as a consequence variation in the electron emission.
- Cold spots: Refractory elements can condensate in the colder parts of the ion source (e.g. insulators).

- Chemical reactivity or evaporation: The elements of interest may react with the materials of the target/ion source assembly or evaporate from the MM due to radiative heating from the cathode. They can then start evaporating even before the capillary in which they are placed is heated (temperature at the location of the MM can reach up to 1400 °C [62]). The HSC software [63] can be used to identify when the chemical elements under study enter the gaseous phase. Elements like Hg and Mg start evaporating at rather low temperatures, therefore the reported efficiencies are underestimated.

4.1.1 Dependence on the cathode temperature

The standard procedure for optimizing the ion source is to heat the cathode until a saturation of the noble gas efficiency is reached. Under these conditions, it can be assumed that the electron current is optimized for maximum ionization efficiency. Typical curves showing the dependence of the efficiency on the cathode temperature are given in Fig. 4.2 for the noble gases helium, neon, krypton and xenon. The drain current (directly related to the electron current drawn from the cathode) and the total ion beam current (measured before the analyzing magnet) are also represented.

For a given element, ignoring volatility concerns and space charge limitation of the extracted ion beam, a further increase in cathode heating will not improve the efficiency, however it will accelerate the cathode ageing, reduce the ion source lifetime and increase susceptibility to other failure mechanisms (such as anode/cathode contact due a thermal distortion of the cathode).

In Section 3.1.3, equation 3.5 is the efficiency model for the FEBIAD, taken from [19]. Here we see that a factor 'f' is used to account for the difference between the calculated ionization efficiency due to electron impact and the experimentally observed ion source efficiency. Plotting this f-factor as a function of different variables (temperature, electron current, chemical element, pressure) offers an insight into the parameters affecting underlying ion source dynamics that are not taken into account in the efficiency calculation. For example, in [19], the f-factor has been interpreted to be a geometrical factor, relating to the ratio of 'active' (fraction of the total volume from where the generated ions are successfully extracted) to total volume of the ion source. Since this ratio is based on the field map of the anode, and since all ion species will be subject to this same field distribution, the f-factor should therefore be the same for all elements.

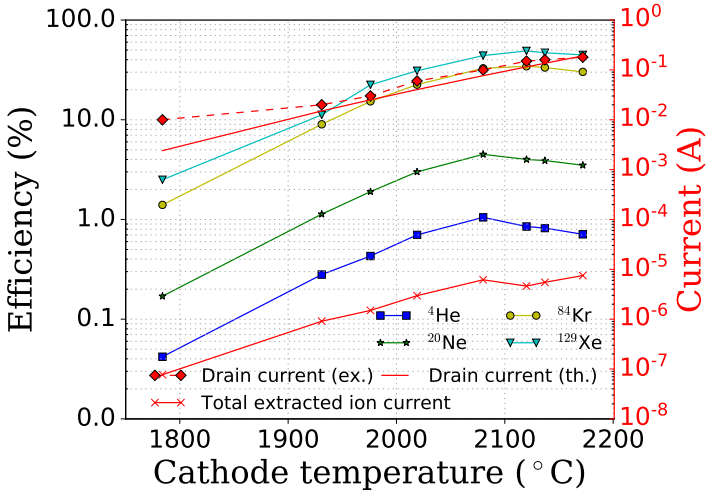

Figure 4.2: Efficiency of the noble gases as a function of the cathode temperature. The anode voltage was kept at 125 V. The red curves (values on the right-hand side axis of the figure) correspond to the drain current, both experimental and theoretical (the latter calculated according to the Richardson-Dushman equation for thermionic emission) and total ion current.

In Fig. 4.3, we see that this is not the case. Even for the noble gases, where we can safely assume no temperature-dependent wall sticking, the f-factors differ by almost an order of magnitude. Nevertheless, when plotting them as a function of the cathode temperature, we see that the influence of cathode temperature on f-factors exhibits no evidence for chemical or mass dependence, consistent with a hypothesis that the electron density in the ion source influences the ratio of 'active' to 'inactive' volumes inside the ion source. Furthermore, f actually decreases with increased cathode temperature. This is expected if the corresponding increase in electron current results in a deepening of the potential well in the ion source, thereby increasing the size of the 'inactive' volume (this effect will be discussed in more details in Section 4.2). Note that this is also consistent with the experimentally observed saturation of ionization efficiency with increased cathode temperature.

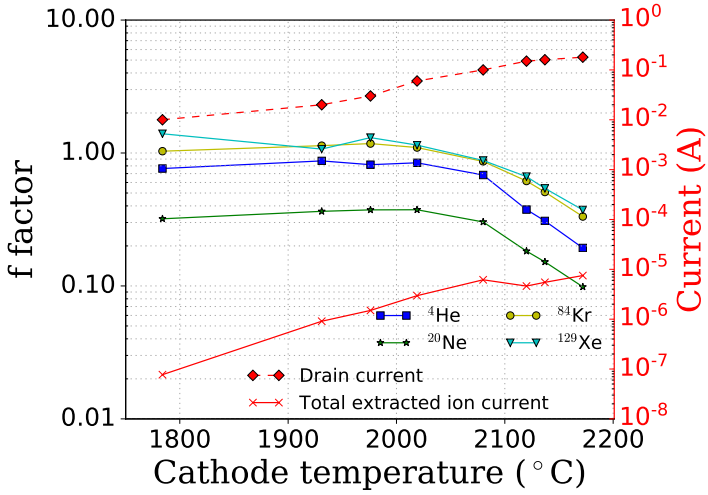

Figure 4.3: f-factor calculated using equation 3.5, for the efficiencies shown in Fig. 4.2.

4.1.2 Dependence on the anode voltage

FEBIAD-like ion sources are usually operated at anode voltages in the range of 100-200 V. This voltage defines the energy of the electrons entering the anode volume. The dependence of the extracted ion current on the anode voltage for gallium and krypton is shown in Fig. 4.4a.

The following regions can be identified in Fig. 4.4a and Fig. 4.4b:

I. The electron energy is too low to cause electron impact ionization. In this region, the presence of surface ionized Ga^{+} can be identified while surface ions are not present for Kr^{+}.

II. The electron energy is high enough to cause ionization but other factors are not optimal (e.g. mean electron energy too low, poor ion survival, poor extraction). The scan of the anode voltage from higher to lower values exhibit a hysteresis (red curve), where for this same region good operation conditions can be achieved.

III. Optimal operation conditions

The following behaviour can be identified in Fig. 4.4a and Fig. 4.4b:

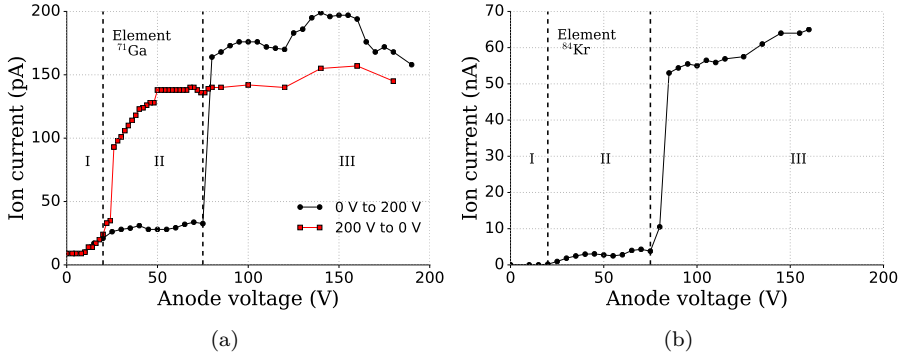

Figure 4.4: Mass separated ion current as a function of the anode voltage (ion source magnet ON). (a) For gallium. Two curves were taken: first with voltage increasing from 0 to 200 V; second one with voltage decreasing from 200 to 0 V. (b) For krypton.

1. When increasing the anode voltage from 0 to 200 V, a sudden increase in ion current occurs at ∼75 V. This onset, or threshold effect, was systematically observed when slowly increasing the anode voltage (no sudden variation in the electron current was observed). This is strong evidence of the ion source performance being governed not only by the electron impact ionization process, but also by the plasma conditions inside the anode cavity. The threshold value (∼75 V in this case) was observed to vary depending on the ion source unit used (different operating temperature and cathode emission properties, creating different electrostatic potential distribution within the source with direct impact in the extraction properties).
2. The characteristics of the anode voltage scan shows hysteresis when the voltage scan is done from a higher to a lower value (red curve). The extracted ion current value (or plasma properties) is maintained over a longer operation voltage range.
3. The ion current onset is independent of the ionization potential of the element: it occurs at ∼75 V for both elements.

A similar effect to the sudden jump in ion current observed in Fig. 4.4 has been reported when studying the discharge characteristics of a relatively low pressure (10^{-4} - 10^{-5} mbar) argon plasma [64]. The phenomenon of hysteresis has also been observed, and the existence of a magnetic field has been reported necessary for this sudden jump and hysteresis to occur. These effects have

been seen when using dedicated discharge devices for plasma physics studies [64, 65, 66]. The reproduction of the curves shown in Fig. 4.4 represents one of the main challenges in the ion source modelling field. Sections 4.2.1 and 4.2.2 give an insight into electron and ion dynamics that could give rise to such a behaviour for the FEBIAD.

Figure 4.5 presents the dependence of the anode drain current as a function of the anode voltage for different cathode temperatures.

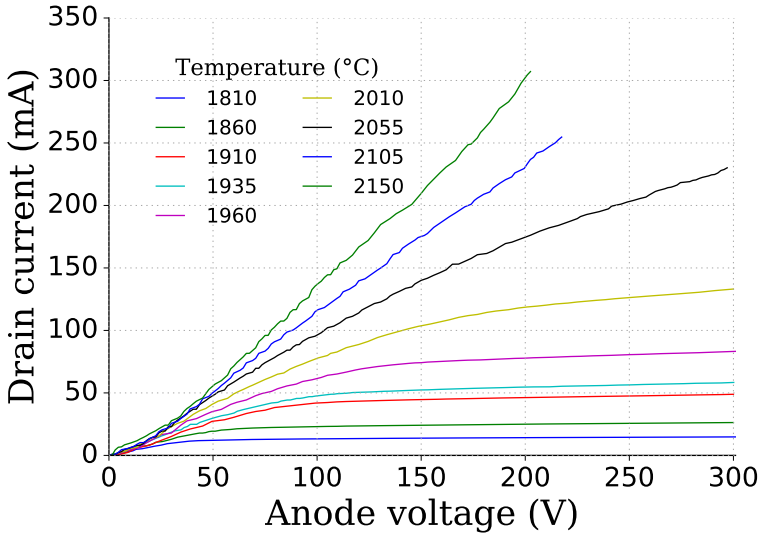

Figure 4.5: Experimental measurement of the cathode current as a function of the anode voltage for different cathode temperatures.

At higher temperatures, in the voltage range studied, the electron current is said to be space-charge limited and it is governed by the Child-Langmuir law Eq. 3.3 (higher voltage results in higher electron current). At lower temperatures, when the voltage becomes large enough to draw all electrons from the surface, the electron emission is limited by the electron production at the cathode (temperature-limited region), and the relationship between anode current and voltage is given by the Richardson-Dushman equation as stated by Eq. 3.4.

By taking these curves at different cathode-anode grid distances, the electron flow into the ion source can be optimized for improved performance of the ion source. These curves provide information about the electron density inside the ion source, which will be used as an input parameter for simulations performed with the VSim software package in Section 4.2.

4.1.3 Dependence on the ion source magnet

An axial magnetic field is applied in the anode volume region by regulating the current of the coils of a fixed solenoid that surrounds the ion source. With a magnetic field strength in the range 0-0.03 T, and since the electron mass is 3-5 orders of magnitude smaller than that of the ions, the mean path of flight of the electrons is affected, but the effect on the ion trajectory is negligible. As a consequence, for a given electron flux to the anode, the probability of interaction of an electron with an atom is enhanced.

The ion current dependence on the ion source magnetic field was partially studied in [19]. It was observed that the dependence of the extraction current on the ion source magnetic field is a succession of maxima and minima. The ratio of maximum to minimum ion current in this investigation was typically 2:1. This behaviour was reproduced [67] using the COMSOL Multiphysics® software package [68].

An investigation into the characteristics of the anode scans with different magnet settings reveals some interesting features of the ion source operation. For example, Fig. 4.6 shows an anode scan for ^{84}Kr under otherwise identical experimental conditions, with and without the source magnet ON. If the ion source is operated below, but close to the threshold anode voltage value seen in Fig. 4.6, the sudden efficiency jump can be irreversibly induced by adjusting the source magnet setting. In this case, at optimal anode voltages (above 80 V), the benefit of the magnet is seen by the increased ion rate for ^{84}Kr (red line). However, below 80 V, the presence of the magnetic field is actually detrimental.

As it is understood, the presence of the magnetic field results in an increased path length for the electrons. On the other hand, the corresponding increase in electron density in the ion source gives rise to a deeper potential well where ions can be trapped. This could increase the mean residence time of an ion inside the ion source thereby increasing the probability of recombination. Clearly, these processes are competing and in the low voltage range detrimental effects in terms of extracted ion current (ion survival or ion extraction probability) outweighs the increased ionization rate due to an increased electron path length.

If the magnet is tuned at each voltage value for maximum ion extraction, a similar behaviour to that observed when the magnet is switched off is seen. A smooth transition to optimal operation conditions is observed. Since the data collected in these two cases (magnet OFF and magnet optimized for maximum ion extraction) corresponded to different experimental conditions (e.g. different cathode temperature and oven heating), it is not possible to determine the impact in terms of efficiency of these modes of operation.

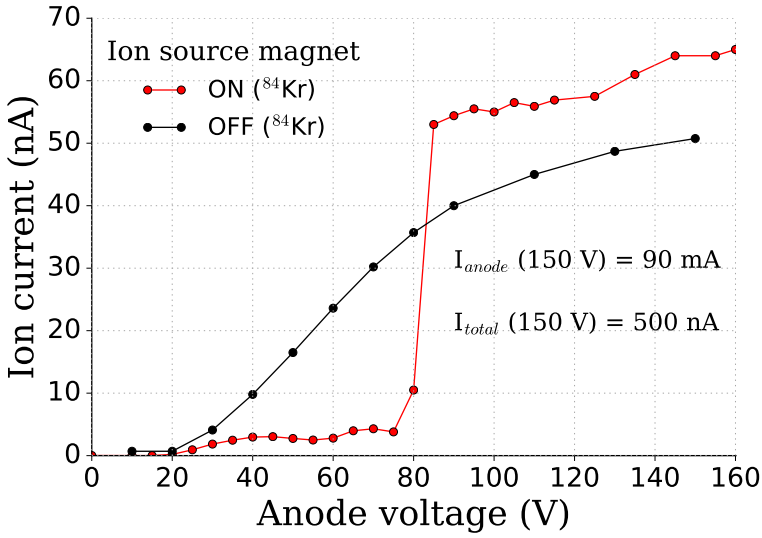

Figure 4.6: Scan of the anode voltage with ion source magnet ON and OFF at 2000 °C. Both curves were taken under identical experimental conditions.

4.1.4 Dependence on the ion load capacity

In the present section we study the influence of the ion load within the VADIS on the ion beam output. Because of the unselective nature of electron impact ionization, it is not possible to independently investigate the dependence on the neutral gas load. However, this will be investigated in Chapter 5, where the VADIS is operated in RILIS-mode and electron impact-ionization doesn't take place.

The gas used in the study was CO_2 and the following mechanisms for the formation of CO^+ were considered:

- Dissociative ionization of CO_2: $CO_2 + e^- \rightarrow CO^+ + O + 2e^-$.
- Thermal dissociation or dissociation by adsorption/chemical reaction of CO_2 when interacting with the surfaces of the target/ion source assembly resulting in CO. CO^+ is then formed by electron impact ionization of CO.

Release efficiencies of CO from a target/ion source assembly were studied in [69]. This study shows that the majority of the CO, in the transformation

from CO_2 to CO comes from a reaction that takes place inside the ion source. Calculations using the HSC software [63] show that the CO_2 that arrives in the ion source reacts with molybdenum (the anode body is made out of Mo) forming CO which gets then extracted as CO^+. More details can be found in Ref. [69].

The role that impurities in the FEBIAD play in the total efficiency of the ion source was discussed by R. Kirchner in [70]. More specifically, Kirchner observed that by reducing the N_2^+ (W_i=15.58 eV) beam output of the FEBIAD the efficiency and stability of the ion source decreased. A similar effect was observed for the case of CO^+ (W_i = 14.0 eV). It was then believed that for an efficient and stable operation of the FEBIAD the presence of impurities at a level where these are seen as few μA ion beam, influences the ion source performance. This is due to possible charge transfer mechanisms when collisions of the elements of interest with these molecular ions take place.

In this work, CO_2 molecules were released into the ion source using a leak valve (the pressure in the target sector of the front-end was kept just below the interlock value of 5×10^{-5} mbar). The leak valve was then closed and the extracted beam current for the noble gases He, Ne, Kr, Xe (W_i = 24.6 eV, 21.6 eV, 14.0 eV and 12.1 eV) was measured at several occasions as well as the CO^+ (W_i = 14.0 eV) output beam. These data were taken over a total period of 4 hours. The noble gases extracted beam current was plotted as a function of the CO^+ beam current as shown in Fig. 4.7.

To some extent, the findings of Kirchner are confirmed; for elements with lower ionization potential than that of CO, with a sufficient CO^+ ion load, a positive effect on the ionization efficiency takes place (as long as the ion source capacity limit is not reached). This is attributed to the additional ionization mechanism of charge exchange collisions with the lower W_i elements. An increase in efficiency for Xe is due to the energy advantage in the formation of a Xe^+ by a CO^+ molecule collision with Xe: $W_i(\mathrm{Xe}) < \mathrm{E}_A(\mathrm{CO}^+)$.

The rapid decrease in efficiency for elements with a higher W_i than the dominant species (in this case the dominant species is the deliberately injected CO_2, but in the case of a target/ion source assembly it could be a source of atoms evaporated from the target material), is cause for concern if trying to operate the ion source with ion loads greatly exceeding several μA. Indeed, high ion current operation is exactly what is required for next generation ISOL facilities and the medical isotope extraction process at MEDICIS.

For example, at ISOLDE, in on-line use, a well outgassed target operates roughly in equilibrium (atom release=in-target production). At MEDICIS on

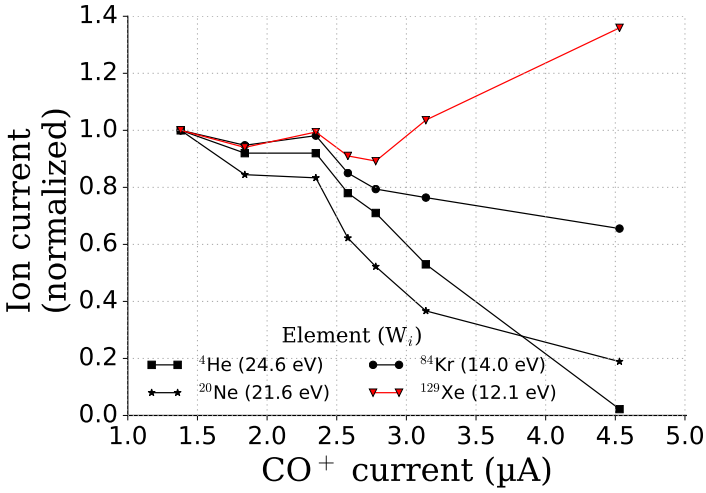

Figure 4.7: Normalized extracted ion current for the noble gases as a function of the extracted CO^+ ion beam.

the other hand, the target works off-line. The radioisotope production may take place inside a cold target for many days but the extraction of the radioisotopes may take place in a fraction of this time. Consequently, the required ion throughput during this extraction may exceed that of an ISOLDE target by an order of magnitude or more.

Figure 4.8 shows the extracted CO^+ ion current as a function of the CO_2 injection (though what is measured is the CO, monitored on a residual gas analyzer (RGA) attached to the side of the vacuum chamber, downstream of the anode exit hole). The actual neutral pressure in the source was not measured directly. These values should be considered relative measurements on the assumption that the pressure measured in the RGA is proportional to the neutral pressure within the ion source.

The maximum current that can be extracted under space-charge limited conditions is given by the Child-Langmuir equation as follows:

$$I[A] = 1.71 \cdot 10^{-7} \cdot \sqrt{\frac{Q}{M}} \left(\frac{a}{d}\right)^2 V^{3/2}[V] \tag{4.2}$$

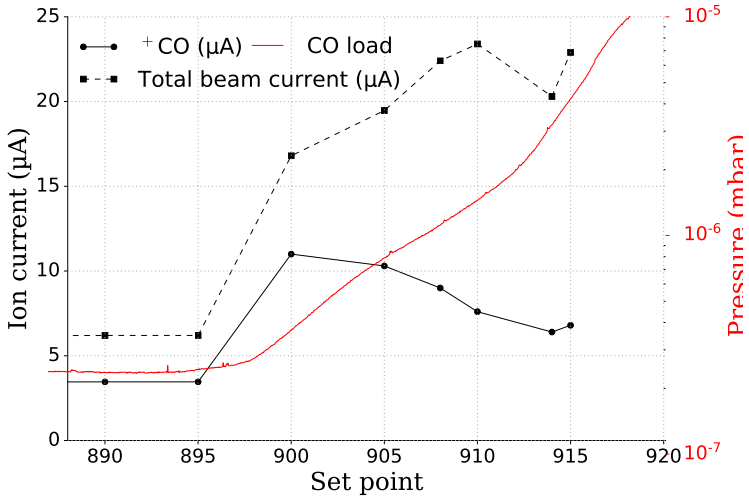

Figure 4.8: Extracted CO^+ ion beam and total current as a function of the CO gas load in the VADIS. The anode voltage is set to 100 V. The set point labelled on the x-axis indicate the position of the leak valve, where 1 is 'closed' and 1000 means 'fully open'

We can use this formula as a guide to the upper limit to the extractable ion current from the ion source. If CO^+ was the only species present in the ion source, applying equation 4.1.4 ($M(CO)$=28, aperture radius a=0.75 mm, gap extraction hole-extraction plates d=1 mm, Q=1 and V=100 V), the space-charge limited CO^+ beam current is 18 μA. In actual fact, despite an increasing CO supply (red curve in Fig. 4.8), the CO^+ ion current saturates at 5 to 10 μA (black curve in Fig. 4.8). This is because CO^+ is not the only ionized species in the ion source. In fact, the total extracted beam current saturates at $\sim$23 μA which is consistent with expected space-charge limitations of the source.

In another experiment, jointly performed with the Paul Scherrer Institute (PSI [71]) (with the goal of determining evaporation rates and transmission of different manganese salts), the ion load capacity of the VADIS was determined using manganese instead of CO. A graphite block was impregnated with a manganese solution and evaporated into the ion source. A gas mixture containing Xe, Ne, Ar, He, Kr (20 % each) was injected into the ion source and their current, together with the CO^+ and total ion current were monitored as the Mn was evaporated into the ion source volume as shown in Fig. 4.9.

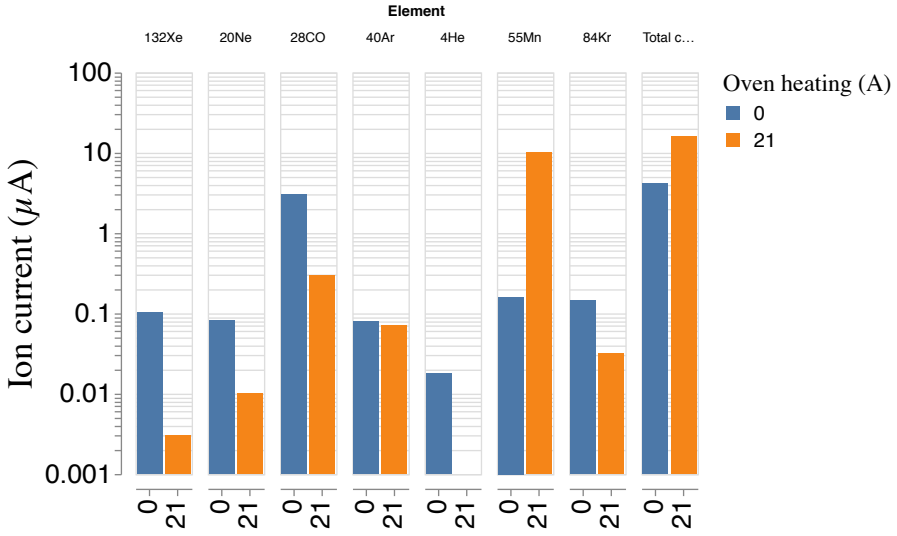

Figure 4.9: Extracted ion beam for different elements at the start of the measurement (blue bars-Mn oven cold) and at maximum Mn ion extraction (orange bar-oven hot). A decrease in efficiency for the main elements contributing to the total beam is observed under the presence of high Mn beam current. A manganese beam of about 160 nA is present at the beginning of the measurement (oven cold) due to indirect heating.

The blue bars correspond to the ion current measured for the different elements when the oven heating was set to 0 A. The orange bars indicate the ion current after the oven has been heated up, therefore the Mn^+ and total ion current are above 10 μA. The latter values correspond to the extracted beam once the total extracted current and Mn^+ ion beam, even when heating further the mass marker, didn't increase any longer. The main contribution to the total beam current was the ^{55}Mn (10 μA out of 16 μA total beam current).

Using the same approach as for CO, the maximum achievable extracted current for ^{55}Mn ions only is 12 μA at 100 V applied to the anode walls. Indeed what we see is that as the experimentally measured current reached this value, the efficiency for all the elements measured decreased, indicating that the space-charge limit for ion extraction has been reached. This is further evidence that, to maintain the efficiency for a chosen species, the ion source should be operated under conditions in which a limitation imposed by the extracted total beam current is not present.

4.1.5 Ionization efficiency measurements

Absolute efficiency measurements of the metallic elements gallium, mercury, magnesium, tin and manganese were performed at the ISOLDE off-line separator using the VADIS ion source. For this purpose, a calibrated mass marker was used. The ions created by electron impact ionization within the ion source are then extracted and the current of the mass-separated beam is integrated using a Faraday cup. An example for the case of a mercury beam is shown in Fig. 4.10.

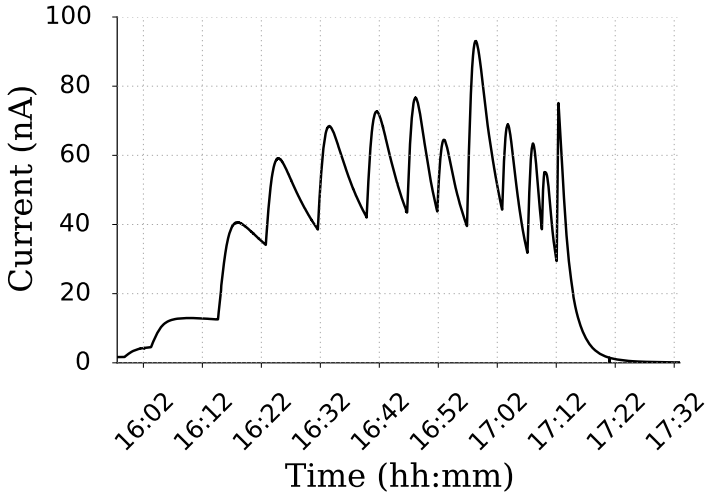

Figure 4.10: Determination of the efficiency of mercury off-line. The extracted current is shown as a function of the necessary time it took to evaporate the sample (x-axis). The 'oscillations' observed correspond to the heating of the mass marker to promote the release of Hg atoms. The measured current is integrated to determine the ion source efficiency.

Table 4.1 shows the experimentally measured efficiencies and the measurement conditions. The efficiencies were measured using 4 different ion sources with the same design (slight modifications may arise during the assembling process, therefore the different units were labelled as 1,2,3 and 4 as indicated in table 4.1). The efficiencies as a function of the cathode temperature are also plotted in Fig. 4.11. The values have been corrected for transmission through the separator ($\sim$76 %).

For the noble gases, it is systematically observed that the efficiency is higher the heavier the element is, regardless of the ionization potential. This is due to

Table 4.1: Experimental efficiencies measured at the ISOLDE off-line laboratory. Unit # refers to the target/ion source assembly used. T is the cathode temperature, A the mass of the element, W_i the ionization potential, V_a the anode voltage, I_a the electron (drain) current, ϵ the ion source efficiency and f the f-factor as defined in equation 3.5. The transmission through the mass separator was 76 %.

Element	Unit #	T (°C)	A	W_i	V_a (V)	I_a (mA)	ϵ (%)	f
Ga	1	2020	71	5.99	125	80	17.7	1.79
	2	2110	71	5.99	150	390	12.4	0.58
	2	2020	71	5.99	150	120	6.1	0.70
Hg	1	2020	202	10.44	125	70	9.2	1.01
	3	2075	202	10.44	98	80	4.0	0.22
	2	2110	202	10.44	150	370	5.1	0.25
	2	2110	202	10.44	150	390	21.4	1.07
Mg	3	2035	24	7.65	95	70	6.2	1.28
	3	2075	24	7.65	103	90	12.6	1.82
Sn	3	2035	120	7.34	100	50	7.8	0.27
	3	2075	120	7.34	100	90	1.5	0.05
Mn	4	1835	55	7.43	100	5	1.3	1.64
	3	2035	55	7.43	100	50	18.7	2.57
	3	2075	55	7.43	100	80	10.6	0.98

the fact that the atoms spends a longer period of time in the ion source volume, which increases the probability of getting ionized.

The observation of a similar trend for metallic elements was attempted with the measurements described in this section. It is seen that the scattering of the efficiency values for a given element is of the same order as the variation in efficiencies measured for the different elements. For this reason, it is not possible to draw a conclusion as to the properties of the element governing the achievable efficiency (mass, ionization potential, vapour pressure, atomic radius, etc). One reason for this is the inability to perform successive measurements under identical experimental conditions and with the same ion source. Understanding the element dependence of the ionization efficiency therefore requires a different experimental approach. One could consider a dual ion source assembly such as the one described in [72] which could enable a known current of a particular

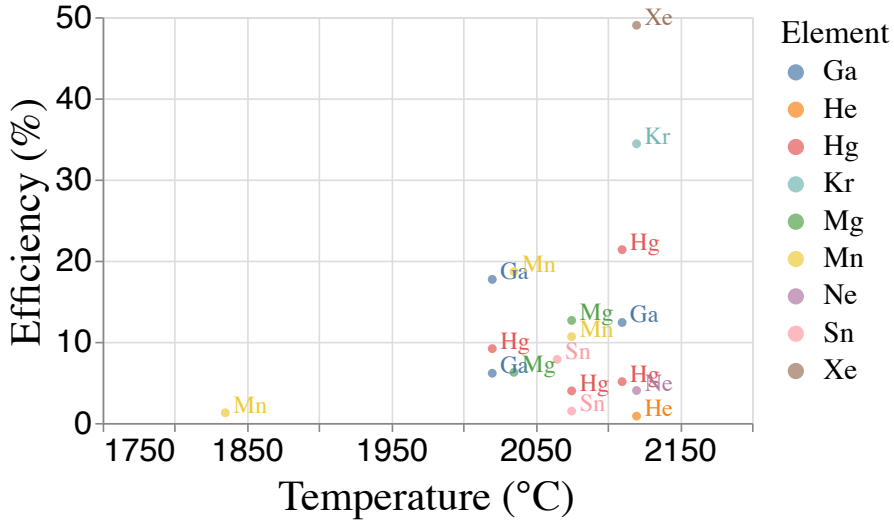

Figure 4.11: Experimentally measured efficiency of metals at the ISOLDE off-line laboratory as a function of the cathode temperature. The efficiency for the noble gases at 2125 °C are also shown, taken from 4.2.

element to be injected in the ion source and then compared with the extracted current of that element from the ion source.

As for the f-factors, these values are calculated from equation 3.5, which doesn't take into account recombination mechanisms, element volatility, surface ionization probability and reactivity with anode materials just to name a few, which would contribute to the large spread in the computed values.

4.2 VSim: A Particle-in-Cell software for the study of the VADIS ion source

The VSim software package [13, 14], which uses a particle-in-cell approach for the modelling of, for example, electron and ion distributions, has been used to gain an insight into the following aspects of the VADIS ion source: field map inside the anode volume; the electron charge density distribution; and the time structure of the ion beam extracted after laser ionization. The evolution of these under varying experimental conditions such as anode voltage, magnetic

field strength, electron current/cathode temperature, extraction voltage, ion density is investigated. The aspects relating the operation of the ion source in RILIS-mode are discussed in Chapter 5.

4.2.1 Influence of the magnetic field on the charge density distribution

Simulations with and without a magnetic field were performed to study its effect on the charge density distribution. In the simulation, electrons are emitted from the wall opposite to the extraction aperture, emulating the cathode emission, with an initial energy of 150 eV. The anode walls are biased positively (150 V, to match the electron injection energy), therefore the electrons enter the anode volume with enough energy to cause ionization by electron impact. The simulation assumes an argon-only environment with a pressure of 10^{-2} mbar inside the anode volume. This would allow an ion creation rate high enough to provide sufficient statistics to study the charge density distribution, while still maintaining simulation timesteps that are suitable for ion tracking. Elastic and inelastic collisions of the electrons and argon gas are considered, as well as electron impact ionization of the argon. The different particles (or species) considered in the simulation are:

- Primary electrons: electrons emitted from the hot cathode that enter the cavity due to the positive 150 V applied to the anode walls.
- Argon ions: Ar^+ as a result of electron impact ionization, left in the 1+ charge state ($\sigma(+)=2.4{\cdot}10^{-16}\text{cm}^2$, $\sigma(2+)=4.9{\cdot}10^{-17}\text{cm}^2$ at 140 eV [73]).
- Recoil electron from ionization: electrons produced by electron impact ionization in the reaction $e^- + Ar = Ar^+ + 2e^-$.
- Secondary electrons: electrons emitted from the anode walls after the impact of primary electrons with it.
- Wall electrons: Electrons emitted from the anode walls, simulating thermionic electron emission due to the fact that the anode is radiatively heated by the cathode.

To carry out the simulations, we have used a special work-flow to allow for meaningful timescales for ion dynamics to be studied. The simulation is left to run for long enough for the electron population to saturate (e.g. number of electrons that enter the volume equals the number of electrons lost in the

walls), with the electrostatic field being computed throughout the evolution of the electrons simulation. At this point, the dominant species in the simulation are the incoming electrons from the cathode (primary electrons), exceeding by several orders of magnitude the other species mentioned above.

The field distribution established when the electron saturation is reached is effectively a convolution of the electron charge density distribution and the electrical field generated by the relative potentials of the anode, extraction plates and extraction electrode. The charge density distribution of the electrons, with and without a magnetic field, and for two different values of the electron current are compared. An homogeneous axial magnetic field of 0.03 T was considered. The results are shown in Fig. 4.12. By comparing the figures in the left hand side (B=0.03 T) with the ones in the right hand side (B=0 T) in Fig. 4.12, we can deduce that the magnetic field provides confinement of the electrons, thereby increasing their path length across the anode, and resulting in a more uniform electron charge density within the anode volume. As a result, an increase in ionization efficiency is expected (as is also observed experimentally).

This simulation was performed for two different electron current values: 40 mA and 100 mA. In both cases, the steady-state electrostatic potential includes a central potential well, that can act as a trap for ions created at this location. This 'trapping' region was discussed in [46] as the 'inactive' volume of the ion source. In fact, the difference in overall ion source efficiency between the MK5 and MK7 FEBIAD variants was shown to correspond to the different ratios of the 'active' to 'inactive' volumes of these two FEBIAD geometries.

When considering a 100 mA electron current, a cloud of electrons is formed at the rear of the ion source as seen in Fig. 4.12 (panel **e**-left). As can be seen in the field map, this results in an electron-suppressing negative potential barrier. The electron charge density (panel **e** in Fig. 4.12) therefore is minimized in the center of the ion source (at the location of the 'inactive' volume - located around the blue–shaded region of panel **d** in Fig. 4.12) and maximized in the 'active' regions of the ion source, closer to the anode walls. Panel **e** does not give information on the electron energy distribution but, the simulation does enable the corresponding ion density distribution to be displayed (panel **f**). This assumes a uniform distribution of atomic vapor, and so is therefore effectively showing the convolution of the electron density and energy distributions. If such a scenario depicted in panel **f** could be sustained in the steady-state, we can imagine this would be an ideal ion source operating mode, resulting in a significant enhancement in ion extraction probability, due to the exclusive creation of ions inside the active volume.

In this respect, the simulation provides an insight into ion source behaviour

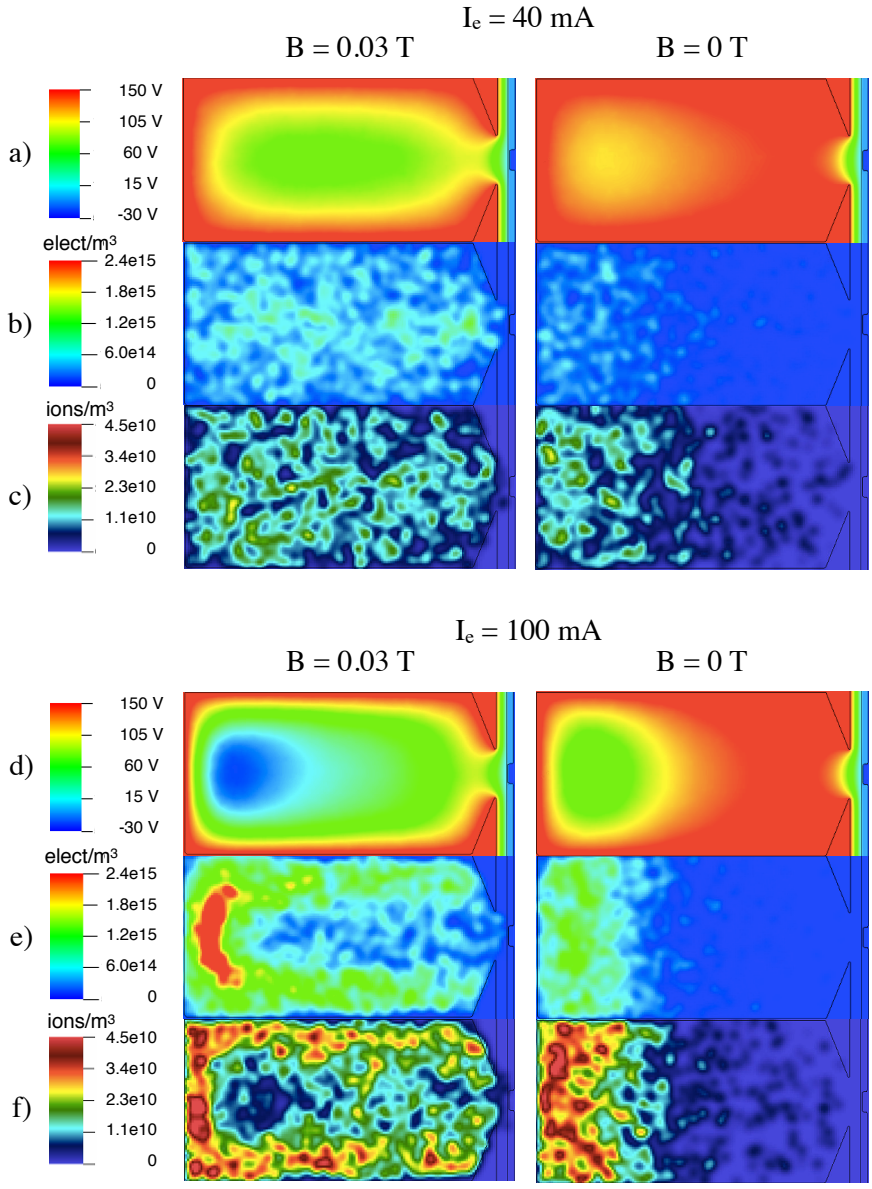

Figure 4.12: Field map, electron and ion density distributions with (left-hand side) and without (right-hand side) the presence of the ion source magnetic field. The results are also shown for two different electron currents: 40 mA (panel **a**, **b**, **c**) and 100 mA (panel **d**, **e**, **f**).

that may help in explaining the experimentally-observed (Fig. 4.4) jump in ionization efficiency and indicate how the hysteresis could occur as a result of a sudden change in ion density and distribution. It is notable also that this operating regime is not achievable without the application of the axial magnetic field, consistent with the experimental data shown in Fig. 4.6.

Further investigating this would require a continuation of the simulations to identify the range of conditions (values of V, B and Ion current) required to generate the favourable ion density distribution shown on the left-hand side of panel **f** of Fig. 4.12, which would be seen experimentally as the onset of the threshold. After the onset of this threshold, the sudden change in ion population and distribution may constitute a significant enough change in experimental conditions, to result in the observed hysteresis effect. This is the subject of the next subsection, where it is seen that the initial electron-dominated conditions described here, evolve with time as the ion density inside the anode volume increases.

4.2.2 Influence of the ion population on the electrostatic field distribution

Here we discuss the influence of the ion population on the electrostatic field distribution. We have so far considered an electron-dominated regime. But in reality, ions present in the volume as a result of the different ionization processes modify the field map, and this becomes non-negligible at an ion density that approaches the value corresponding to a total extracted ion beam of several μA.

Ideally, a simulation would include and couple all physics phenomena taking place in the ion source: electron and ion motion, ionization, recombination, secondary electron emission (from the wall/collisions), thermal electron emission amongst others. But the charge to mass ratio of the electrons is 3-5 orders of magnitude smaller than that of the ions. As a result, the time-scales of the ion and electron dynamics are very different.

To overcome the computational issue, the simulation is split in two main steps as follows:

Step 1 - Electrons are launched from the back of the ion source as described in Subsection 4.2.1. As they enter the ion source volume, the ion population increases as a result of electron impact ionization. The simulation is left to run for long enough for the electrons to equilibrate. The information collected in

this step (e.g. ion population distribution, electrostatic field distribution) are used as an input for step 2.

Step 2 - A new simulation is run in which the ions generated in the first step of the simulation are left to move in the electrostatic field previously defined by the electron distribution and the external fields. The electron dynamics are not considered in this step. This enables the simulation to run with timesteps that are appropriate for ion, rather than electron, dynamics. A new charge distribution for the ions is obtained. At this point, maintaining the same ion density distribution, the actual ion density is uniformly increased by adjusting the number of particles per macro-particle in the simulation. This is done to ensure that a non-negligible number of ions are considered in the next iteration, without necessitating the use of impractically long simulation times. This is then used as a starting point for the next iteration (returning to *Step 1*).

With this approach, it is not necessary to simultaneously use a timestep short enough to resolve the electron dynamics and also simulate for a long enough duration to track the ions from the anode volume out to the extraction electrode.

The number of ions and electrons as this iterative process takes place is shown in Fig. 4.13. It can be seen that as the ion number increases, the electron number keeps increasing as well. This is because the positive charge of the ions compensate for the space charge of the electron population, allowing a higher number to enter the ion source volume.

Then we proceed to study the electrostatic field, electron and ion distributions at 5 different stages as highlighted in Fig. 4.13: t_1, t_2, t_3, t_4, and t_5 for an electron current of 100 mA. This will show how it evolves as the ion number increases. The five stages are depicted in Fig. 4.14.

We start (at t_1) with the electron-dominated system, similar to that seen in Fig. 4.12 (**d**,**e**,**f**). After each time-step (each of roughly 12 μs), the ion distribution influences the potential field map, and in turn the electron density and energy distribution. We see that, as the iterative simulation progresses, the minimum of the axial potential moves towards the center of the ion source and eventually, at t_5 is almost eliminated, and a smooth slope or ion 'funnel' is established. In this case, electrons penetrate further into the ion source and lose less energy in doing so, resulting in a more uniform ion density distribution.

Further simulation time would confirm the expectation that, once completed (possibly requiring several more time steps), a complete transition to a downward sloping longitudinal potential will be made. This would result in a

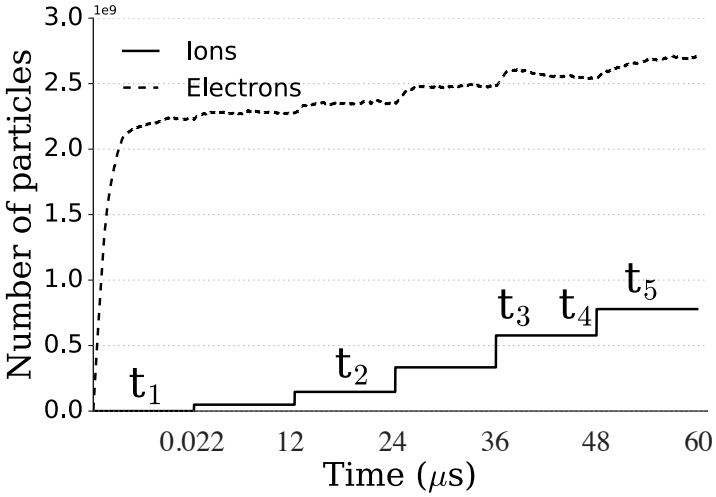

Figure 4.13: Number of electrons and ions in the ion source volume. The ion number is 'boosted' during the iterative process to gain an insight on how the electron number and electrostatic field distribution evolve.

steady-state operation of the ion source, because newly introduced ions then efficiently drain out of the anode volume, analogous to water filling a bath to the level of the overflow drain. In this mode, we can expect that the ionization efficiency is optimal since the residency time of the ions is minimized while the extraction probability is maximized. If this is indeed the case, it should be possible to experimentally determine this time from ion source 'switch on', t_{on} to 'full ignition', t_i, where the ionization efficiency is at its maximum. For example, if, as is suggested here, this process is entirely dependent on the filling of the potential well with ions, it must be dependent on the neutral flux of the species being ionized.

Testing this experimentally could be rather simple: for example, using a time-resolved (ns resolution) ion detection system (an MCP or channeltron), the ion bunch arrival time downstream of the ion source after the onset of a fast (nanosecond-range) rise-time anode voltage pulse could be recorded. As an additional measurement, if the anode pulse duration and repetition rate is changed (from Hz to kHz) while maintaining a fixed duty cycle (20 % anode on, 80 % anode off for example), the influence of the anode pulse length on the ion rate could be monitored using the Faraday cup[1]. Any deviation from a

[1]The experimental setup described here is already available at the ISOLDE off-line separator, and has been previously applied for FEBIAD pulsing tests [74]

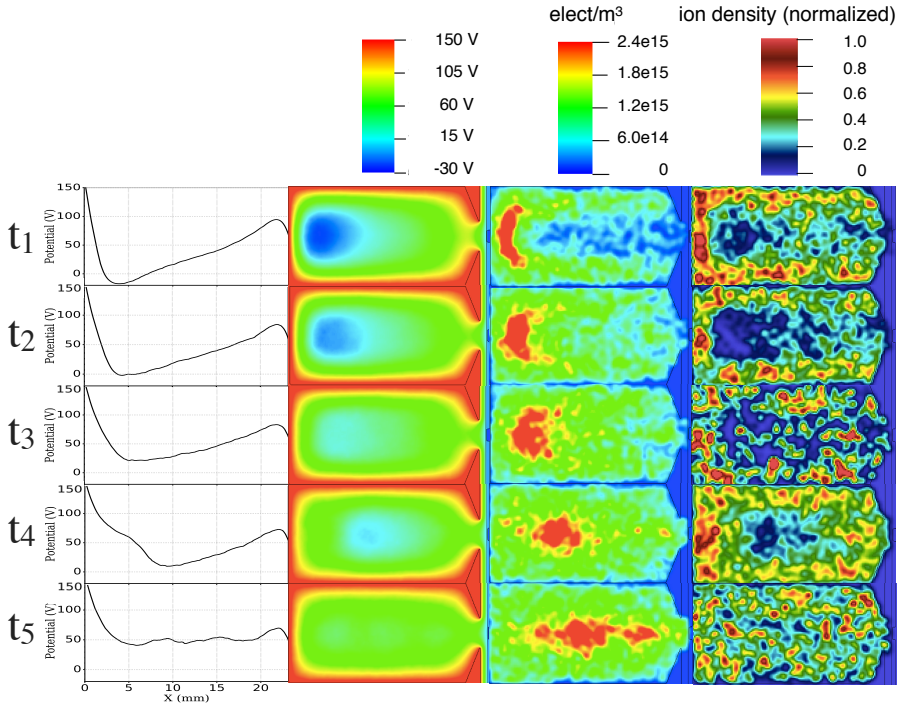

Figure 4.14: Evolution of the electrostatic field, electron and ion distribution as the ratio of ions and electrons in the ion source varies (see stages shown in Fig. 4.13). The first column shows the potential along the axis of ion source.

measurement of 20% of the ion current with a fixed voltage anode, would then be attributed to the need for a FEBIAD ignition time. This same measurement could be performed under different experimental conditions: anode voltage, neutral species, magnetic field strength, and neutral pressure.

Coming back to the subject of the hysteresis in the anode voltage plot of Fig. 4.4, it can be imagined that, once the steady-state conditions are reached and the ion extraction rate equals the ion creation rate, the system becomes more resilient to parameter changes (such as the anode voltage). However, it may be that, to reach this state in the first place, a certain minimum anode voltage is required. This can be investigated in an extended simulation campaign by performing the iterative study at several values of anode voltage, with the goal of determining the minimum voltage, V_f (forward) required to enable t_i to be reached. In the same way, a voltage V_b (backward) could be determined by continuing the simulation in Fig. 4.14 for more time steps but with a range

of lower anode voltages. If V_b (backward) is less than V_f (forward), hysteresis is shown to be present in the system.

Finally, going back to the experimental study, if t_i can be determined using the anode pulsing test for a given ion source and set of experimental conditions and for a range of anode voltages, then a comparison of anode voltage scans performed in a way that ensures the anode voltage pulses either always shorter or always significantly longer than t_i could be performed. Depending on the appearance (or not) of the characteristic hysteresis curve, we could then understand which of the two scenarios presented here (electron dominated, or ion-influenced) are most relevant to describing the FEBIAD operation.

Chapter 5

The Versatile Arc Discharge and Laser Ion Source (VADLIS)

The Versatile Arc Discharge and Laser Ion Source (VADLIS) has been an available option for ISOLDE users since 2015. The ability to switch from VADIS-mode to RILIS-mode of operation has been crucial to the success of a series of experiments [50, 75, 76]. This chapter investigates, and later demonstrates how the extraction efficiency of laser-ionized species can be improved when operating the VADLIS in RILIS-mode, through the application of an extraction potential to the exit aperture.

In Section 5.1 an article is presented [51] which proposes a way to overcome the reduction in extraction voltage when the VADLIS is operated in RILIS-mode, due to the decrease in the anode voltage that is required. A series of simulations using the VSim software [13, 14] were carried out to investigate the enhancement of extraction efficiency with a modified electrical configuration of the VADLIS. Prototypes were built and tested and results compared to simulations. The off-line studies were performed using gallium. Results from on-line operation at ISOLDE of the modified VADLIS are also discussed.

Section 5.2 gives more details of the performance of the modified VADLIS when operated at ISOLDE at the end of 2017 and the enhancement in extraction efficiency for stable magnesium, molybdenum and mercury. Section 5.3 gives

information on how the ion extraction is influenced by changes in the electrostatic field distribution based on VSim simulations while Section 5.4 shows the influence (experimentally measured) of changing the extraction voltage using the modified VADLIS on the mass resolving power. Section 5.5 provides experimental results when operating the VADLIS in RILIS-mode in the presence of abnormally high neutral atom and ion densities, the former is achieved by injecting CO_2 gas and the latter is achieved by evaporating a rubidium atom dispenser, which is surface ionized inside the ion source due to its low ionization potential.

Finally we discuss ongoing and proposed developments for the VADLIS, which can potentially broaden its use at ISOL facilities.

5.1 Paper: Enhancing the extraction of laser-ionized beams from an arc discharge ion source volume

Nuclear Inst, and Methods in Physics Research B 431 (2018) 59–66

Contents lists available at ScienceDirect

Nuclear Inst. and Methods in Physics Research B

journal homepage: www.elsevier.com/locate/nimb

Enhancing the extraction of laser-ionized beams from an arc discharge ion source volume

Y. Martinez Palenzuela[a,c,*], B.A. Marsh[a], J. Ballof[a,b], R. Catherall[a], K. Chrysalidis[a,d], T.E. Cocolios[c], B. Crepieux[a], T. Day Goodacre[a,e,f], V.N. Fedosseev[a], M.H. Huyse[c], P.B. Larmonier[a,g], J.P. Ramos[a], S. Rothe[a], J.D.A. Smith[h], T. Stora[a], P. Van Duppen[c], S. Wilkins[a]

[a] CERN, CH-1211 Geneva 23, Switzerland
[b] Institut für Kernchemie, Johannes Gutenberg Universität, D-55099 Mainz, Germany
[c] KU Leuven, Instituut voor Kern- en Stralingsfysica, B-3001 Leuven, Belgium
[d] Institut für Physik, Johannes Gutenberg Universität, D-55099 Mainz, Germany
[e] School of Physics and Astronomy, The University of Manchester, Manchester M13 9PL, United Kingdom
[f] TRIUMF, 4004 Wesbrook Mall, Vancouver, BC V6T 2A3, Canada
[g] Ministère des Affaires Étrangères et Européennes, 37 Quai d'Orsay, 75007 Paris, France
[h] Tech-X UK Ltd, Sci-Tech Daresbury, Warrington, UK

ARTICLE INFO

Keywords:
Ion source
Resonance laser ionization
Arc discharge ionization
Radioactive ion beams
Particle-in-cell simulation

ABSTRACT

The Versatile Arc Discharge and Laser Ion Source (VADLIS) is a recently established ion source for the CERN-ISOLDE radioactive ion beam facility. It offers either electron-impact ionization (VADIS-mode) or resonance laser ionization (RILIS-mode). The choice of operating mode depends on the element of interest or the required beam purity. Particle-in-cell simulations using the VSim software show that the ion extraction efficiency of the VADLIS in RILIS-mode can be improved if it is equipped with an insulated extractor plate, to which an optimal voltage can be applied. This enables optimization of the RILIS-mode ion extraction independently of the electron density. Experiments have been performed using a prototype VADLIS with an adjustable extractor plate voltage for the generation of gallium ion beams at the off-line separator as well as magnesium, molybdenum and mercury ion beams at ISOLDE. A factor > 2 increase of the VADLIS efficiency in RILIS-mode has been achieved.

1. Introduction

The Versatile Arc Discharge and Laser Ion Source [1] (VADLIS) combines the FEBIAD (Forced Electron Beam Induced Arc Discharge) ion source [2] and the RILIS (Resonance Ionization Laser Ion Source) [3], both employed at Isotope Separator On Line (ISOL) facilities for the production of radioactive ion beams. The ISOLDE variant of the FEBIAD is known as the VADIS (Versatile Arc Discharge Ion Source) [4] but they share the same design and operating principle based on electron impact ionization. At ISOLDE [5], reaction products (radioactive isotopes) produced in the high-temperature target effuse as atomic vapor towards the anode volume of the ion source, via a transfer line. The transfer line is connected to the cathode tube (see Fig. 1) through which the atoms effuse into the anode cavity, where they are ionized, primarily by electron bombardment. Electrons are emitted by thermionic emission from the flat surface of the cathode which is resistively heated to typically 2000 °C. A positive voltage is applied to the anode cavity (typically in the range of 100 V to 150 V). Electrons are therefore accelerated towards the grid. Those that pass into the anode do so as a mono-energetic electron beam with an energy corresponding to the anode voltage. An axial magnetic field, regulated by the current applied to the coils of a fixed solenoid installed around the ion source volume, increases the mean path length of the electron trajectory thus increasing the probability of an electron/atom interaction. The VADIS series of ion sources all use the anode geometry of the MK5 FEBIAD [6] though the material of the grid was replaced from graphite to molybdenum in an effort to reduce the CO^+ ion formation. The total ion load of the cavity decreases creating a low density plasma [4]. Previous experimental studies indicate a complex relationship between the anode voltage (electron energy) and the overall ion source performance [4]:

- The electron energy must exceed the ionization potential of the element of interest. The ionization cross section varies with electron energy and peaks at a value typically equal to 2–3 times the ionization potential.
- If the electron emission from the cathode is space-charge limited,

* Corresponding author.
E-mail address: yisel.martinez@cern.ch (Y. Martinez Palenzuela).

https://doi.org/10.1016/j.nimb.2018.06.006
Received 3 April 2018; Received in revised form 6 June 2018; Accepted 8 June 2018
Available online 06 July 2018

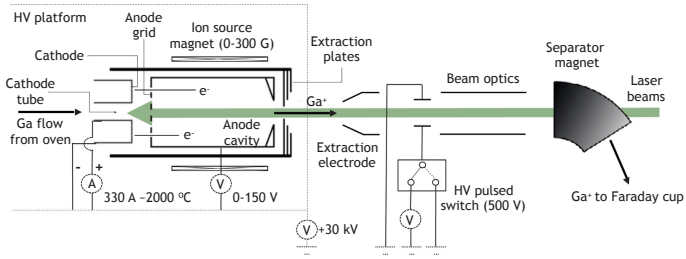

Fig. 1. Sketch of the VADLIS and general description of the experimental set-up. (not to scale).

then the electron flux is proportional to $V^{\frac{3}{2}}/d^2$, where V is the voltage difference and d the distance between the cathode and the anode [7].

- The anode body temperature is determined by its proximity to the hot cathode (~2000 °C). The anode is also heated by electron bombardment, which is determined by the electron current and the anode voltage. The anode temperature influences the surface ionization rate of the atoms and wall sticking times as well as electron emission from the walls. Theoretical estimations are given in [8].
- For the standard VADIS configuration, the extraction plates are held at the potential of the high voltage platform as indicated in Fig. 1 (locally grounded). The voltage difference between the anode and extraction plates is therefore equivalent to the anode voltage.

It is challenging to experimentally determine the relative importance of each of these aspects of the ion source in terms of the resulting ionization efficiency for a given species. For this reason, particle-in-cell (PIC) simulations of the ion source, for which individual physical effects can be switched on and off, can therefore provide a valuable insight. The CPO software [9] has been used in the past to demonstrate the impact of the so called 'active' volume in the overall efficiency of the ion source. A model describing the dependance between efficiency and the active volume was then inferred from experimental results over a wide range of operational parameters. More details can be found in [4,10].

Recently it was demonstrated that the VADIS cavity could be used as an effective laser-atom interaction region provided that the lasers can be transmitted through the 1.5 mm diameter exit aperture of the anode [1]. In this case the ion source is operated in so-called RILIS-mode, with the source magnet and the anode voltage optimized for laser-ion survival and extraction, whilst keeping the anode voltage below the required value for electron impact ionization to occur.

The development of this multi-purpose ion source (known as the VADLIS) has been crucial to the success of several experiments at ISOLDE since its first on-line use in 2015. For example, this approach enabled the first operation of RILIS with molten lead targets for the study of mercury isotopes by in-source laser spectroscopy [11] since a reliable means of coupling the standard hot cavity RILIS ion source with liquid targets does not currently exist. On-line experiments for the production of mercury, cadmium and magnesium beams have shown that RILIS-mode achieves a beam purity comparable to that of the standard hot-cavity RILIS ion source as well as an operating efficiency comparable to VADIS-mode for the laser-ionized species [1,11]. This additional degree of ion source flexibility proved vital to the success of the ISOLTRAP [12] experiment at ISOLDE described in Ref. [13,14] for which magnesium and neon beams were required in a single experiment and thus one target/ion source assembly should be used. Beams of neon isotopes need an electron impact ionization mechanism while magnesium can be ionized by both electron impact and laser ionization (RILIS). The RILIS-mode allowed the ^{23}Mg yield to be preserved with a much cleaner isobaric spectrum compared to the VADIS-mode (electron impact ionization).

In this work we characterize the performance of a modified VADLIS, equipped with an adjustable-voltage extractor plate, primarily intended to improve the performance of the RILIS-mode of operation in terms of selectivity and extraction efficiency. This is highly desirable at ISOL facilities: e.g users would benefit from a reduced number of shifts necessary to perform their experiments without any apparent drawback. Even though the VADIS operation mode can also benefit from these modifications, the enhancement in extraction efficiency was observed to be not as significant as for the RILIS-mode. We demonstrate that the source can perform as a standard VADIS with no loss of performance or drop in lifetime. The particle-in-cell software VSim [15,16] is used to study improved RILIS-mode extraction characteristics. VSim is also used to simulate the ion extraction time profile which shows good agreement with experimental results. In the outlook we discuss the prospects of this modified VADLIS as the new standard configuration, and suggest further modifications for improved ion source flexibility, diagnostics and performance.

2. Experimental set-up

The study performed in Ref. [1], which identified the different modes of operation of the VADLIS served as a starting point for a better understanding and optimization of the anode cavity as an efficient laser-atom interaction volume. The experimental studies were carried out at the ISOLDE off-line laboratory described in Ref. [8]. Gallium vapor was released from a $GaNO_3$ precipitate contained in a resistively-heated capillary oven, connected to the rear of the tubular cathode tube. Atomic Ga (ionization potential ~6.0 eV) effusing along the cathode tube is able to enter the anode cavity by passing through the anode grid, located 1 to 2 mm downstream of the cathode exit. The Ga atoms were ionized via a two-step, one-resonance ionization scheme (294.36 nm,532 nm) [17]. The first step involves a transition from the thermally-populated low-lying atomic energy level $3d^{10}4s^24p^2P^0_{3/2}$ to the $4s^24d^2D_{5/2}$ state. Up to 200 mW of 294.36 nm light was produced using a frequency-doubled Rhodamine 6G dye laser, pumped by 20W of 532 nm radiation from a frequency-doubled Nd:YAG laser (Edgewave IS series). The second step, non-resonant ionization to the continuum made use of up to 15W of residual 532 nm light from the dye pump laser. An optical delay line ensured coincidence of the ~8ns laser pulses in the ion source. The laser pulse repetition rate was fixed to 10 kHz for these studies.

The laser beams are transmitted to the ion source through a fused silica window in the separator vacuum chamber and enter the anode volume through the 1.5 mm diameter aperture of the anode extractor plate. A portion of the laser beams passes through both the anode cavity and the central hole of the anode grid, entering the cathode tube

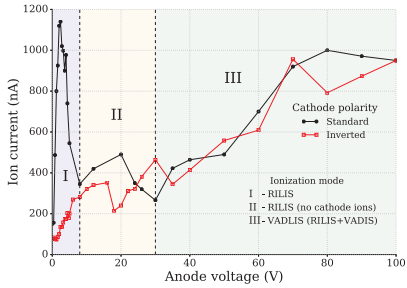

Fig. 2. Ga^+ beam intensity as a function of the anode voltage (black line). The different regions show the Ga^+ signal from ions created by the laser beams in the anode and cathode (region I, V_a ~[0, 7 V]), ions created only inside the anode (region II) and by electron impact ionization plus resonance ionization (region III). Details on the contribution of different ionization mechanisms to the Ga^+ signal are discussed in [1]. The red line represents the Ga^+ beam intensity as a function of the anode voltage when the cathode polarity is inverted (see subSection 2.1)

(diameter 1.2 mm, length 22 mm) as shown in Fig. 1. The ion source assembly is on a high voltage platform, held at +30 kV. A grounded extraction electrode, located ~60 mm downstream of the anode exit, extracts ions as a 30keV, effectively mono-energetic beam, which is transmitted through a magnetic dipole mass separator for isotope selection. After mass/charge selection the ion beam is transported to a Faraday cup as shown in Fig. 1.

The beamline is equipped with a high voltage pulsed switch (BEHLKE GHTS60) connected to a vertical deflector downstream of the extraction electrode, also shown in Fig. 1. By using a sliding beam gate technique, the time structure of the extracted beam can be obtained as discussed in Section 3.2.

The dependence of the $^{71}Ga^+$ current while sending the lasers into the anode cavity, as a function of the anode voltage V_a, is shown in Fig. 2. In the analysis of the ion source performance we assume a constant atomic Ga flux into the anode (i.e. the effect of the electron-bombardment heating of the anode on the Ga evaporation rate from the oven is negligible).

Three regions can be identified in the anode voltage scan. Below $V_a = 30$ V laser-ionization is the dominant ionization mechanism. The highest ion signal is recorded at values of V_a for which the kinetic energy of the ions created by the laser pulse within the cathode tube is sufficient to overcome the voltage of the anode grid (region I). As the anode voltage increases region II is reached. At this stage, the positive anode grid potential exceeds the potential difference along the resistively heated cathode tube (Fig. 1). Laser-ions originating from inside the cathode tube are therefore prevented from entering the anode volume and the ion current decreases. At around 30 V, electron impact ionization becomes the predominant ionization mechanism and the ion source operates in the standard VADLIS regime (region III).

2.1. Cathode with inverted polarity

The survival of ions created inside the cathode tube is expected to be enhanced by the 'hot cavity effect' [18,19]. The voltage drop along the resistively heated cathode tube acts as a drift field for any ions created in that region. The direction of ion flow depends on the polarity of the power supply. In the standard configuration, there is a negative voltage gradient towards the anode-end of the cavity, attracting positively-charged ions towards the anode. These ions can be generated either by laser or surface ionization. If the polarity of the cathode is inverted, the ion flow along the cathode towards the anode is suppressed.

Fig. 2 compares the Ga^+ ion rate (combined effect of laser, surface and electron-impact ionized) dependence on the anode voltage with standard and inverted cathode heating current polarity. The disappearance of the ion current peak in region I in the case of inverted polarity confirms our interpretation that the observed ions at low anode voltage originate from inside the hot cathode tube itself.

Alkali suppression could be achieved by equipping the target assembly with a resistively heated transfer line, with inverted polarity, between the RILIS cavity and the target as discussed in Ref. [20]. In Section 4.3 we will discuss this aspect and how the overall RILIS-mode selectivity can be increased under certain conditions by making use of the same mechanism for surface ion suppression using the cathode itself. This is possible since the MK5-type ISOLDE ion sources are capable of operation with an inverted polarity [20].

3. Particle-in-cell simulations for the characterization of the VADIS electrostatic cavity

The software VSim from Tech-X Corporation [15,16] is used in the present work to model the electrostatic field distribution within the VADIS cavity and gain an insight into the RILIS-mode ion dynamics. It contains a well validated implementation of the electrostatic particle-in-cell (PIC) algorithm with Monte Carlo treatment for the field ionization, impact ionization as well as elastic and inelastic scattering processes.

In this study we focus on the electric field distribution caused by the electrons reaching the anode cavity, combined with the voltages applied to the ion source walls and external electrostatic fields reaching the extraction zone. When the rate of electron supply to the anode (electrons incident from the cathode, plus those generated through collisions with the atoms and anode walls) matches the rate of electron absorption on the walls of the anode, a quasi-steady state is reached for the electron population and, accordingly for the electric field distribution. The electron current extracted from the cathode and injected into the anode volume in VADIS-mode is of the order of some tens of mA while the typical ion current extracted from the anode volume through the exit aperture reaches at maximum several μA. We therefore consider in the present study that the ion density inside the anode volume has a negligible influence on the quasi-steady state electric field distribution. The impact of the ion source external magnetic field in the electron/ion dynamics was not included in the present study.

3.1. Electrostatic field distribution within the anode volume

Fig. 3 shows the contour lines for the electrostatic field distribution (after the quasi-steady state described above has been reached) when applying 100 V to the anode walls (VADIS-mode of operation). Electrons are launched from a circular surface with an initial homogeneous spacial distribution representing the cathode. An electron current of

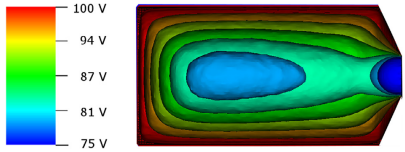

Fig. 3. Simulated electrostatic field distribution inside the anode (exit aperture on the right hand side) with an anode voltage of 100 V (VADIS-mode) and the electron current to 20 mA. Ions created at a location corresponding to an equipotential field line linked to the extraction aperture will be successfully extracted while those created in the potential well (blue region in the center of the source) will be trapped.

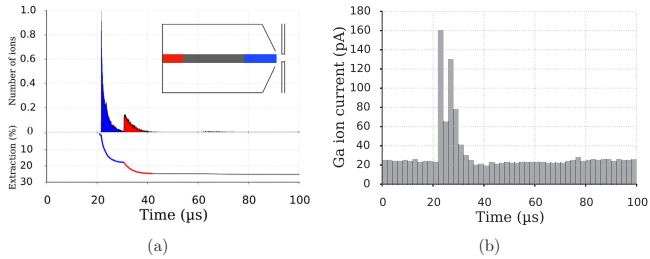

Fig. 4. (a) Simulated time structure of Ga^+ with VSim – extraction plates at 0 V and anode at 20 V (top panel) and integrated number of ions from 0 to 100 μs (time between two laser pulses) normalized to the total number of ions created during one laser pulse (lower panel). The inset represents the ion's origin in the anode volume and the color code is the same as in the figure. (b) Experimental time structure of $^{71}Ga^+$ measured with a Faraday cup at the focal plane of the dipole separator magnet.

20 mA is used as an input parameter for the simulation taking into account that the anode grid transparency is ~50%. This value is comparable with the 40 mA current measured experimentally for a cathode operation temperature of 1935 °C. The results are in broad agreement with earlier studies [8] which used the CPO software [9].

The ion source efficiency depends on the ionization efficiency, ion survival and extraction probability. Since the anode exit aperture is small compared to its internal surface area it is particularly important for the electrostatic field distribution to provide ion confinement (preventing anode wall collisions) and to result in ion flow towards the exit aperture.

The consequence of this, however, is that satisfying this requirement typically results in a region of the potential well in the centre of the anode volume where ions are confined from reaching the anode walls and the exit aperture. They are therefore trapped. This is illustrated in Fig. 3 – where the central blue area corresponds to this trapped region. In [8] the ratio of this trapped region to the active region (ion confinement but with access to anode aperture) was identified as the primary difference between MK5 and MK3 FEBIAD geometries responsible for the different efficiencies of these two ion sources. Based on these considerations, a reduction in the volume of this inactive region will result in an increase in ion source efficiency. In VADIS-mode, ion creation takes place throughout the full anode volume while in RILIS-mode ions are created only where the laser beam is present: a well defined central region in a cylinder with a diameter of 1.5 mm (the exit hole diameter of the VADIS). The initial VADLIS investigations suggested this potential well, which also appears when the ion source is operated in RILIS-mode, resulted in a comparatively slow release of laser-ionized ions from this region [1].

3.2. Laser ionization as a probe to study the electrostatic field distribution and ion extraction time structure

The histogram of the ion arrival time at the detection system, relative to the moment of ion creation (the laser pulse arrival time), provides the time structure of the ion beam generated at the ion source. The field distribution inside the ion source has a strong impact on the time structure of the laser-ionized beam. The time structures from the first VADLIS investigations [1] were qualitatively interpreted as resulting from ionization in three distinct regions along the length of the anode cavity. An analysis of the time structures can provide information about the field distribution, as well as the ion survival and the probability for an ion to be extracted.

To validate and better describe the time structure interpretation given in Ref. [1], a column of uniformly distributed ions is placed in the calculated electrostatic field along the axis of the ion source, representing the ions created in the region of interaction of the laser beam with the atoms. The length of the laser pulse is in the ns range, small compared to the ion motion time scale. Therefore we consider the ions are created instantaneously. Because of the relative low atom density, the number of photo-electrons created by the laser pulse is sufficiently small not to perturb the static electrical field simulated previously. It is therefore assumed in the calculation that ions are subject to this predefined and unchanging electric field distribution. These approach is advantageous given the charge to mass ratio of the electrons is 3–5 orders of magnitude smaller than that of the ions and as a result the ions experience much smaller acceleration due to the same field magnitude. These assumptions are therefore necessary to enable the simulation to run in time steps suitable for ion, rather than electron, motion. Since we do not model explicitly the electron–ion dynamics at the same time, ion–electron neutralization mechanisms were not taken into account.

With the anode voltage set at 20 V in the simulations we study the ion time structure (this voltage value was chosen to study the time profile of the ions created within the anode volume and will be compared to the time structure measured experimentally at this same voltage). The electron current which determines the electrostatic field distribution was set to 1.5 mA since just half of the electrons reach the anode volume due to the 50% grid transparency (3 mA was measured experimentally at 1935 °C though this number was observed to go up to 12 mA for a different ion source). Considering a 1 nA laser-ionized Ga^+ beam with a 1.5 mm diameter (defined by the aperture of the extraction plates) and 23.16 mm length (length of the anode cavity) ion creation cylinder, the ion density along the laser beam path from a single overlapped set of laser pulses is of the order of $10^{11}/cm^3$.

The simulated results show good agreement with the qualitative interpretation given in [1], with the time structure (Fig. 4a (top panel)) showing two distinct peaks. A prompt release peak, appearing after ~21 μs, (corresponding to the time-of-flight of the ions from the source to the Faraday cup) was associated to the ions created by the laser pulse in the region close to the exit-hole aperture and first to feel the extraction field. The second peak of the prompt release, appearing ~10 μs later can be associated to regions where the potential is high enough to overcome the potential well present at the rear of the ion source, which is the case for the ions created near the anode grid (see Fig. 1 and Fig. 3). These statements were validated by tagging each ion inside the ion source according to their horizontal coordinate with a color code and observing how the particles are extracted from the volume as a function time. Fig. 4a (lower panel) shows that up to 18% of the ions are extracted within 10 μs after ion creation and 10 μs later, the percentage of ions extracted from the ion source equals 25%.

According to the simulation, approximately 75% of the ions are not released within 100 μs, but remain confined within the region of enclosed electrical potential (Fig. 4a (lower panel)). In fact, it is demonstrated in Ref. [11] that, by operating the lasers with a 2kHz repetition rate, the laser related ions residency time within the cavity exceeds 500 μs.

To validate these results, the experimental time structure of the extracted beam was obtained through a sliding beam gate technique: by applying a pulsed high voltage source to a vertical deflector plate downstream of the extraction electrode a fast beam gate was realized.

The variable-width beam gate was operated at the repetition rate of the pulsed RILIS lasers (10kHz) and triggered, with adjustable delay from the master clock that triggered the laser.

The Ga^+ signal was recorded while a 10kHz beam gate (gate open) of 2 μs duration was applied. The measurement was repeated for different gate delay times across the 100 μs interval between laser pulses. The results are shown in Fig. 4b. The ions generated within the central (grey) region on Fig. 4a (inset), are not extracted within the time-window between laser pulses, and therefore form a 'DC' background in the experimentally-observed time structure (Fig. 4b). A laser on/off measurement proved that 50% of this DC background current is attributed to laser-ionized Ga. One notices also two distinct time structures on top of the DC background current. We can evaluate the ratio of ions found in the prompt release (from a single laser pulse) to this slow-release DC component to be 1:1.3 (calculated after subtraction of the non laser-ionised DC background). This is in agreement with earlier studies which indicated that the majority of the ions are slowly extracted on a time scale which is long compared to the time between laser pulses [1,11]. The ion survival time in the anode volume is therefore sufficiently long for the ion population to build up, exceeding the capacity of the potential well.

The general features of both the experimental and theoretical time structures are consistent. The two peaks appearing in the experimental time structure, separated by ~4 μs as shown in Fig. 4b is consistent with the existence of a voltage depression. The spacing in time of these peaks as well as their intensity will depend on the electron density in the cavity and anode voltage, since it is the electron density that determines the field distribution and depth of the potential well.

The information provided by the simulated and experimental time structures shown in Fig. 4 enables an estimation of the extraction efficiency of the slow-release component of the laser-ions. From the simulation (Fig. 4a), we see that the prompt release accounts for 25% of the ions generated by one laser pulse. The remaining ions are either not released (trapped or re-neutralised), or released slowly with respect to the 100 μs between laser pulses. Using the assumption that the electrostatic field used for the simulation in Fig. 4a remains unchanged after many laser pulses, and that the ion-survival for the ions originating in the prompt release regions (colored regions in Fig. 4a (inset)) is 100%, the extraction efficiency for the ions generated in the 'trapped' region is estimated to be 42%, resulting in an overall ion extraction efficiency of 57%. As will be shown in Section 4.3, even with an anode voltage of 20 V, the application of an optimal voltage to the extraction plates (see Fig. 1) results in an enhancement in overall efficiency of ~30%.

4. VADLIS with improved extraction characteristics of laser-ions

The electrical field distribution inside the anode due to the potential difference between the anode body and the locally grounded extraction plates, has an effect on the ion extraction. Here we investigate the recovery of an effective potential difference, that can be optimized for maximum ion extraction probability while operating in RILIS-mode. This can be achieved by applying a negative voltage to the extraction plates aperture of the ion source. The present study was performed using the VSim software, leading to the construction of a VADLIS prototype that presents improved ion extraction characteristics as demonstrated experimentally.

4.1. Dependence of electrical field distribution on the extractor-plate voltage

A comparison between the field distribution inside the anode cavity of the VADIS when the extraction plates are set to 0 V and −100 V is shown in Fig. 5. For both cases, the anode voltage is set to 1.35 V and the electron drain current (the electron current from the cathode to the anode) to 0.2 mA, corresponding to the value measured during optimal RILIS-mode operation. At such low voltages no significant electron impact ionization takes place (1.35 eV is below the threshold for electron impact ionization of Ga). As shown in Fig. 5a, an electrical potential well of ~1 V depth with respect to the anode walls is established towards the rear of the source. This means that ions created in this region will not be extracted (or the extraction will be slow since it will require the accumulation of enough ions to exceed the capacity of this potential depression) since their thermal energy is insufficient to overcome this potential well.

Biasing the voltage of the extraction plates to −100 V (Fig. 5b) results in an extraction field which penetrates deeper into the anode volume to better satisfy the efficiency requirements discussed earlier: ion confinement to prevent wall collisions, a field distribution that results in ion flow towards the exit aperture, and a reduction of ion trapping effect in the 'inactive' anode space.

Fig. 6a represents the potential along the axis of the anode cavity. Only the positive voltage values are displayed, however the curves corresponding to the extraction voltages of 0 V and −100 V reach a value of −6 V and −39 V at the anode exit respectively.

The solid curve in Fig. 6a represents the simulated potential along the axis of the ion source when the extraction plates are at 0 V. Ions created in the light grey regions shown in Fig. 6a will be extracted. This is due to the fact that their initial positions lie outside the potential barrier defined by the solid vertical lines (trapping region). In the same way, when applying −100 V to the extraction plates, this trapping region is reduced (defined by the vertical dashed lines). As a result, the volume of the region from which ions can be successfully extracted increases and is represented by the dark grey area in Fig. 6a.

The percentage of ions extracted within the first 100 μs can be related to the length along the x-axis defined by the shaded regions shown in Fig. 6a. This is because the laser-ions are assumed to be created and uniformly distributed in a cylinder of laser illumination along the axis of the ion source. For 0 V, this percentage equals 32% and increases to 48% for −100 V applied to the extraction plates.

The percentage of ions remaining within the ion source as a function of time is represented in Fig. 6b for 0 V (Fig. 5a) and −100 V (Fig. 5b) respectively. It shows a faster and more efficient extraction of the ions when the extraction plates are biased to −100 V. The extraction efficiency within the first 100 μs is calculated to improve from 32% to 48%, in agreement with the evaluation from Fig. 6a. After many laser pulses and accumulation of ions in the potential well region, ions will be able to escape more easily when −100 V are set in the extraction plates due to a shallower potential well compared to the standard configuration. It can also be noticed that when comparing Fig. 6b and Fig. 4a (lower panel), the extraction efficiency of the prompt release it is higher for the case of 1.35 V applied to the anode walls (32%) compared to when the voltage of the anode is 20 V (25%). For 20 V more electrons are drawn from the cathode, which results in a higher electron density and deeper potential well.

The ions created near the exit aperture will suffer from a larger energy spread. Considering an energy spread that the ISOLDE mass separators can accept of 20 eV, only ions created at a position within the ion source higher than 22.4 mm will not be transmitted through a slit corresponding to the standard resolving power of the mass separator. This means that for the case in which the extraction plates are set to −100 V, the relative fraction of ions with an energy spread larger than 20 eV is only of 3% of the total extracted beam.

The increase in energy spread of the extracted ions when applying a voltage of −200 V on the extraction plates was also visible in the experimentally measured mass spectra. The mass resolution M/ΔM for ^{71}Ga decreased from 1200 (at 0 V) to 600 (at −200 V).

4.2. Adjustable-extractor VADLIS prototype

In order to validate the improved ion extraction suggested by the aforementioned simulations, a VADIS with an adjustable-voltage extraction plate has been constructed and tested at the ISOLDE off-line

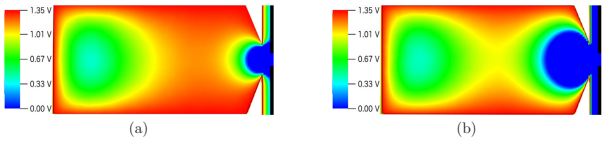

Fig. 5. Electrostatic field distribution simulated with VSim with anode walls at 1.35 V (optimal value for RILIS-mode efficiency) and 0.2 mA electron current: (a) 0 V extraction plates; (b) −100 V extraction plates. The color scale is adjusted to best visually depict the [0 V, 1.35 V] region. Values at 0 V and below appear as dark blue. The consequences in terms of energy spread of the ions generated in this region are discussed in the text.

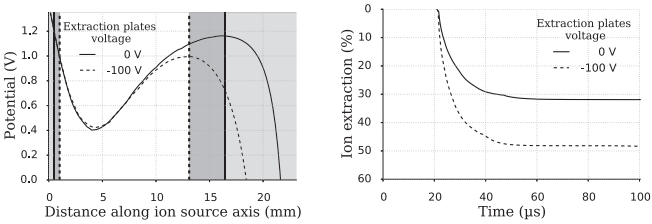

Fig. 6. (a) Potential along the axis of the anode cavity for 0 V (solid line) and −100 V (dashed line) set on the extraction plates. The x-axis represents the full length of the anode cavity (23.1 mm). The y-axis shows the potential within the source just in the range [0 V, 1.35 V] b) Percentage of ions extracted from the anode volume as a function of time. Details about the meaning of the shadowed areas are given in the text.

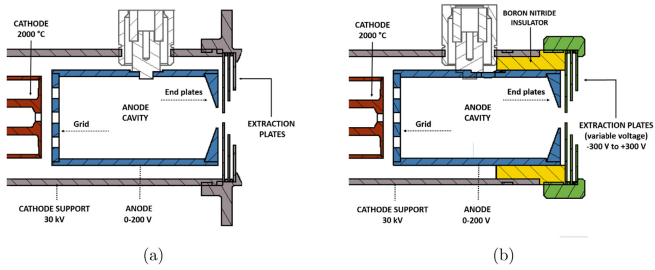

Fig. 7. (a) Standard VADIS used at ISOLDE based on the MK5 FEBIAD geometry (just one out of three anode holders shown); (b) VADIS with BN insulator. In this case just one anode holder was used to allow the electrical connection of the anode. Extraction plates can be biased with a voltage in the range from −300 to +300 V.

laboratory. The differences between the standard VADIS and the new version are highlighted in Fig. 7b. The extraction plates are mounted in a boron nitride (BN) cylinder, leaving them insulated from the target unit and allowing the application of an independent voltage.

This modification has the additional advantage of improving the structural stability of the ion source: the anode cylinder is screwed into the BN insulator, rather than being held by three insulating screws as can be seen in Fig. 7a. The relevant distances for the standard performance of the source when operated both on-line and off-line were kept the same (cathode-grid distance = 1.5 mm, extraction plate aperture diameter = 1.5 mm). The source was operated for a period of more than a month in which multiple cycles of cooling and heating were performed demonstrating its reliability and showing the new BN component withstands thermal expansion of the metal parts.

The new configuration showed typical ion source performance under standard operation conditions. The $^{84}Kr^{+}$ ion current produced by electron impact ionization in the VADIS operation mode was monitored during the whole period of operation. The obtained total efficiency remained between 16 and 25% at the cathode temperature of 2030 °C when operated at 100 V anode voltage, which is comparable to typically measured values with a standard VADIS unit. This is a typically used reference parameter at ISOLDE for testing the VADIS ion source performance.

4.3. Experimental results using the adjustable-extractor VADLIS prototype

The performance of the new VADLIS source was investigated by measuring the intensity of $^{71}Ga^{+}$ ion beam produced in the RILIS-mode under different combinations of the anode voltage (V_a) and the extraction plates voltage (V_e). The obtained results are presented in Fig. 8 and Table 1.

Fig. 8a shows the $^{71}Ga^{+}$ beam intensity for the extractor voltage range V_e [0, −140 V] and an anode voltage range V_a [0, 2 V] (falling within region I in Fig. 2). Fig. 8b shows the same in the ranges V_e [0, −60 V] and V_a[10, 25 V] (corresponding to region II in Fig. 2). At V_e = 0 V, corresponding to the standard VADIS configuration, the maximum current measured in the range V_a [0, 2 V] is 113 pA at 1.35 V and decreases as the anode voltage increases. The decrease in laser-ionized Ga^{+} current for V_a > 1.35 V is due to the anode voltage exceeding the voltage drop of the resistively heated cathode. Ga^{+} ions originating from the cathode tube are therefore suppressed since they are unable to pass the anode grid to enter the anode volume.

For V_a < 1.35 V, the ion current is less sensitive to changes in the voltage of the extraction plates compared to V_a > 1.35 V as can be observed in Fig. 8a. When V_a < 1.35 V, the ions created by the laser light inside the cathode flow towards the anode cavity due to the voltage gradient that exists inside the cathode. These ions can be

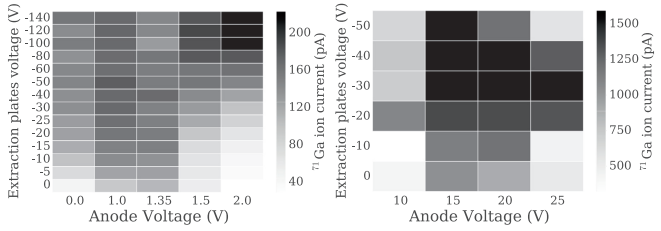

Fig. 8. Voltage scan of V_a and V_e for (a) region I and (b) region II as defined in Fig. 2. Note: the data represented in Fig. 8a and Fig. 8b were taken during different measurement periods and consistency in terms of all experimental conditions (laser alignment, power, ion beam purity, electron emission etc) could not be guaranteed. Therefore, the intensity ratios observed when going from region I to region II do not correspond to the ion signal ratios observed in the anode scan shown in 2.

Table 1
Experimentally measured ion rates for different anode voltages with and without the application of the extractor plate voltage for region I. Here V_{eopt} refers to the value of V_e for which the ion signal is the highest.

V_a (V)	I [V_e = 0 V] (pA)	I [V_{eopt}] (pA)	V_{eopt} (V)
0.0	50	170	−140
1.0	100	187	−50
1.35	113	179	−40
1.5	60	200	−120
2.0	30	223	−120

Table 2
Enhancement factor obtained when optimizing the extraction plates voltage for maximum ion extraction in RILIS-mode. The anode voltage V_a and the source magnet current were optimized in each case for maximum ion extraction efficiency.

Isotope	Background V_e = 0 V	Lasers On V_e = 0 V	Lasers On(*) V_{eopt}	Enhancement factor	Laser scheme (nm)) [λ_1|λ_2|λ_3]
^{24}Mg	8 pA	8.5 nA	23.5 nA	2.8	[285|553|532] [17]
^{98}Mo	0 pA	13.4 pA	103 pA	7.7	[380|416|635] [21]
^{196}Hg	18 pA	58 pA	133 pA	2.3	[256|313|532] [22]

(*) The Lasers Off signal for V_{eopt} is also expected to increase, however this value was not measured.

successfully extracted once they traverse the anode grid. All ions passing the anode grid enter the active region of the anode volume and are therefore rapidly and efficiently extracted.

With $V_a > 1.35$ V (within the region represented in Fig. 8a), most of the observed Ga^+ ions are generated inside the anode volume rather than in the hot cathode. Since these ions have a point of origin that is not necessarily in the active region of the anode, a higher proportion of these ions have an extraction probability that is dependent upon the extraction aperture voltage V_e.

The maximum Ga^+ signal when $V_e = 0$ V equals 113pA (for $V_a = 1.35$ V), see Table 1. When tuning the voltage of the extraction plates to maximize the extracted Ga^+ beam current, a value of 223pA was achieved. These results demonstrate that, by having an independently-adjustable extractor plate voltage, the ion extraction efficiency of the VADLIS in RILIS-mode can be improved by a factor 2. In a similar way for region II, a 30% increase in the Ga^+ signal was observed. Operating the ion source in this region has the advantage of suppressing the incoming ions from the cathode. This is desirable if the required beam suffers from surface-ionized isobaric contamination.

In November 2017 the first on-line test of the modified VADLIS was performed at ISOLDE. The target material was a magnesium oxide (MgO − 9.8 g) and uranium oxide (UO_2 − 92.2 g) mixture, specifically chosen for the production of molecular beams for a separate beam-development activity. Magnesium and molybdenum atoms were available from the target-ion source assembly, with magnesium evaporating from the target material and molybdenum from the anode grid, whilst mercury was either radiogenically produced or present as a contaminant in the target material. The target was operated in the range of 780 to 1200 °C while the cathode of the ion source was kept at ~2000 °C. The enhancement in the magnesium, molybdenum, and mercury laser-ion signal when optimizing V_e for maximum ion extraction in the RILIS-mode of operation is shown in Table 2. The optimal anode voltages V_a for ^{24}Mg,^{98}Mo and ^{196}Hg were 1, 0 and 1 V respectively.

In our tests magnesium, mercury and gallium reach the anode by travelling along the cathode tube. In contrast, the anode body itself is the source of the molybdenum atoms. This difference is reflected in the enhancement factor achieved when optimizing the extraction voltage V_e for Mg, Hg and Ga (2 to 3), compared to Mo (7.7). This is as expected, since ions originating outside of the anode volume (Mg, Ga, Hg) enter the anode through the grid and therefore have enough kinetic energy to reach the extraction aperture as shown in Fig. 6a. Their extraction probability is therefore independent of the extraction voltage settings. The situation for Mo (factor 7.7 enhancement) is analogous to that of ^{71}Ga depicted in the right-hand column in Fig. 8a, when the anode voltage ($V_a = 2$) is sufficient to suppress the cathode ions. At this point, the enhancement factor achieved by optimizing the extractor voltage becomes 7.3.

The VADIS efficiency for Ga, Mg and Hg have been measured at the off-line laboratory in a separate set of measurements to be 12%, 6% and 9% respectively [23]. Assuming an equal VADIS-mode and RILIS-mode efficiency (as is typically shown in the laser-on anode scans), the RILIS-mode efficiency of the VADIS with optimally biased extraction plates is expected to be 24% (Ga), 12% (Mg) and 18% (Hg).

5. Conclusions and outlook

Previous studies have demonstrated that the anode cavity of the VADIS ion source serves as an efficient laser-atom interaction region. We used the VSim particle-in-cell software to study the electrostatic field distribution inside the anode cavity and the ion time structure. The general features observed in the calculated time structure with the help of VSim simulation code matched the experimentally measured values and the interpretations of previous work.

The simulated electrostatic field distribution within the anode

volume of the VADLIS when operating in RILIS-mode was compared to a simulation of a cavity with better laser-ion extraction characteristics. The simulations showed an increase in the active region of the latter, favourable for the extraction of laser-ions created in the anode volume within the first 100 μs of ionization when biasing the voltage of the extraction plates to negative values, which gives the flexibility of optimizing the extraction field for maximum ion extraction probability.

Based on the input of the simulations, a new prototype ion source was designed. During off-line tests of the prototypes, no loss of reliability was observed. On the contrary, the insulator design enables a more structurally-sound means of securing the anode chamber, and potentially eliminates some VADIS failure modes such as short circuit caused by tilting of the anode chamber. A twofold increase in efficiency was observed in RILIS-mode with this prototype for gallium during the off-line testing period. This modified VADLIS was also operated on-line at the ISOLDE facility showing an enhancement factor greater than 2 for the stable isotopes tested (^{24}Mg, ^{98}Mo and ^{196}Hg). The extraction voltage V_e allows for the operation of the ion source in a regime for which surface ions created inside the cathode tube are suppressed while an enhancement in overall signal can still be achieved.

The agreement between the experimental and simulated results obtained so far indicate that VSim can be used to optimize the anode cavity geometry for improved RILIS and VADIS mode performance. Following the validation of this approach to optimizing ISOLDE ion sources, we will aim to continue this work to find the optimal RILIS-mode VADLIS geometry and design. Re-purposing the anode grid, and decoupling its polarization from the anode body, offers an additional parameter which can be used to change the electron energy and electron flux. This would enable a switching from RILIS-mode to VADIS-mode without changing the extracted beam energy. This is important for maintaining optimal conditions for energy-sensitive beam manipulations downstream (such as for injection in the REXTRAP/EBIS [24,25]). Such modification allows better diagnostics of the ion source, enabling the measurement of the electron drain current at different anode components (grid, body, extractor).

The modified VADLIS ion source has been shown to be reliable and highly versatile, while offering an improved efficiency compared to the standard VADLIS. These characteristics are expected to be particularly important for next-generation ISOL facilities (SPES [26], SPIRAL2 [27], ISOL@MYRRHA [28]) where the target lifecycle is expected to be long (weeks-months), or for cases where a wide variety of species will need to be extracted from a single target-ion source assembly (e.g. CERN-MEDICIS [29]). Regular target/ion source changes to suit specific experiments are therefore less practical.

This work represents an important step forward in the development and exploitation of the VADLIS as the most versatile ion source for ISOL facilities. We propose this could be a favourable standard configuration for operation at ISOLDE. It would offer unmatched versatility combined with the option of high selectivity, without compromising standard VADIS performance and reliability.

Acknowledgements

This work has been funded by FWO-Vlaanderen (Belgium), by GOA/2010/ 010 (BOF KU Leuven), by the IAP Programme initiated by the Belgian Science Policy Office (BriX network P7/12), by the European Commission within the European Nuclear Science and Application Research ENSAR2 (Grant agreement No. 654002) and by a Grant from the European Research Council (ERC-2011- AdG-291561-HELIOS). The authors would like to thank the support received from the European Union's Horizon 2020 research and innovation programme under grant agreement No. 642889 MEDICIS-PROMED.

References

[1] T. Day Goodacre, J. Billowes, R. Catherall, T.E. Cocolios, B. Crepieux, D.V. Fedorov, V.N. Fedosseev, L.P. Gaffney, T. Giles, A. Gottberg, K.M. Lynch, B.A. Marsh, T.M. Mendonça, J.P. Ramos, R.E. Rossel, S. Rothe, S. Sels, C. Sotty, T. Stora, C. Van Beveren, M. Veinhard, Blurring the boundaries between ion sources: the application of the RILIS inside a FEBIAD type ion source at ISOLDE, Nucl. Instrum. Methods Phys. Res., Sect. B: Beam Interact. Mater. At. 376 (2015) 39–45.
[2] R. Kirchner, E. Roeckl, A novel ISOL ion source, Nucl. Instrum. Methods 139 (1976) 291–296.
[3] V.N. Fedosseev, Yu. Kudryavtsev, V.I. Mishin, Resonance laser ionization of atoms for nuclear physics, Phys. Scr. 85 (5) (2012) 058104.
[4] L. Penescu, R. Catherall, J. Lettry, T. Stora, Development of high efficiency Versatile Arc Discharge Ion Source at CERN ISOLDE, Rev. Sci. Instrum. 81 (2) (2010) 1–5.
[5] R. Catherall, W. Andreazza, M. Breitenfeldt, A. Dorsival, G.J. Focker, T.P. Gharsa, T.J. Giles, J.-L. Grenard, F. Locci, P. Martins, S. Marzari, J. Schipper, A. Shornikov, T. Stora, The ISOLDE facility, J. Phys. G: Nucl. Part. Phys. 44 (9) (2017) 094002.
[6] S. Sundell, H. Ravn, Ion source with combined cathode and transfer line heating, Nucl. Instrum. Methods Phys. Res., B 70 (1–4) (1992) 160–164.
[7] C.D. Child, Discharge from hot CaO, Phys. Rev. (Series I) 32 (5) (1911) 492–511.
[8] L. Penescu, Techniques to Produce and Accelerate Radioactive Ion Beams (Ph.D. thesis), Polytechnic Inst., Bucharest, 2009 https://cds.cern.ch/record/2259078?ln=en.
[9] CPO programswww.electronoptics.com.
[10] L. Penescu, R. Catherall, J. Lettry, T. Stora, Numerical simulations of space charge effects and plasma dynamics for FEBIAD ion sources, Nucl. Instrum. Methods Phys. Res., Sect. B 266 (19–20) (2008) 4415–4419.
[11] T. Day Goodacre, Developments of the ISOLDE RILIS for Radioactive Ion Beam Production and the Results of their Application in the Study of Exotic Mercury Isotopes (Ph.D. thesis), The University of Manchester, 2016 https://cds.cern.ch/record/2254839.
[12] D. Lunney, Extending and refining the nuclear mass surface with ISOLTRAP, J. Phys. G: Nucl. Part. Phys. 44 (6) (2017) 064008.
[13] M. Breitenfeldt, D. Atanasov, K. Blaum, T. Eronen, P. Finlay, F. Herfurth, M. Kowalska, S. Kreim, Yu. Litvinov, D. Lunney, V. Manea, D. Neidherr, T. Porobic, M. Rosenbusch, L. Schweikhard, N. Severijns, F. Wienholtz, R.N. Wolf, K. Zuber, Q-values of Mirror Transitions for fundamental interaction studies. CERN INTC proposal P-369, 2013.
[14] J. Karthein, Precision mass Measurements using the Phase-Imaging Ion-Cyclotron-Resonance Detection Technique (Master thesis), University of Heidelberg, 2017 https://cds.cern.ch/record/2300223?ln=en.
[15] C. Nieter, J.R. Cary, VORPAL: a versatile plasma simulation code, J. Comput. Phys. 196 (2) (2004) 448–473.
[16] VSimhttps://www.txcorp.com.
[17] V.N. Fedosseev, L.E. Berg, D.V. Fedorov, D. Fink, O.J. Launila, R. Losito, B.A. Marsh, R.E. Rossel, S. Rothe, M.D. Seliverstov, A.M. Sjödin, K.D.A. Wendt, Upgrade of the resonance ionization laser ion source at ISOLDE on-line isotope separation facility: new lasers and new ion beams, Rev. Sci. Instrum. 83 (2) (2012) 02A903.
[18] R. Kirchner, On the thermoionization in hot cavities, Nucl. Instrum. Methods Phys. Res., Sect. A 292 (2) (1990) 203–208.
[19] V.I. Mishin, V.N. Fedoseyev, H.-J. Kluge, V.S. Letokhov, H.L. Ravn, F. Scheerer, Y. Shirakabe, S. Sundell, O. Tengblad, Chemically selective laser ion-source for the CERN-ISOLDE on-line mass separator facility, Nucl. Instrum. Methods Phys. Res., Sect. B 73 (4) (1993) 550–560.
[20] J. Lettry, R. Catherall, U. Köster, U. Georg, O. Jonsson, S. Marzari, V. Fedosseev, Alkali suppression within laser ion-source cavities and time structure of the laser ionized ion-bunches, Nucl. Instrum. Methods Phys. Res., Sect. B 204 (2003) 363–367.
[21] RILIS Databasehttp://riliselements.web.cern.ch/riliselements/.
[22] T. Day Goodacre, J. Billowes, K. Chrysalidis, D.V. Fedorov, V.N. Fedosseev, B.A. Marsh, P.L. Molkanov, R.E. Rossel, S. Rothe, C. Seiffert, K.D.A. Wendt, RILIS-ionized mercury and tellurium beams at ISOLDE CERN, Hyperfine Interact. 238 (1) (2017) 41.
[23] Y. Martinez Palenzuela, (Ph.D. Thesis). KU Leuven. In preparation.
[24] B.H. Wolf, J. Cederkäll, O. Forstner, F. Wenander, F. Ames, K. Reisinger, L. Liljeby, Ö. Skeppstedt, B. Jonson, G. Nyman, First radioactive ions charge bred in REXEBIS at the REX-ISOLDE accelerator, Nucl. Instrum. Methods Phys. Res., Sect. B: Beam Interact. Mater. At. 204 (2003) 428–432.
[25] P. Schmidt, F. Ames, G. Bollen, O. Forstner, G. Huber, M. Oinonen, J. Zimmer, Bunching and cooling of radioactive ions with REXTRAP, Nucl. Phys. A 701 (1–4) (2002) 550–556.
[26] G. de Angelis, G. Fiorentini, The Legnaro National Laboratories and the SPES facility: nuclear structure and reactions today and tomorrow, Phys. Scr. 91 (11) (2016) 113001.
[27] M. Lewitowicz, The SPIRAL2 Project and experiments with high-intensity rare isotope beams, J. Phys: Conf. Ser. 312 (5) (2011) 052014.
[28] L. Popescu, Nuclear-physics applications of MYRRHA, EPJ Web Conf. 66 (2014) 10011.
[29] R.S. Augusto, L. Buehler, Z. Lawson, S. Marzari, M. Stachura, T. Stora, the CERN-MEDICIS Collaboration, CERN-MEDICIS (Medical Isotopes Collected from ISOLDE): a new facility, Appl. Sci. 4 (2) (2014) 265–281.

5.2 Performance of the modified VADLIS on-line at ISOLDE

After the first off-line studies demonstrating a factor >2 enhancement in extraction of gallium, follow-up tests and characterization of the modified VADLIS took place at ISOLDE. A summary of the results obtained while operating the modified VADLIS in RILIS-mode on-line for the extraction of magnesium, molybdenum and mercury beams are given in Section 5.1. In the present section, more details are given regarding the operation of the modified VADLIS at ISOLDE during such tests, carried out in November 2017 (unit #630). These measurements were possible since an experiment intended to extract refractory transition metals as oxides or fluorides as proposed in [77] was scheduled. It gave the opportunity to test the new device under on-line conditions. Information on the target material used is given in Section 5.1. The modified VADLIS with which the unit was equipped would allow for favourable extraction of laser-ions by biasing the extraction plates to negative voltages.

Figure 5.1a shows the boron nitride (BN) insulator with a thread in which the extraction plates and anode body were mounted. Figure 5.1b shows the connection to the anode body and extraction plates.

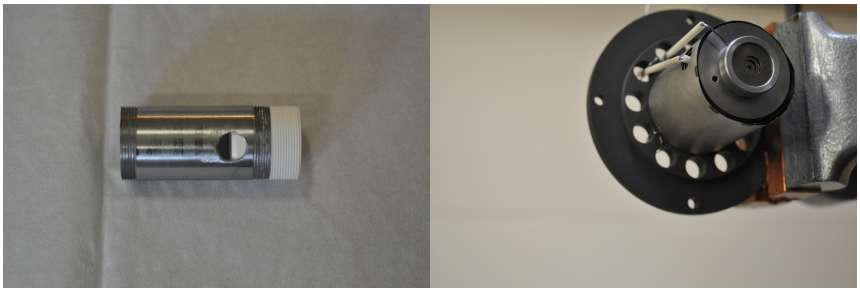

(a) (b)

Figure 5.1: Building of the modified VADLIS with extraction plates for first off-line tests. a) Anode body mounted on BN insulator with thread. b) Connections to anode body and extraction plates.

RILIS-ionized beams of magnesium (which evaporates from the target material), molybdenum (atoms evaporate from the molybdenum anode surface) and mercury (either radiogenically produced or present as a contaminant in the target material) were extracted. The ionization schemes used during the measurements are shown in Fig. 5.2. The summary of the measurements and

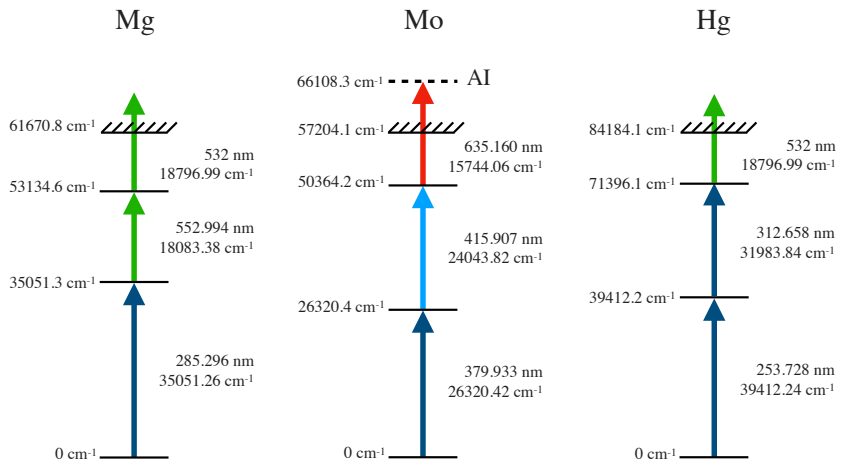

Figure 5.2: Ionization schemes used for the study of laser-ionized beams of magnesium [42], molybdenum [78] and mercury [42].

more details on the target/ion source assembly specificities can be found in Table 2 of Section 5.1.

5.2.1 Magnesium

Magnesium atoms evaporate from the target material and reach the anode via the cathode tube. The extraction of $^{24}Mg^{+}$ was studied by scanning the extraction plate voltage (V_e) in the range from [0 V,-300 V]. Results are shown in Fig. 5.3 for three anode voltages: 1, 5 and 250 V. The enhancement factor when the anode is at 1 V (RILIS-mode) equals 2.8. When the anode is set at 5 V (RILIS-mode, no cathode ions) this factor increases to 4.7.

These results are in agreement with the off-line results for gallium: when V_a=5 V only the ions produced within the anode volume by the laser pulse are present, then applying an additional extraction voltage plays a more important role in extracting a higher percentage of the ions that otherwise would have been trapped in the potential well. More information in this regard can be seen in Fig. 8 in Section 5.1.

In cases where surface ions are present as an isobaric contaminant in the RILIS-ionized beam, the VADLIS offers an opportunity for increased selectivity. For example, when magnesium beams are desired, isobaric sodium contaminants

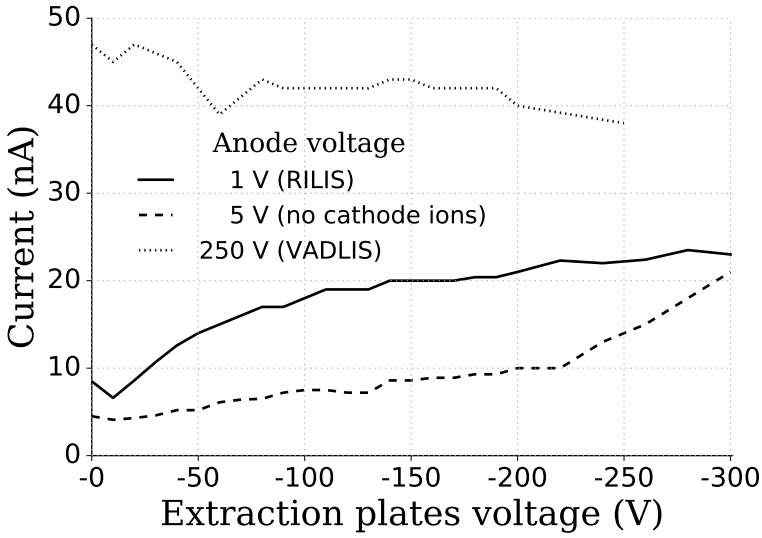

Figure 5.3: ^{24}Mg ion current as a function of the voltage applied to the extraction plates for 1, 5 and 250 V anode settings.

can also be present (sodium is surface ionized). By operating the ion source in RILIS-mode at 5 V, the incoming sodium contribution from the cathode tube can be suppressed while maintaining the same magnesium extraction efficiency.

RILIS-ionization of magnesium required the use of a non-resonant ionization step, provided by a 40 W, 532 nm Nd:YVO_4 laser (Coherent Blaze) [79]. Approximately 25 W is directed to the ion source, and can cause localized heating of the cathode surfaces. This heating increased the total (VADLIS) signal considerably (see Fig. 5.3). The cooling effect was observed at the end of the anode voltage when blocking the Blaze laser as shown in Fig.5.4.

5.2.2 Molybdenum

It was discussed in Section 5.1 that a higher enhancement factor is achieved for ions created within the anode volume when biasing the extraction plates to negative values. Molybdenum atoms evaporate from the anode body, and are not volatile enough to exist in large quantities outside of the anode. This makes it a suitable element to study the extraction enhancement of ions with a creation point within the anode volume. Figure 5.5 shows the results of scanning V_a and

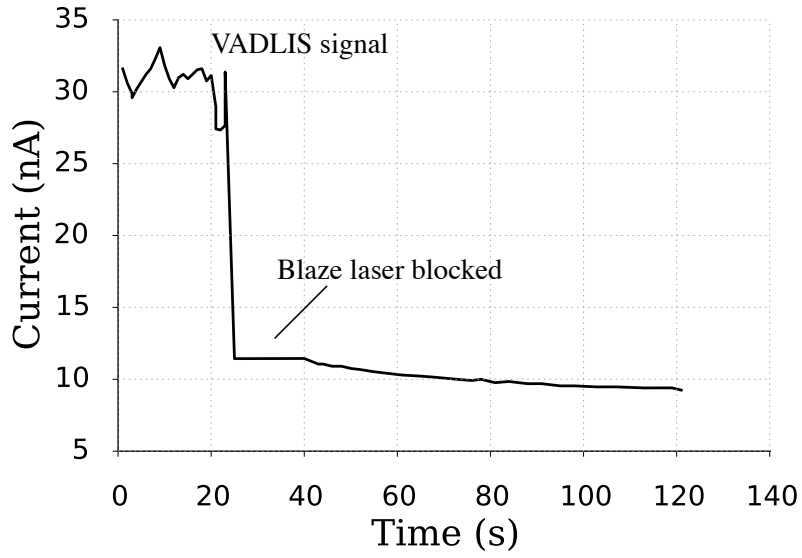

Figure 5.4: ^{24}Mg ion current before and after blocking the Blaze laser to observe heating effect.

V_e to determine the regions for which the extraction enhancement is highest. The isotope used was ^{98}Mo, which has an isotopic abundance of 24.39 %.

The highest signal is obtained at V_a=0 V. The anode scan for Mo does not exhibit the characteristic low V_a ion peak corresponding to the combined effects of extracting ions created inside both the cathode and the anode. This is because the anode walls themselves are the source of Mo atoms. For this reason, Mo is a good candidate for investigating the ion extraction enhancement of the additional extraction voltage for ions created inside the anode only. In this case, the enhancement factor was higher (7.7) when optimizing the extraction voltage.

5.2.3 Mercury

The versatility of the VADLIS for selective ionization of mercury has been demonstrated in various occasions. For example, in 2017 a successful run for SSP (Solid-State Physics) experiments (IS602, IS640, IS585 and IS515) and

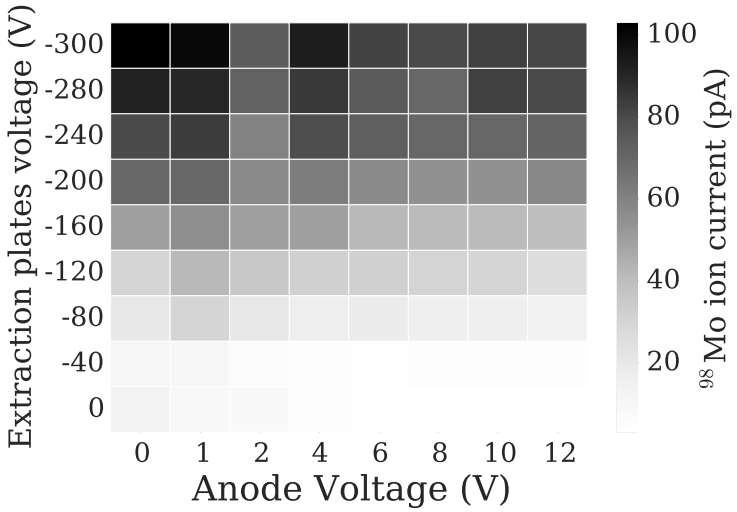

Figure 5.5: Scan of the voltages V_a and V_e to optimize the extraction of ^{98}Mo.

MINIBALL took place in which both teams (SSP and MINIBALL) required beams of ^{199}Hg and ^{206}Hg respectively. A liquid-Pb target was used (#619). VADIS-mode provided enough beam intensity for SSP collections while RILIS-mode provided the required purity for MINIBALL (isobaric Pb contamination was dominant in VADIS-mode). Switching from one mode of operation to the other allowed for a more efficient exploitation of the available time without the intervention of the RILIS team to correct for the isotope shift each time, when switching from mass 199 to mass 206.

In this work we used the modified VADLIS for enhanced extraction of laser-ionized mercury ion beams. Mercury atoms (present in the target material as a contaminant or radiogenically produced) are laser-ionized in both the cathode tube and the anode. Surface ionization of mercury is negligible due to its high ionization potential, however an ion current of an unidentified species at this mass was observed. The 'lasers OFF' signal has therefore been labelled as 'background'.

Table 5.1 shows the enhancement in ion signal when V_e is optimized in RILIS-mode, compared to the signal when V_e is kept at 0 V, showing that a factor 2 improvement can be achieved.

Table 5.1: ^{196}Hg ion current enhancement when V_e is optimized for maximum ion extraction in the RILIS region. (This dataset is different from the one used to get the results shown in Table 2, Section 5.1).

V_a (V)	Lasers On V_e=0 V (pA)	Background V_e=0 V (pA)	Lasers On V_{e_opt} (pA)
0.0	30	18	97
0.2	50	35	90
0.4	50	34	100
0.6	56	31	86
0.8	44	34	85
1.0	45	34	85
1.3	50	37	99
1.6	58	40	90
1.9	60	40	114

5.3 Electrostatic field distribution in the VADLIS: other considerations

For the purpose of these studies, the simulations are divided in two parts (same procedure was followed to obtain the results in Section 5.1). First, we find the electrostatic fields at a quasi-steady state for the electron population, where the electrons incident from the cathode plus those generated through ionization processes in the anode match those absorbed in the walls.

Figure 5.6 (obtained from a simulation) shows the number of electrons in the ion source and the electron current as a function of time. The anode voltage is set to 1.35 V to ensure RILIS-mode of operation (region I in Fig. 2 Section 5.1). The electron current emitted from the cathode is 0.2 mA (taken from Fig. 4.4), and using 0.1 mA as an input for the simulation due to the 50 % transparency of the anode grid) for an operation temperature of 1935 °C.

Under these conditions, the quasi-steady state for the electron population is

reached at ∼30 ns (Fig 5.6 (top panel)). The evolution of the electron current can be observed in Fig 5.6 (lower panel). At this point, the electrostatic fields are established and it is assumed that these conditions will not change when photo-ions are created on the axis of the anode volume (see Fig. 5a in Section 5.1).

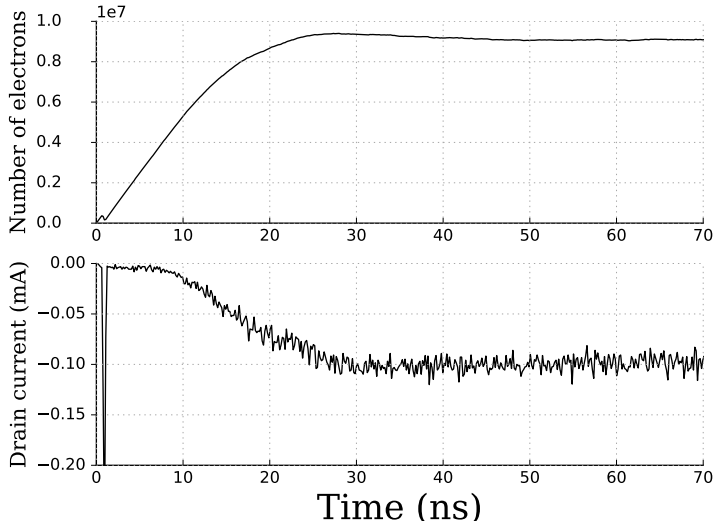

Figure 5.6: Simulated number of electrons as a function of time in the anode cavity (top panel) and electron current (drain current) emitted by the cathode as a function of time (lower panel).

As a second step, a cylinder of ions is placed along the axis of the ion source representing the ions created in the region of interaction of the laser beam with the atoms.

Figure 5.7 (top-left) shows the initial position of the ions within the ion source, marking the arrival of the laser pulse. In the four stages represented, the color scale stays the same. The blue dots represent ions with initial position near the back of the ion source and red dots represent ions near the exit hole of the ion source. The beam formation and extraction is depicted in the top-right panel (5 μs). Ions nearer the exit hole are extracted first, contributing to the prompt peak release in Fig. 4a) in Section 5.1. After $\sim$ 30 μs (bottom-left), ions initially at the back start being extracted. These are the ones that contribute to the second peak in Fig. 4a) in Section 5.1. The ions that are not extracted within the ∼100 μs window are trapped in the potential well, or come out slowly

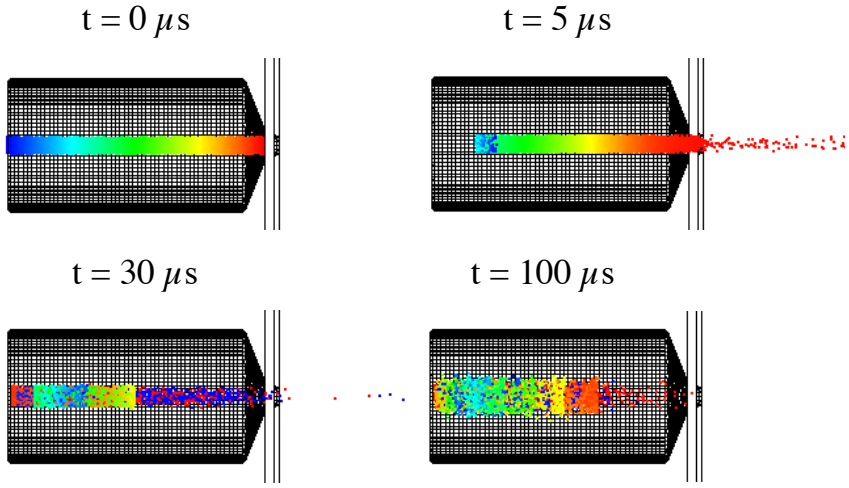

Figure 5.7: Temporal evolution of the location of the ions in a 100 μs window (time between two laser pulses at 10 kHz repetition rate, 5 to 30 ns laser pulse duration). The particles are color-tagged according to their initial position from left (blue) to right (red), as shown in the top-left figure (0 μs). See text for a description of the four stages depicted in the figure.

compared to the time between pulses, contributing to the background signal measured in Fig. 4b) in Section 5.1.

5.4 Influence of the extraction voltage on the mass resolving power

As discussed in Section 5.1, biasing the voltage of the extraction plates increases the energy spread of the ions created in the region close to the extraction aperture as shown in Fig. 5b), Section 5.1. The influence of setting the extraction plates to -200 V while operating the ion source in RILIS-mode was studied experimentally by observing the mass resolving power as shown in Fig. 5.8. The peaks correspond to ^{69}Ga and ^{71}Ga. The peaks were fitted with a Gaussian function and the mass resolution decreased from 1200 (0 V bias on the extraction plates) to 600 (-200 V bias on the extraction plates). A mass resolving power of 600 is sufficient to separate the masses of interest.

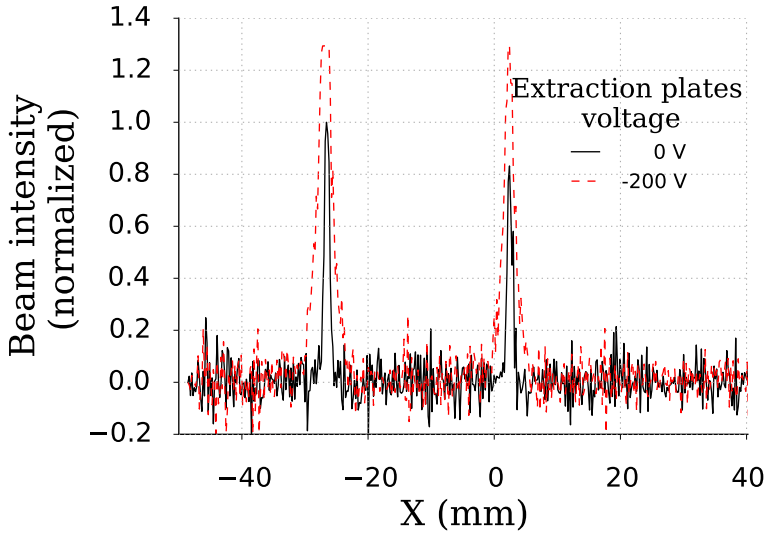

Figure 5.8: Beam profile measured at the scanner position (focal plane downstream of the dipole magnet) when the extraction plates are set to 0 and -200 V.

5.5 Effect of neutral atom density and ion load

By introducing an additional ionization mechanism that is independent of temperature, electron dynamics and collisional processes, the RILIS-mode offers an opportunity to study the effect on the ion survival or extraction, without altering the dominant ion creation process itself. In this case, the effect of neutral atom or molecule presence on the RILIS-mode ionization efficiency is studied. In standard FEBIAD operation (with electron impact ionization being the dominant ionization mechanism) it is not possible to inject a neutral gas, without in turn increasing the ion production rate (due to ionization of the gas itself).

Similarly, when operating in RILIS-mode, it has been possible to study the effect on the RILIS ionization efficiency as the ion load of the ion source is varied. This is done by evaporating a dispenser of rubidium atoms which are readily surface ionized on the metallic parts of the ion source.

Both aspects of this study are of interest since, at laboratories producing radioactive beams on-line, particularly next-generation facilities, it is important

to be able to maintain the ionization efficiency under a variety of experimental conditions. Aspects such as target and material cleanliness, volatility, volume, production rate and required temperature, all influence the evaporation rate of neutrals and, in turn, ion densities in the ion source. It is therefore important to understand the operating limits of the ion source options that are available.

The advantage of injecting neutrals in the ion source was discussed by Kirchner for the case of the hot cavity [36] in which an increase in efficiency was observed. Kirchner discusses how the probability of a surface ionized particle leaving the ion source as an ion is enhanced when the neutral atom density is increased. Xenon gas was used for such studies, showing that the extraction efficiency for the surface ionized elements can be increased up to a factor 5. The reason for this was associated to the suppression of the recombination probability in the walls of the ion source. An ion created in the surface of the cavity loses its excess energy by colliding with the neutral atoms, not having enough energy anymore to traverse the ionizer cavity and overcome the plasma potential when approaching the wall of the ion source. The ion is therefore confined, unable to recombine with the cavity walls, and efficiently extracted after being guided along the cavity under the influence of the longitudinal cavity heating voltage.

Fig. 5.9 shows how the laser-ionized (RILIS-mode of the VADIS) ^{71}Ga beam intensity varies while adjusting the neutral CO_2 pressure (by injecting CO_2 in a controlled way using a leak valve, which decomposes into CO at high temperatures). Gallium is either surface or laser ionized (laser off shown as sharp dips). Electron-impact ionization of Ga in RILIS-mode is negligible.

It can be seen how, as the pressure increases (which is dominated by the CO gas load in the ion source), the extraction efficiency of ^{71}Ga also increases by a factor 3. When the leak valve was closed, (see maximum value in Fig. 5.9), the extracted ^{71}Ga started to decrease. Since the CO remains neutral, the enhancement in the ^{71}Ga signal cannot be explained by charge exchange mechanisms. A more plausible mechanism is inelastic collisions between Ga^+ ions and CO molecules, which improves the confinement of the Ga^+ ions in the potential well, reducing their probability of reaching the anode walls, where neutralization could occur.

A direct observation that suggests the presence of a collisional environment (for the hot cavity) was reported by the ISOLTRAP collaboration. The RILIS scheme for ionizing elemental Cu was used, yet the laser wavelength scan, corresponding to the atomic Cu resonance, was seen when observing the $CuCH_2$ peak (mass separator set to maximize transmission of $CuCH_2$) in the ISOLTRAP MR-ToF-MS. This proves that the Cu^+ ion formed a $CuCH_2$ molecule inside

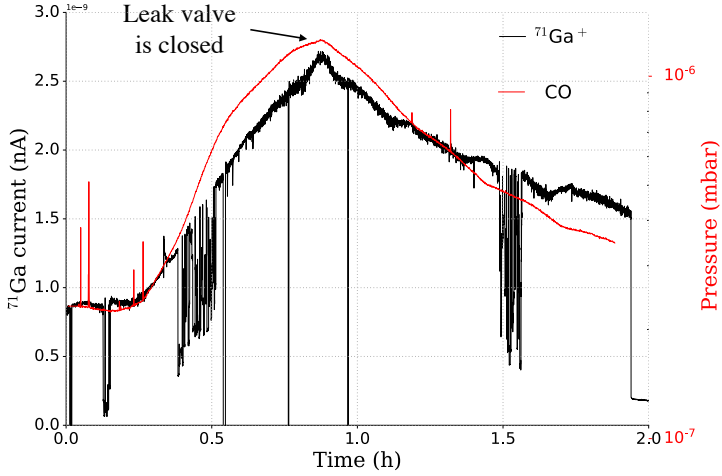

Figure 5.9: $^{71}Ga^+$ signal enhancement as CO_2 is injected into the source in RILIS-mode (again, we measure the CO content in the RGA). The 'dips' going to zero correspond to the insertion of the Faraday cup in the way of the beam for total current measurements. The large 'dips' correspond to periods where the laser beams were blocked or the wavelength was being readjusted.

the laser ion source, after resonance ionization. More details can be found in [80].

Another more probable mechanism that could be the factor leading to the increase in Ga^+ signal, is the enhancement in surface and laser-ion survival of Ga^+ in the cathode tube due to the CO gas load present. In the cathode tube, the gas pressure is higher (smaller volume) as compared to the anode volume and the ion confinement is weaker (based only on the cavity plasma potential). The enhancement mechanism is then explained by the one proposed by Kirchner. Further investigation is required to better understand the effect of the CO gas load (or using non-surfaced ionized species) such as using gas injection from elsewhere (not through the cathode), by inverting the cathode polarity to suppress ions created inside the cathode tube, or by using a closed cathode, therefore measuring only ions created in the anode volume.

To test this hypothesis (enhancement in surface and laser-ion survival of

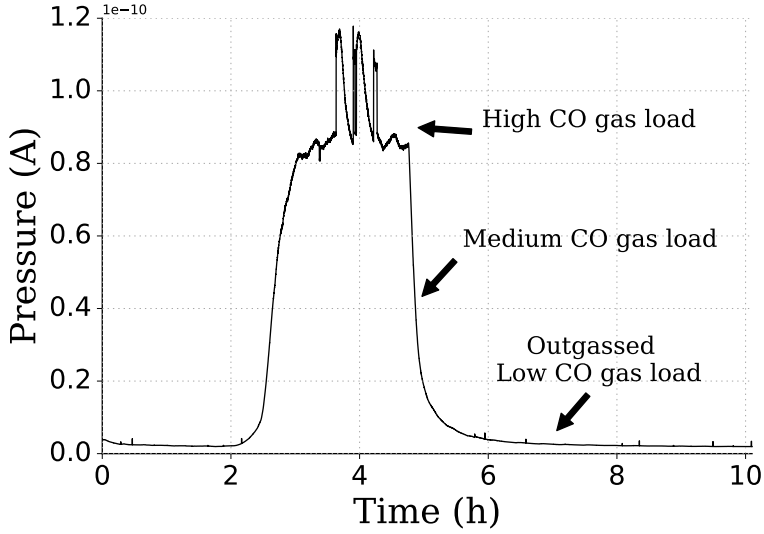

Figure 5.10: Amount of CO in the ion source as a function of time measured by the residual gas analyzer, placed at the exit of the ion source. (The y-axis shows relative values since a calibration of the RGA is not available.)

Ga^+ in the cathode tube due to the CO gas load present), anode voltage scans with different CO pressures were performed. During the anode voltage scans, the Ga signal with lasers ON and lasers blocked was recorded. Three situations were studied. In the first one, the ion source is loaded with CO (leak valve open and stable conditions reached) yielding an extracted CO^+ ion current of 10 μA in VADIS mode. In the second one, the leak valve was closed and the scan was performed when the CO pressure was 50 % of the initial value. The last anode scan was performed after more than 40 hours of outgassing, meaning the ion source was operating under typical CO^+ ion extracted ion currents of the order of $\sim$ 500 nA. The relative amount of CO measured by the residual gas analyzer is displayed in Fig. 5.10.

Figure 5.11 shows the three anode scans performed. The 'Lasers on (VADLIS)' curve refers to the total signal recorded for gallium which includes all possible ionization mechanisms. The 'Lasers off' scan was performed while blocking the lasers, the main ionization mechanisms are therefore surface ionization and electron impact ionization (or VADIS). The 'RILIS' curve is the result of subtracting the 'Lasers on' and 'Lasers off' curves, showing the contribution from laser ions only.

The data displayed in Fig. 5.11a and Fig. 5.11b were taken under the same experimental conditions (Ga evaporation rate from the oven and laser performance were kept stable during the time the measurement was done). A higher total ion rate in Fig. 5.11a in the low voltage region suggests, given that the RILIS signal did not increase noticeably, an increase of the surface ions created within the hollow cathode.

Once the ion source has been outgassed and the CO content brought back to the nominal value, the ion source performs as usual and the ratios VADLIS: (surface + VADIS): RILIS are as expected as shown in Fig. 5.11c (see also Fig. 2 in Section 5.1). In this case the absolute values cannot be compared to those shown in Fig. 5.11a and Fig. 5.11b since the lasers were re-tuned and the same evaporation rate of Ga atoms from the oven couldn't be guaranteed.

Since the results obtained here points out an enhancement for cathode tube-originating ions occurs, it hints to the prospect that, the hot cavity SIS can be used for higher ionization potential elements with enhanced efficiency if neutral species are added. This would improve ion survival through inelastic collisions to reduce wall contact probability. This would be highly beneficial mainly for facilities without a laser ion source available, for which the injection of CO would be of great advantage (e.g. MEDICIS). The plasma ion source is more complicated from the technical point of view and less robust than the hot cavity. It also creates undesired contamination. The emittance is worse compared to the hot cavity and it has larger energy spread. Intermediate ionization potential elements for which high temperatures are needed would benefit from the option of improving the properties of the cavity for surface ionization. A calibrated leak could be added to the standard units to further investigate the influence of CO (and other gases) on the ionization enhancement. Adding the gas would allow for better surface ionization while laser ionization, if available, can be used when selectivity is desired.

The influence of ion load on the ion source efficiency was investigated by measuring the ^{71}Ga output when the Rb^+ ion density is increased. Rubidium atoms (W_i=4.2 eV) were evaporated into the ion source volume from an oven. Due to its low ionization potential, Rb is easily surface-ionized and several μAs of ^{85}Rb beam can be extracted.

Figure 5.12 shows how an excess of ions in the ion source influences the extracted Ga^+ beam. The Ga^+ beam almost disappears, decreasing from 3.4 nA to 0.1 nA. At this point the total beam current is 9.4 μA, Rb^+ being the biggest component (6.3 μA at the end of the measurement).

From this study it is not possible to draw conclusions about the ion capacity

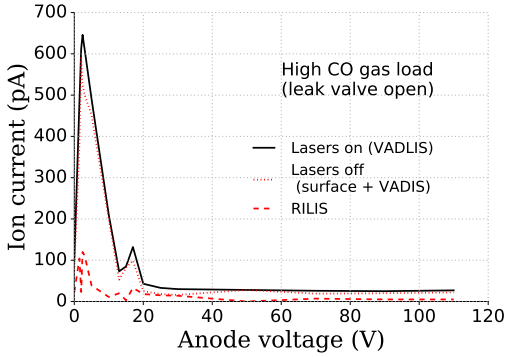

(a) High CO load.

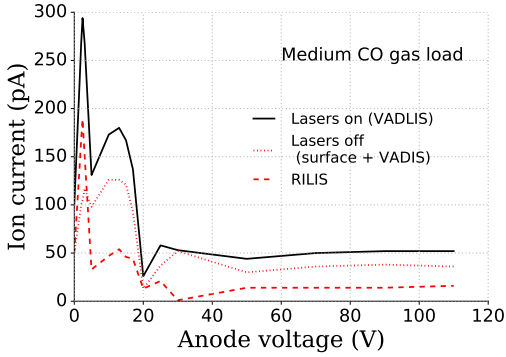

(b) Medium CO load.

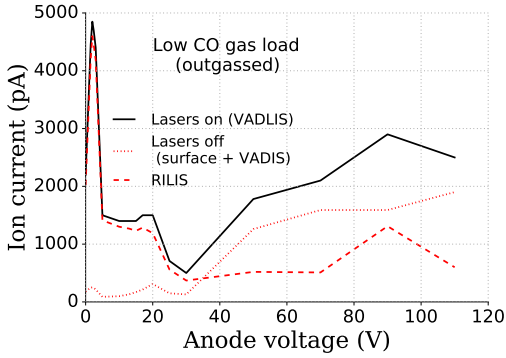

(c) Low CO load.

Figure 5.11: Anode voltage scan for different pressures of CO within the anode volume.

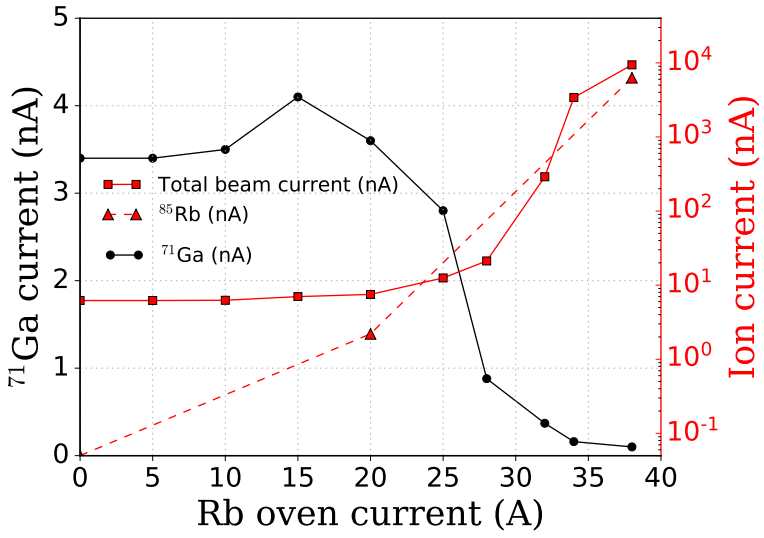

Figure 5.12: ^{71}Ga ion current in RILIS-mode dependence on the ion load capacity. The cathode temperature is 2035 °C.

of the VADLIS on its own because the measured signal has several sources of origin:

- Ga^+ and Rb^+ surface ions originating in the cathode tube
- Ga^+ and Rb^+ surface ions originating in the anode
- laser ionized Ga^+ from the cathode tube and anode volume

Increasing the Rb^+ ion rate ends up having an influence in the extracted Ga^+ ion beam as observed in Fig. 5.12. A different experimental configuration would be required to understand the influence of the ion load capacity on the extracted beam for ions generated inside the anode volume. Such an approach would be important for determining the ion capacity limits of the VADLIS itself. For example, inverting the cathode polarity, measuring the Ga^+ signal in an anode voltage region that guarantees suppression of ion created in the cathode tube or using a closed cathode configuration. Under these conditions, it would also be possible to investigate the influence of the extraction plates voltage on the VADLIS ion capacity.

Chapter 6

Conclusions

6.1 Contribution of this work

This thesis work investigated two aspects of radioactive beam production at CERN using the isotope separator on-line (ISOL) method:

- The optimization, commissioning and first beams of a new facility (MEDICIS), dedicated to the production of potentially interesting new medical isotopes.
- A detailed characterization and optimization of the VADIS and newly established VADLIS ion sources, of interest for ISOL facilities around the globe.

The MEDICIS infrastructure and operating regime are introduced. The application of ion beam transport simulations to drive the design and commissioning of the MEDICIS beamline has been described. The experimental beam properties have been used to validate the ion optics simulation approach used in this work. The agreement between simulations and experiments showed that the facility is operating in line with expectations and indicate its suitability for full scale operation. Details on the first beams produced at MEDICIS, both stable and radioactive, are provided.

With the goal of improving our understanding of FEBIAD ion sources, and thereby enhancing their performance for ISOL facilities in general (in

our case ISOLDE and MEDICIS), a study of the ISOLDE FEBIAD (VADIS) has been conducted, using a mixture of experimental work and particle-in-cell simulations. For example, the dependence of the ion source extraction efficiency on operational parameters such as cathode temperature, anode voltage, ion source magnet and ion load was studied. In addition, the VADIS efficiency for gallium, mercury, manganese, tin and magnesium were investigated experimentally.

Using the VSim software package, and by employing a novel iterative approach to mitigate the computational challenge of accounting for both the electron and ion dynamics, a deeper insight into the FEBIAD operation has been achieved. Although largely qualitative, the evolution of the potential field lines generated by the combined effect of the electrostatic potentials and the electron and ion densities has been shown. The role of the ion source magnetic field in enabling the electrons to penetrate further into the ion source has been demonstrated.

The simulations also imply a transition between ion source 'modes' during the initial 'ignition' phase. This does not suggest an arc discharge, as the acronym FEBIAD suggests, but rather a filling of the electrostatic potential well with ions, leading to the creation of a sustainable electrostatic ion funnel, providing favourable and self-sustaining ion extraction conditions.

Such an interpretation is consistent with the notion that the ion source is not simply an electron-dominated electron-impact ionization volume but rather that the optimum conditions for ionization efficiency require a certain balance of electron and ion densities. This implies an ion start-up (ignition) time, estimated to be several tens of microseconds depending on the ion creation rate. A next step, but out of the scope of this work, would be to test this experimentally using one or both of the methods described in Section 4.2.2.

Particular attention has been devoted to the newly developed VADLIS, which is a combination of the VADIS and the RILIS, offering unique versatility amongst ion sources used for radioactive ion beam production through the ability to quickly switch between a selective laser ionization mode and a universal electron impact ionization mode. For example, the VSim software has been used to demonstrate that the VADLIS, operated in RILIS-mode, suffers from a lower ion extraction voltage which reduces the ion extraction probability. This led to the development of a modified VADLIS prototype for enhanced laser-ion extraction by means of extraction voltage optimization. The results of using this device for the first off-line and on-line tests are presented, confirming the efficiency improvement expected from simulations. This ion source is now proposed as the most versatile ion source for use at ISOLDE.

The ion load investigation carried out in this thesis indicates that, by combining the RILIS and the VADIS, and now with the ability to optimize ion extraction, progress has been made towards realizing a high ion capacity laser ion source. This conclusion is based on the comparison of the experimentally-observed ion load limits of the hot-cavity laser ion source (several hundreds of nA, observed during ISOLDE operation) and the calculated space-charge limited ion extraction rate from the VADIS (in the range of 10 μA). This is particularly important for a facility such as MEDICIS, for which in-target production takes place over several days inside a room-temperature target unit. The subsequent extraction of the radioisotopes of interest takes place later on at MEDICIS, with the goal of extracting the sample in the form of an ion beam with minimal loss of specific activity. To further complicate matters, when the target is heated, any sufficiently volatile radiogenic species that was accumulated during the target irradiation, will enter the ion source alongside the sample of interest. To handle this, the ion source should have a sufficient ion capacity, or be sufficiently selective to minimize the ionization of the unwanted species. By offering the ability to switch between selective and non-selective ionization modes the VADLIS offers the advantage of enabling detailed evaporation or outgassing monitoring (in VADIS mode) of the target unit, followed by selective-laser ionization of the isotope of interest (in RILIS mode). Further experimental characterization of the modified VADLIS is required to test the assumption that this ion source offers an ion-capacity advantage over the standard hot-cavity RILIS. Such a test could be carried out by monitoring the effect on the laser-ion rate while varying the ion density of a surface ionized species (such as Rb, through the use of a Rb ion dispenser). By measuring the laser-ion current versus total extracted current (ensuring the ions are created in the anode volume) while maintaining the same atom density of the laser ionized species, the ion capacity of the VADLIS could be evaluated.

6.2 Future directions

Based on the validation of the VSim software for the study of the electrostatic field distribution and ion dynamics in the VADIS and VADLIS, further use of this modelling approach could be devoted to the optimization of the physical parameters of the ion source (extraction hole and ion source diameter, length, grid shape, cathode-grid distance). Such an approach will undoubtedly streamline the process of realizing an optimal FEBIAD configuration.

Although this work has provided further insight into various aspects, it also points out certain areas of uncertainty which require further investigation. For

example, the importance of collisional ionization/charge exchange processes occurring under high gas load has been demonstrated but so far the investigation has been limited to a small variety of gases and a restricted pressure range. For example, similar work at GANIL indicates that, under certain conditions, the presence of xenon enhances the ionization rates for certain species [81].

The attempt to understand the chemical dependence of the VADIS efficiency through a series of standard efficiency measurements was unable to reveal any correlations. This was because the measurement method does not allow to preserve all operational parameters between measurements. An alternative method that enables an interrupted use of the same ion source, and therefore maintaining the same experimental conditions, is clearly required.

Making use of the independent control of the extraction voltage of the VADLIS should be investigated as a possible means of improving RILIS selectivity. This could be achieved by optimizing the timing of a pulsed extraction voltage, with respect to the laser-ion creation time.

Bibliography

[1] G. Dumont, H. Pattyn, M. Huyse, G. Lhersonneau, J. Verplancke, J. Van Klinken, J. De Raedt, and D. L. Sastry. LISOL, the Leuven isotope separator on-line at the "cyclone"-cyclotron. *Nuclear Instruments and Methods*, 153(1):81–92, 1978.

[2] M.J.G. Borge and K. Blaum. Focus on Exotic Beams at ISOLDE: A Laboratory Portrait. *Journal of Physics G: Nuclear and Particle Physics*, 45(1):010301, 2018.

[3] C. Müller, C. Vermeulen, U. Köster, K. Johnston, A. Türler, R. Schibli, and N.P. van der Meulen. Alpha-PET with terbium-149: evidence and perspectives for radiotheragnostics. *EJNMMI Radiopharmacy and Chemistry*, 1(1):5, 2016.

[4] C. Muller, K. Zhernosekov, U. Koster, K. Johnston, H. Dorrer, A. Hohn, N.T. van der Walt, A. Turler, and R. Schibli. A unique matched quadruplet of terbium radioisotopes for PET and SPECT and for alpha- and beta-radionuclide therapy: an in vivo proof-of-concept study with a new receptor-targeted folate derivative. *Journal of nuclear medicine : official publication, Society of Nuclear Medicine*, 53(12):1951–1959, 2012.

[5] C. Müller, E. Fischer, M. Behe, U. Köster, H. Dorrer, J. Reber, S. Haller, S. Cohrs, A. Blanc, J. Grünberg, M. Bunka, K. Zhernosekov, N. van der Meulen, K. Johnston, A. Türler, and R. Schibli. Future prospects for SPECT imaging using the radiolanthanide terbium-155 - production and preclinical evaluation in tumor-bearing mice. *Nuclear Medicine and Biology*, 41:e58–e65, 2014.

[6] R. S. Augusto, L. Buehler, Z. Lawson, S. Marzari, M. Stachura, T. Stora, and the CERN-MEDICIS Collaboration. CERN-MEDICIS (Medical Isotopes Collected from ISOLDE): A New Facility. *Applied Sciences*, 4(2):265–281, 2014.

[7] P. Van Duppen. Isotope Separation On Line and Post Acceleration. In *The Euroschool Lectures on Physics with Exotic Beams, Vol. II*, pages 37–77, Leuven, 2006.

[8] M.D. Lunney and R.B. Moore. Cooling of mass-separated beams using a radiofrequency quadrupole ion guide. *International Journal of Mass Spectrometry*, 190-191:153–160, 1999.

[9] E. Mané, J. Billowes, K. Blaum, P. Campbell, B. Cheal, P. Delahaye, K.T. Flanagan, D.H. Forest, H. Franberg, C. Geppert, T. Giles, A. Jokinen, M. Kowalska, R. Neugart, G. Neyens, W. Nörtershäuser, I. Podadera, G. Tungate, P. Vingerhoets, and D.T. Yordanov. An ion cooler-buncher for high-sensitivity collinear laser spectroscopy at ISOLDE. *The European Physical Journal A*, 42(3):503–507, 2009.

[10] M Mukherjee, D Beck, K Blaum, G Bollen, J Dilling, S George, F Herfurth, A Herlert, A Kellerbauer, H J. Kluge, S Schwarz, L Schweikhard, and C Yazidjian. ISOLTRAP: An on-line Penning trap for mass spectrometry on short-lived nuclides. *The European Physical Journal A*, 35(1):1–29, 2008.

[11] F. J. C. Wenander. Charge Breeding of Radioactive Ions. *CAS-CERN Accelerator School: Ion Sources*, 2014.

[12] SIMION https://simion.com/.

[13] C. Nieter and J.R. Cary. VORPAL: A versatile plasma simulation code. *Journal of Computational Physics*, 196(2):448–473, 2004.

[14] VSim https://www.txcorp.com/vsim.

[15] Tech-X Corporation https://www.txcorp.com/.

[16] Boris. J. Proceedings of the Fourth Conference on Numerical Simulation of Plasmas. page 3, Washington DC, 1970.

[17] OPERA https://operafea.com/magnet-design-software/.

[18] M. Turrión, M. Eller, R. Catherall, L. M. Fraile, U. Herman-Izycka, U. Köster, J. Lettry, K. Riisager, and Th Stora. Management of ISOLDE yields. *Nuclear Instruments and Methods in Physics Research, Section B: Beam Interactions with Materials and Atoms*, 266(19-20):4674–4677, 2008.

[19] L. Penescu. *Techniques to produce and accelerate radioactive ion beams https://edms.cern.ch/document/1902501/5.* PhD thesis, Bucharest, Polytechnic Inst., 2009.

[20] Y. Kadi, Y. Blumenfeld, W. Venturini Delsolaro, M. A. Fraser, M. Huyse, A. Papageorgiou Koufidou, J. A. Rodriguez, and F. Wenander. Post-accelerated beams at ISOLDE. *Journal of Physics G: Nuclear and Particle Physics*, 44(8), 2017.

[21] J. Riegert, R. Catherall, T. Stora, and A.P. Bernardes. CERN-MEDICIS Organization of the operation https://edms.cern.ch/document/1902501/5, 2018.

[22] T. Stora. MEDICIS Operation and Target Life Cycle https://edms.cern.ch/document/1701216/1, 2016.

[23] Y. Amador and B. Conde Fernandez. MEDICIS Safety file - Descriptive part https://edms.cern.ch/document/1541088/0.6, 2018.

[24] J. A. Ferreira Somoza and C.Y. Vallgren. Vacuum Work Package description https://edms.cern.ch/document/1303144/4, 2017.

[25] ANSYS® Academic Research https://www.ansys.com/academic.

[26] M. Ballan, J. P. Ramos, S. Marzari, and T. Stora. Development of the ISOLDE-MEDICIS target oven: a large diameter tantalum container https://edms.cern.ch/document/2020611/1. Technical report, 2018.

[27] J P Ramos, M Ballan, L Egoriti, D Houngbo, S Rothe, R S Augusto, A Gottberg, L Popescu, M Dierckx, S Marzari, and T Stora. The design and tests for the new CERN-ISOLDE spallation source: an integrated tungsten converter surrounded by an annular UC$_{x}$ target operated at 2000°. 2019.

[28] FLUKA http://www.fluka.org/fluka.php.

[29] R. S. Augusto. Private communication.

[30] V Gadelshin, T Cocolios, V Fedoseev, R Heinke, T Kieck, B Marsh, P Naubereit, S Rothe, T Stora, D Studer, P Van Duppen, and K Wendt. Laser resonance ionization spectroscopy on lutetium for the MEDICIS project. In *HYPERFINE INTERACTIONS*, volume 238. Springer Verlag, 2017.

[31] S. Marzari, A.P. Bernardes, and Y. Martinez. MEDICIS Frontend https://edms.cern.ch/document/1734868/1.

[32] A.L. Septier. *Focusing of charged particles.* Number v. 2 in Focusing of Charged Particles. Academic Press, 1967.

[33] IRA https://www.chuv.ch/fr/ira/ira-home/.

[34] C2TN http://c2tn.tecnico.ulisboa.pt/.

[35] I. Langmuir and K.H. Kingdon. Thermionic Effects Caused by Vapours of Alkali Metals. *Proceedings of the Royal Society of London. Series A*, 107(741):61 LP – 79, 1925.

[36] R. Kirchner. On the thermoionization in hot cavities. *Nuclear Instruments and Methods in Physics Research Section A: Accelerators, Spectrometers, Detectors and Associated Equipment*, 292(2):203–208, 1990.

[37] R. Kirchner. Progress in ion source development for on-line separators. *Nuclear Instruments and Methods*, 186:275–293, 1981.

[38] V N. Panteleev, A E Barzakh, L Kh. Batist, D V Fedorov, V S. Ivanov, F Moroz, Pavel Molkanov, S Yu. Orlov, and Yu M. Volkov. The radioisotope complex project "RIC-80" at the Petersburg Nuclear Physics Institute. *Review of Scientific Instruments*, 86:123510, 2015.

[39] V N. Panteleev, A E Barzakh, L Kh. Batist, D V Fedorov, V S. Ivanov, F Moroz, Pavel Molkanov, S Yu. Orlov, Yu M. Volkov, and M. D. Seliverstov. Highly efficient ion source for surface and laser ionization. In *International Conference on Electromagnetic Isotope Separators and Related Topics-EMIS. In preparation*, Geneva, 2018.

[40] ISOLDE yield database https://isoyields2.web.cern.ch/.

[41] V. Fedosseev, K. Chrysalidis, T. Day Goodacre, B. Marsh, S. Rothe, C. Seiffert, and K. Wendt. Ion beam production and study of radioactive isotopes with the laser ion source at ISOLDE. *Journal of Physics G: Nuclear and Particle Physics*, 44(8):84006, 2017.

[42] RILIS Database http://riliselements.web.cern.ch/riliselements/.

[43] U. Köster, V.N. Fedoseyev, V.I. Mishin, L. Weissman, M. Huyse, K. Kruglov, W.F. Mueller, P. Van Duppen, J. Van Roosbroeck, P. Thirolf, H.G. Thomas, D. Weisshaar, W. Schulze, R. Borcea, M. La Commara, H. Schatz, K. Schmidt, S. Röttger, G. Huber, V. Sebastian, K.L. Kratz, R. Catherall, U. Georg, J. Lettry, M. Oinonen, H.L. Ravn, H. Simon, and ISOLDE collaboration. Isomer separation of Cu and Cu with a resonance ionization laser ion source. *Nuclear Instruments and Methods in Physics Research Section B: Beam Interactions with Materials and Atoms*, 160(4):528–535, 2000.

[44] R. Kirchner and E. Roeckl. A novel ISOL ion source. *Nuclear Instruments and Methods*, 139:291–296, 1976.

[45] S. Sundell and H. Ravn. Ion source with combined cathode and transfer line heating. *Nuclear Inst. and Methods in Physics Research, B*, 70(1-4):160–164, 1992.

[46] L. Penescu, R. Catherall, J. Lettry, and T. Stora. Development of high efficiency Versatile Arc Discharge Ion Source at CERN ISOLDE. *Review of Scientific Instruments*, 81(2):1–5, 2010.

[47] R Kirchner and E Roeckl. Investigation of gaseous discharge ion sources for isotope separation on-line. *Nuclear Instruments and Methods*, 133(2):187–204, 1976.

[48] CPO programs www.electronoptics.com.

[49] Y. Liu, D. W. Stracener, and T. Stora. Production of negatively charged radioactive ion beams. *New Journal of Physics*, 19(8):085005, 2017.

[50] T. Day Goodacre, J. Billowes, R. Catherall, T. E. Cocolios, B. Crepieux, D. V. Fedorov, V. N. Fedosseev, L. P. Gaffney, T. Giles, A. Gottberg, K. M. Lynch, B. A. Marsh, T. M. Mendonça, J. P. Ramos, R. E. Rossel, S. Rothe, S. Sels, C. Sotty, T. Stora, C. Van Beveren, and M. Veinhard. Blurring the boundaries between ion sources: The application of the RILIS inside a FEBIAD type ion source at ISOLDE. *Nuclear Instruments and Methods in Physics Research, Section B: Beam Interactions with Materials and Atoms*, 376:39–45, 2015.

[51] Y. Martinez Palenzuela, B.A. Marsh, J. Ballof, R. Catherall, K. Chrysalidis, T.E. Cocolios, B. Crepieux, T. Day Goodacre, V.N. Fedosseev, M.H. Huyse, P.B. Larmonier, J.P. Ramos, S. Rothe, J.D.A. Smith, T. Stora, P. Van Duppen, and S. Wilkins. Enhancing the extraction of laser-ionized beams from an arc discharge ion source volume. *Nuclear Instruments and Methods in Physics Research, Section B: Beam Interactions with Materials and Atoms*, 431, 2018.

[52] B. A. Marsh, T. Day Goodacre, S. Sels, Y. Tsunoda, B. Andel, A. N. Andreyev, N. A. Althubiti, D. Atanasov, A. E. Barzakh, J. Billowes, K. Blaum, T. E. Cocolios, J. G. Cubiss, J. Dobaczewski, G. J. Farooq-Smith, D. V. Fedorov, V. N. Fedosseev, K. T. Flanagan, L. P. Gaffney, L. Ghys, M. Huyse, S. Kreim, D. Lunney, K. M. Lynch, V. Manea, Y. Martinez Palenzuela, P. L. Molkanov, T. Otsuka, A. Pastore, M. Rosenbusch, R. E. Rossel, S. Rothe, L. Schweikhard, M. D. Seliverstov, P. Spagnoletti, C. Van Beveren, P. Van Duppen, M. Veinhard, E. Verstraelen, A. Welker, K. Wendt, F. Wienholtz, R. N. Wolf, A. Zadvornaya, and K. Zuber. Characterization of the shape-staggering effect in mercury nuclei. *Nature Physics*, 2018.

[53] K. Blaum, C. Geppert, H.-J. Kluge, M. Mukherjee, S. Schwarz, and K. Wendt. A novel scheme for a highly selective laser ion source. *Nuclear Instruments and Methods in Physics Research Section B: Beam Interactions with Materials and Atoms*, 204:331–335, 2003.

[54] D. A. Fink, T. E. Cocolios, A. N. Andreyev, S. Antalic, A. E. Barzakh, B. Bastin, D. V. Fedorov, V. N. Fedosseev, K. T. Flanagan, L. Ghys, A. Gottberg, M. Huyse, N. Imai, T. Kron, N. Lecesne, K. M. Lynch, B. A. Marsh, D. Pauwels, E. Rapisarda, S. D. Richter, R. E. Rossel, S. Rothe, M. D. Seliverstov, A. M. Sjödin, C. Van Beveren, P. Van Duppen, and K. D .A. Wendt. In-Source Laser Spectroscopy with the Laser Ion Source and Trap: First Direct Study of the Ground-State Properties of 217,219Po. *Phys. Rev. X*, 5(1):11018, 2015.

[55] D. A. Fink, S. D. Richter, K. Blaum, R. Catherall, B. Crepieux, V. N. Fedosseev, A. Gottberg, T. Kron, B. A. Marsh, C. Mattolat, S. Raeder, R. E. Rossel, S. Rothe, F. Schwellnus, M. D. Seliverstov, M. Sjödin, T. Stora, P. Suominen, and K. D. A. Wendt. On-line implementation and first operation of the Laser Ion Source and Trap at ISOLDE/CERN. *Nuclear Instruments and Methods in Physics Research Section B: Beam Interactions with Materials and Atoms*, 344:83–95, 2015.

[56] V.I. Mishin, A.L. Malinovsky, and D.V. Mishin. Resonant Ionization Laser Ion Source (RILIS) with improved selectivity achieved by ion pulse compression using insource time-of-flight technique. In *AIP Conf. Proc. 1104*, pages 207–212.

[57] S. Rothe, R. Catherall, B. Crepieux, T. Day Goodacre, V. N. Fedosseev, T. Giles, B. A. Marsh, J. P. Ramos, and R. E. Rossel. Advances in surface ion suppression from RILIS: Towards the Time-of-Flight Laser Ion Source (ToF-LIS). *Nuclear Instruments and Methods in Physics Research, Section B: Beam Interactions with Materials and Atoms*, 376:86–90, 2016.

[58] R. Heinke, T. Kron, S. Raeder, T. Reich, P. Schönberg, M. Trümper, C. Weichhold, and K. Wendt. High-resolution in-source laser spectroscopy in perpendicular geometry. *Hyperfine Interactions*, 238(1):6, 2016.

[59] K. Chrysalidis, S. Wilkins, R. Heinke, A. Koszorus, R. De Groote, V. N. Fedosseev, B. A. Marsh, S. Rothe, R. Garcia Ruiz, D. Studer, A. Vernon, and K. Wendt. First demonstration of Doppler-free two-photon in-source laser spectroscopy at the ISOLDE-RILIS. In *International Conference on Electromagnetic Isotope Separators and Related Topics-EMIS. In preparation*, Geneva, 2018.

[60] M. Kronberger, A. Gottberg, T. M. Mendonca, J. P. Ramos, C. Seiffert, P. Suominen, and T. Stora. Production of molecular sideband radioisotope beams at CERN-ISOLDE using a Helicon-type plasma ion source. *Nuclear Instruments and Methods in Physics Research Section B: Beam Interactions with Materials and Atoms*, 317:438–441, 2013.

[61] Pekka Suominen, Thierry Stora, Pascal Sortais, J Médard, and Lpsc Grenoble. Ionization efficiency of a COMIC ion source equipped with a quartz plasma chamber. 2010.

[62] L. Kirkby. Préparation et domaine d'exploitation des Mass-Marker des cibles ISOLDE. Technical report, CERN Summer Student Project.

[63] HSC https://www.outotec.com/products/digital-solutions/hsc-chemistry/.

[64] Robert L. Merlino and Steven L. Cartier. Hysteresis in a low pressure argon discharge. *Applied Physics Letters*, 44(1):33–34, 1984.

[65] T Gyergyek. Experimental study of the nonlinear dynamics of a harmonically forced double layer. *Plasma Physics and Controlled Fusion*, 41(2):175, 1999.

[66] Deli Tang and Paul K. Chu. Anode double layer in magnetized radio frequency inductively coupled hydrogen plasma. *Journal of Applied Physics - J APPL PHYS*, 94, 2003.

[67] F. Maldonado, T. Day Goodacre, and A. Gottberg. Multiphysics simulations for FEBIAD ion source developments at TRIUMF. In *International Conference on Electromagnetic Isotope Separators and Related Topics-EMIS. In preparation*, Geneva, 2018.

[68] COMSOL https://www.comsol.com/comsol-multiphysics.

[69] C. Seiffert. *Production of radioactive molecular beams for CERN-ISOLDE*. PhD thesis, Darmstadt, Tech. U, http://cds.cern.ch/record/2064456?ln=en, 2015.

[70] R. Kirchner, D. Marx, O. Klepper, V.T. Koslowsky, T. Kühl, P.O. Larsson, E. Roeckl, K. Rykaczewski, D. Schardt, J. Eberz, G. Huber, H. Lochmann, R. Menges, and G. Ulm. Intense beams of mass-separated, neutron-deficient indium, tin, thallium and lead isotopes. *Nuclear Instruments and Methods in Physics Research Section A: Accelerators, Spectrometers, Detectors and Associated Equipment*, 234(2):224–229, 1985.

[71] PSI https://www.psi.ch/.

[72] A. Pichard. Development of a surface ionization source for the SPIRAL 2 project. *Review of Scientific Instruments*, 81(2):1–4, 2010.

[73] H. C. Straub, P. Renault, B. G. Lindsay, K. A. Smith, and R. F. Stebbings. Absolute partial and total cross sections for electron-impact ionization of argon from threshold to 1000 eV. *Physical Review A*, 52(2):1115–1124, 1995.

[74] B. A. Marsh et al. The application of laser resonance ionization inside FEBIAD-type ion sources for ISOL facilities. https://ecos-eurisol14.sciencesconf.org/conference/ecos-eurisol14/pages/Marsh_RILIS_FEBIAD_BM_1.pdf, 2014.

[75] T. Day Goodacre. *Developments of the ISOLDE RILIS for radioactive ion beam production and the results of their application in the study of exotic mercury isotopes*. PhD thesis, The University of Manchester. https://cds.cern.ch/record/2254839, 2016.

[76] M. Breitenfeldt, D. Atanasov, K. Blaum, T. Eronen, P. Finlay, F. Herfurth, M. Kowalska, S. Kreim, Yu. Litvinov, D. Lunney, V. Manea, D. Neidherr, T. Porobic, M. Rosenbusch, L. Schweikhard, N. Severijns, F. Wienholtz, R.N. Wolf, and K. Zuber. Q-values of Mirror Transitions for fundamental interaction studies. *CERN INTC proposal P-369*, 2013.

[77] U. Köster, P. Carbonez, A. Dorsival, J. Dvorak, R. Eichler, S. Fernandes, H. Frånberg, J. Neuhausen, Z. Novackova, R. Wilfinger, and A. Yakushev. (Im-)possible ISOL beams. *European Physical Journal: Special Topics*, 150(1):285–291, 2007.

[78] T. Day Goodacre et al. The ISOLDE RILIS in 2016, achievements, developments and future plans. In *ISOLDE Workshop and Users Meeting*, CERN, Geneva, Switzerland, 2016.

[79] B. A. Marsh, V. N. Fedosseev, D. Fink, T. Day Goodacre, S. Rothe, M. Seliverstov, N. Imai, A .M. Sjødin, and R. E. Rossel. Suitability test of a high beam quality Nd:YVO4 industrial laser for the ISOLDE RILIS installation. *Cern Technical Note*, (CERN-ATS-Note-2013-007 TECH), 2013.

[80] A. Welker, N. A.S. Althubiti, D. Atanasov, K. Blaum, T. E. Cocolios, F. Herfurth, S. Kreim, D. Lunney, V. Manea, M. Mougeot, D. Neidherr, F. Nowacki, A. Poves, M. Rosenbusch, L. Schweikhard, F. Wienholtz, R. N. Wolf, and K. Zuber. Binding Energy of Cu 79: Probing the Structure of the Doubly Magic Ni 78 from only One Proton Away. *Physical Review Letters*, 119(19):1–6, 2017.

[81] P. Delahaye et al. New exotic beams from the SPIRAL 1 upgrade. In *International Conference on Electromagnetic Isotope Separators and Related Topics-EMIS. In preparation*, Geneva, 2018.

FACULTY OF SCIENCE
DEPARTMENT OF PHYSICS AND ASTRONOMY
INSTITUTE FOR NUCLEAR AND RADIATION PHYSICS
Celestijnenlaan 200D - box 2418
B-3001 Leuven
yisel.martinez@kuleuven.be
https://fys.kuleuven.be/iks/ns/home